

# INVESTIGATION OF FLUIDIC HIGH INTENSITY SOUND GENERATOR

*B. R. TEITELBAUM*

*L. B. TAPLIN*

*BENDIX RESEARCH LABORATORIES*

TECHNICAL REPORT AFFDL-TR-70-98

MAY 1971

DISTRIBUTION OF THIS REPORT IS UNLIMITED

AIR FORCE FLIGHT DYNAMICS LABORATORY  
AIR FORCE SYSTEMS COMMAND  
WRIGHT-PATTERSON AIR FORCE BASE, OHIO

20070919083

## NOTICE

When Government drawings, specifications, or other data are used for any purpose other than in connection with a definitely related Government procurement operation, the United States Government thereby incurs no responsibility nor any obligation whatsoever; and the fact that the government may have formulated, furnished, or in any way supplied the said drawings, specifications, or other data, is not to be regarded by implication or otherwise as in any manner licensing the holder or any other person or corporation, or conveying any rights or permission to manufacture, use, or sell any patented invention that may in any way be related thereto.

Copies of this report should not be returned unless return is required by security considerations, contractual obligations, or notice on a specific document.

# INVESTIGATION OF FLUIDIC HIGH INTENSITY SOUND GENERATOR

*B. R. TEITELBAUM*

*L. B. TAPLIN*

DISTRIBUTION OF THIS REPORT IS UNLIMITED

## FOREWORD

This report was prepared by the Research Laboratories of The Bendix Corporation, Southfield, Michigan, for the Aero-Acoustics Branch, Vehicle Dynamics Division, Air Force Flight Dynamics Laboratory, Wright-Patterson Air Force Base, Ohio, under Contract F33615-68-C-1406. This research was conducted under Project 4437 "High Intensity Sound Environment Simulation for Air Force Systems Testing" Task 443705 "Noise Source Development for Air Force Systems Testing". The Air Force Project Engineer was Mr. O. F. Maurer.

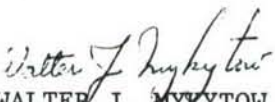
The authors wish to acknowledge the contributions of the following Bendix personnel to the research effort: J. H. Tarter, B. Tuller, D. R. Sproule, R. Spencer, J. S. Jurko, and O. K. Mattice.

The inclusive dates of the research effort were 26 February 1968 through 24 April 1970.

The Bendix Research Laboratories number corresponding to this report is 5335.

The manuscript was released by the authors in April 1970 for publication as a technical report.

This report has been reviewed and is approved.

  
WALTER J. MYKYTOW  
Asst. for Research & Technology  
Vehicle Dynamics Division



## ABSTRACT

This report summarizes the results of an investigation of a fluidic high-intensity sound generator concept. The investigation concerned the evaluation of a new type of proportional fluidic amplifier geometry, the annular slot amplifier. This geometry lends itself well to compact and symmetric interconnections between sound generator stages, and connection to a radiating horn at the final stage. The annular slot amplifier was found to have significantly higher pressure gain than the conventional planar jet proportional amplifier, 4 to 12.5 versus 3 to 5. An annular slot amplifier model was tested over a frequency range from 300 hz to over 2000 hz. Its control port impedance was studied particularly, and the impedance as well as the amplifier gain were found to vary with frequency. The frequency dependence is attributed to a distributed-parameter feedback phenomenon in the vent region.

An experimental two-stage sound generator was designed, fabricated and tested. The second stage is an annular slot amplifier with its critical areas scaled up ten times over those of the first stage. The first stage control flow source is an electrodynamic driver of the kind used with conventional loudspeakers. The second stage power jet area is  $5.78 \text{ in}^2$ , and the supply pressure is 10 psig. The radiating horn is exponential with a cutoff frequency of 180 hz and an exit diameter of 42 inches.

## TABLE OF CONTENTS

	<u>Page</u>
SECTION 1 - INTRODUCTION	1
SECTION 2 - ANNULAR SLOT JET AMPLIFIER	2
2.1 Amplifier Description	2
2.2 Initial Tests and Adjustments	6
2.3 Load Lines	10
2.4 Static Characteristic Maps	17
SECTION 3 - CONTROL FLOW SOURCE	22
3.1 Electrodynamic Driver	22
3.2 Piezoelectric Valve	26
3.3 Control Flow Source Status	28
SECTION 4 - GENERATOR DYNAMICS	29
4.1 General	29
4.2 Amplifier Gain	30
4.2.1 Static Gain	30
4.2.2 A Lumped Parameter Small Signal Steady State Analysis	31
4.2.3 Control Port Input Conductance ( $g_c$ )	36
4.2.4 Receiver Output Conductance ( $g_o$ )	40
4.2.5 Load Conductance ( $g_l$ )	41
4.2.6 Amplification Factor ( $\alpha$ )	42
4.2.7 Determination of Amplifier Parameters	42
4.3 Initial Frequency Response Tests	45
4.4 A.C. Impedance and Gain Measurement Tests	56
4.5 The Additional Distributed Signal Path	66
4.6 Amplifier Nominal Gain (No Feedback)	70
4.7 Compensation of Output Response Curves by Selection of Control Line Parameters	77
4.8 Noise	86
SECTION 5 - SOUND GENERATOR DESIGN	88
SECTION 6 - EXPERIMENTAL GENERATOR PERFORMANCE	94
6.1 First Stage with Interstage Transformer	94
6.2 Generator in Original Configuration	99
6.3 Generator with Vent Region Similitude	103
6.4 Generator with Vent Region Similitude and Changed D.C. Load	106
SECTION 7 - SUMMARY AND CONCLUSIONS	112
REFERENCES	115

# LIST OF ILLUSTRATIONS

<u>Figure No.</u>	<u>Title</u>	<u>Page</u>
1	Schematic Drawing of Annular Slot Jet Amplifier	3
2	Annular Slot Amplifier Model	4
3	Alternate Control Flow Deflector	7
4	Output Pressure Versus Control Static Pressure, Annular Slot Model	9
5	Test Schematic for Load Characteristic Map	11
6	Test Schematic for Control Characteristic Map	11
7	Arbitrary Set of Characteristic Curves	12
8	Load Lines Superimposed on Characteristic Curves	14
9	Load Characteristic Map for Annular Slot Model	18
10	Qualitative Comparison of Amplifier Types	19
11	Control Characteristic Map for Annular Slot Model	21
12	Frequency Response of Loudspeaker Driver and Audio Amplifier	24
13	Piezoelectric Valve Module	27
14	Lumped Parameter Equivalent Circuit	32
15	Equivalent Circuit (Nodal Analysis)	34
16	Input Characteristic Curves for Planar Proportional Jet Amplifier in Single-Ended Configuration	38
17	Plot of Equivalent Circuit Parameters	44
18	Pressure Transducer Installation	46
19	Thevenin Equivalent Circuit for 10 percent Efficient Driver with Design Load Value	53
20	Frequency Response of Annular Slot Model	55
21	Frequency Response (80 percent Control Port Area)	57
22	Frequency Response (60 percent Control Port Area)	58
23	Frequency Response (40 percent Control Port Area)	59
24	Typical Standing Wave Plot	61
25	Smith Chart of Control Port Impedance Obtained from Standing Wave Data	63
26	Control Port Dynamic Characteristics	65
27	Simplified Circuit with Distributed Feedback	68
28	Inside-Out Configuration with Large Control Line Duct Area	76
29	Amplifier Configuration with Large, Flared Ducts	78
30	Driver and Transformer Circuit	79
31	Standing Wave Ratio Versus Impedance and Transformer Ratio Parameter	82
32	Calculated Versus Measured Output Response	84
33	Annular Slot Amplifier Model Noise	87
34	Sound Generator Schematic Diagram	89
35	Experimental Sound Generator	90

<u>Figure No.</u>	<u>Title</u>	<u>Page</u>
36	First Stage Output Pressure Frequency Response with Interstage Transformer and with Concentric Tube Load	96
37	Effect of Supply Pressure Change on First Stage Pressure Frequency Response	98
38	Frequency Response of Generator in Original Configuration, $p_{L2}$ and $p_3$	101
39	Frequency Response of Generator in Original Configuration, $p_{L1}$ and $p_{c2}$	102
40	Frequency Response of Generator with Modified Second Stage Vent Region, $p_{L2}$ and $p_{c2}$	105
41	Frequency Response of Generator with Modified Second Stage Vent Region and Changed d.c. Load, $p_{L2}$ and $p_{c2}$	108
42	Generator Frequency Response in Terms of Sound Pressure Level, Horn Exit, $p_3$ and $p_{L2}$	109
43	Generator Frequency Response in Terms of Sound Pressure Level, $p_{c2}$ , $p_{L1}$ , and $p_{c1}$	110



# SYMBOLS

$A$	Duct cross section area, orifice area	$\text{in}^2$
$A_c$	Control port area	$\text{in}^2$
$(A_L)$	Duct area where $p_L$ is instrumented	$\text{in}^2$
$A_{\min}$	Minimum duct area downstream of amplifier receiver	$\text{in}^2$
$A_r$	Area at control port or receiving end of duct	$\text{in}^2$
$A_s$	Power jet nozzle area, area at driver or sending end of duct	$\text{in}^2$
$(A)_t$	Duct area where $p_t$ is instrumented	$\text{in}^2$
$a_1$	A constant to provide a consistent set of units	-
$c$	Speed of sound in gas	$\text{in}/\text{sec}$
$c_1$	Gas flow constant for orifice flow	$(\text{deg R})^{1/2}/\text{sec}$
$c_d$	Orifice discharge coefficient	dimensionless
$D_1$	Distance from power jet nozzle exit plane to receiver entrance plane	$\text{in}$
$D_2$	Distance from control flow deflector base surface to receiver entrance plane	$\text{in}$
$d_m$	Distance from control port to first minimum of standing wave pattern	$\text{in}$
$E$	Open-circuit a.c. pressure of an equivalent generator (rms)	$\text{psi}$
$f$	Frequency	$\text{hz}$
$f_o$	Quarter wavelength resonant frequency	$\text{hz}$



G	Amplifier pressure gain	dimensionless
g	(Without subscript) Acceleration due to gravity, 386	in/sec <sup>2</sup>
g <sub>c</sub>	Control port conductance	in <sup>2</sup> /sec
g <sub>f</sub>	Transconductance of flow source	in <sup>2</sup> /sec
g <sub>L</sub>	Circuit parameter, $g_L = g_o + g_\ell$	in <sup>2</sup> /sec
g <sub>ℓ</sub>	External load conductance	in <sup>2</sup> /sec
g <sub>nc</sub>	Normalized control port conductance	dimensionless
g <sub>o</sub>	Amplifier output conductance	in <sup>2</sup> /sec
h	Transport lag	sec
j	$\sqrt{-1}$	dimensionless
K <sub>r</sub>	Parameter, $K_r = (r - 1)/(r + 1)$	dimensionless
K <sub>1</sub> , K <sub>2</sub>	Transfer function parameters	dimensionless
L	Duct length	in
ℓ	Feedback path length	in
m	Normalized resistive component of impedance	dimensionless
n	Normalized reactive component of impedance	dimensionless
P <sub>cs</sub>	Static control pressure (steady state)	psig
P <sub>d</sub>	Absolute pressure downstream of orifice	psia
P <sub>L</sub>	Load pressure (steady state)	psig
P' <sub>L</sub>	Absolute output or load pressure (steady state)	psia
P <sub>out</sub>	Output pressure (steady state)	psig

$P_s$	Supply pressure	psig
$P_u$	Absolute pressure upstream of orifice	psia
$P_v$	Absolute back pressure on load	psia
$p$	a.c. component of pressure (rms)	psi
$P_c$	Amplitude of a.c. effective control port pressure (rms)	psi
$P_g$	Open-circuit a.c. pressure of a generator (rms)	psi
$P_L$	Amplitude of a.c. component of load pressure (rms)	psi
$P_{min}$	Amplitude of a.c. pressure at a standing wave minimum (rms)	psi
$P_{out}$	Amplitude of a.c. component of output pressure (rms)	psi
$p_s$	Duct input or sending end a.c. pressure (rms)	psi
$p_t$	Amplitude of a.c. pressure just downstream of interstage transformer outlet (rms)	psi
$R$	Transformer ratio, $R = A_r/A_s$	dimensionless
$R'$	Normalized control port resistance	dimensionless
$R_L$	Load resistance	psi-sec/lb or sec/in <sup>2</sup>
$r$	(Without subscript) Standing wave ratio	dimensionless
$r_c$	Control port resistance	sec/in <sup>2</sup>
$r_f$	Feedback path resistance	sec/in <sup>2</sup>

$r_\ell$	External load resistance	$\text{sec/in}^2$
$r_o$	Amplifier output resistance	$\text{sec/in}^2$
$T$	Absolute gas temperature	deg R
$v$	Phase velocity of wave	$\text{in/sec}$
$v_r$	Propagation velocity along feedback path	$\text{in/sec}$
$W$	Weight flow (steady state)	$\text{lb/sec}$
$W_c$	Control weight flow (steady state)	$\text{lb/sec}$
$W_L$	Output or load weight flow (steady state)	$\text{lb/sec}$
$W'_L$	Added flow component for deriving amplifier output impedance	$\text{lb/sec}$
$W_s$	Supply flow	$\text{lb/sec}$
$w$	a.c. component of weight flow (single amplitude zero-to-peak, or rms, as specified)	$\text{lb/sec}$
$w_c$	Amplitude of a.c. component of control weight flow (rms)	$\text{lb/sec}$
$w_L$	Amplitude of a.c. component of output weight flow (rms)	$\text{lb/sec}$
$w_r$	Duct receiving end a.c. weight flow (rms)	$\text{lb/sec}$
$X'$	Normalized control port reactance	dimensionless
$Y_c$	Amplifier input admittance	$\text{in}^2/\text{sec}$
$Y_{\text{out}}$	Amplifier output admittance	$\text{in}^2/\text{sec}$
$Z_c$	Control port impedance	$\text{sec/in}^2$
$Z_g$	Generator impedance (equivalent constant-area duct)	$\text{sec/in}^2$

$Z'_g$	Generator impedance evaluated at driver or sending end of duct	$\text{sec/in}^2$
$Z_{in}$	Duct input impedance (equivalent constant-area duct), same as $Z_s$	$\text{sec/in}^2$
$Z_o$	Acoustic characteristic impedance (equivalent constant-area duct)	$\text{sec/in}^2$
$Z_{oc}$	Acoustic characteristic impedance evaluated at control port end of duct	$\text{sec/in}^2$
$Z_r$	Termination impedance (equivalent constant-area duct)	$\text{sec/in}^2$
$Z'_r$	Duct termination impedance evaluated at control port or receiving end	$\text{sec/in}^2$
$Z''_r$	Duct termination impedance transformed to sending end position	$\text{sec/in}^2$
$Z_s$	Duct input impedance (equivalent constant-area duct), same as $Z_{in}$	$\text{sec/in}^2$
$Z'_s$	Duct input impedance evaluated with respect to receiving end area	$\text{sec/in}^2$
$Z''_s$	Duct input impedance evaluated with respect to sending end area	$\text{sec/in}^2$
$Z_T$	Duct transfer impedance, $Z_T = p_s/w_r$	$\text{sec/in}^2$
$\alpha$	(Without subscript) Amplification factor	dimensionless
$\alpha_t$	Wave attenuation constant	$\text{in}^{-1}$
$\beta$	(Without subscript) Transfer function factor variable with frequency	dimensionless
$\beta_t$	Wave phase constant	$\text{in}^{-1}$
$\gamma$	Wave propagation constant	$\text{in}^{-1}$
$\eta_t$	Interstage transformer power loss factor	dimensionless

$\lambda$	Wavelength	in
$\rho$	Mass density of gas	$\text{lb sec}^2/\text{in}^4$
$\omega$	Angular frequency, $\omega = 2\pi f$	rad/sec
$P$	Power	in lb/sec or watts (depending on context)
$P_1$	Power delivered to load by driver	in lb/sec
$P_2$	Total input power to driver	in lb/sec
<u>Subscripts:</u>		
o	Quiescent value of variable	
$\lambda/2, \lambda/4$	Variable value at half-wavelength, quarter-wavelength conditions	
1, 2, 3	Variable measured at station denoted (see Figure 34)	



## SECTION 1

### INTRODUCTION

This report summarizes the results of a program to investigate the characteristics of a fluidic high-intensity sound generator concept. The program follows a previous analytical and experimental effort in which the feasibility of the fluidic sound generator concept was demonstrated.

Sound generators of this type have application in the testing of structures and components in a high-intensity sound environment. The fluidic approach offers potential advantages over current approaches in the elimination of wear, fatigue, and drift of critical adjustments in the high-power transducing stage. To meet requirements for acoustic environmental testing, the sound generator should be an amplifier system capable of responding to any arbitrary electrical waveform whose components are within a specified frequency range. This is in contrast to a variable frequency oscillator system which may be appropriate for other testing applications. The overall objective of the present program was to provide information to support the future design and fabrication of a full-scale prototype. During the present program, three significant steps were accomplished:

- (1) a new type of fluidic amplifier geometry (the annular slot) was evaluated,
- (2) the fluidic amplifier was operated over a broad band of acoustic frequencies, and
- (3) the staging of two of the fluidic amplifiers was demonstrated in the form of an experimental generator.

These aspects will be described in detail in the main body of the report.

## SECTION 2

### ANNULAR SLOT JET AMPLIFIER

#### 2.1 AMPLIFIER DESCRIPTION

The annular slot jet amplifier geometry is shown schematically in Figure 1. The power jet and receiver are annular slots wrapped around a central axis. The power jet exits from the supply pressure region in a direction parallel to the central axis. Also, the plane of the receiver entrance is perpendicular to the central axis. The control flow is injected through an annular port inside and concentric with the power jet exit and receiver entrance. Variations in control flow and pressure modulate the amount of power jet momentum which is incident on the receiver entrance.

This geometry lends itself well to compact and symmetric interconnections between stages, particularly when large port sizes are used. In the case of a final stage, the receiver entrance can blend into a center body horn contour very conveniently, as in a siren. Also, the annular slot geometry was found to have high a.c. gain values. This will be discussed in detail in Section 4.

An annular slot amplifier model was designed and constructed to determine experimentally the characteristics of this type of amplifier. The results of tests with a large amplifier (0.2 to 0.4 in<sup>2</sup> power jet area) of the more conventional straight slot geometry were used to guide the design of the annular slot model.\* The straight slot amplifier had been constructed under the previous fluidic sound generator effort, and the tests were run both during the previous and the current efforts.

Figure 2 shows a cross-section of the annular slot model. Views of various bolts have been omitted for the sake of clarity. By the use of shims, the distance  $D_1$ , the power jet-to-receiver distance, can be readily varied. Also, the distance  $D_2$  can be varied by the use of shims to alter the control port geometry just upstream of the jet interaction region. The mean diameters and widths of the power jet and receiver annular slots are less convenient to vary.

The basic dimensions of the annular slot model were selected to be large enough that adjustment and instrumentation would not be difficult, and so that a power level at least as high as that of the previous straight slot model would be obtained. However, it was desired that the model size not be too large, since this would impose a difficult requirement

---

\* Reference 1.

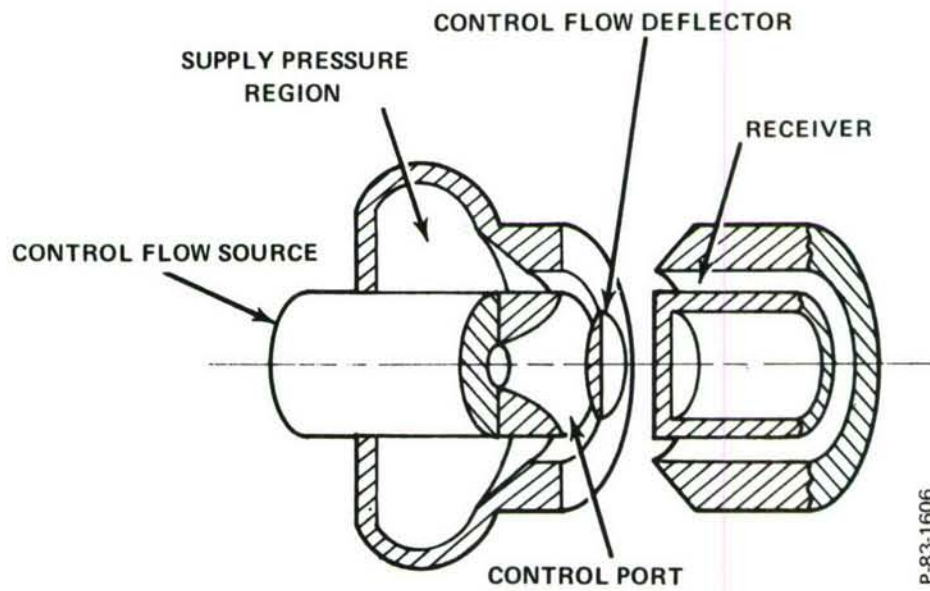
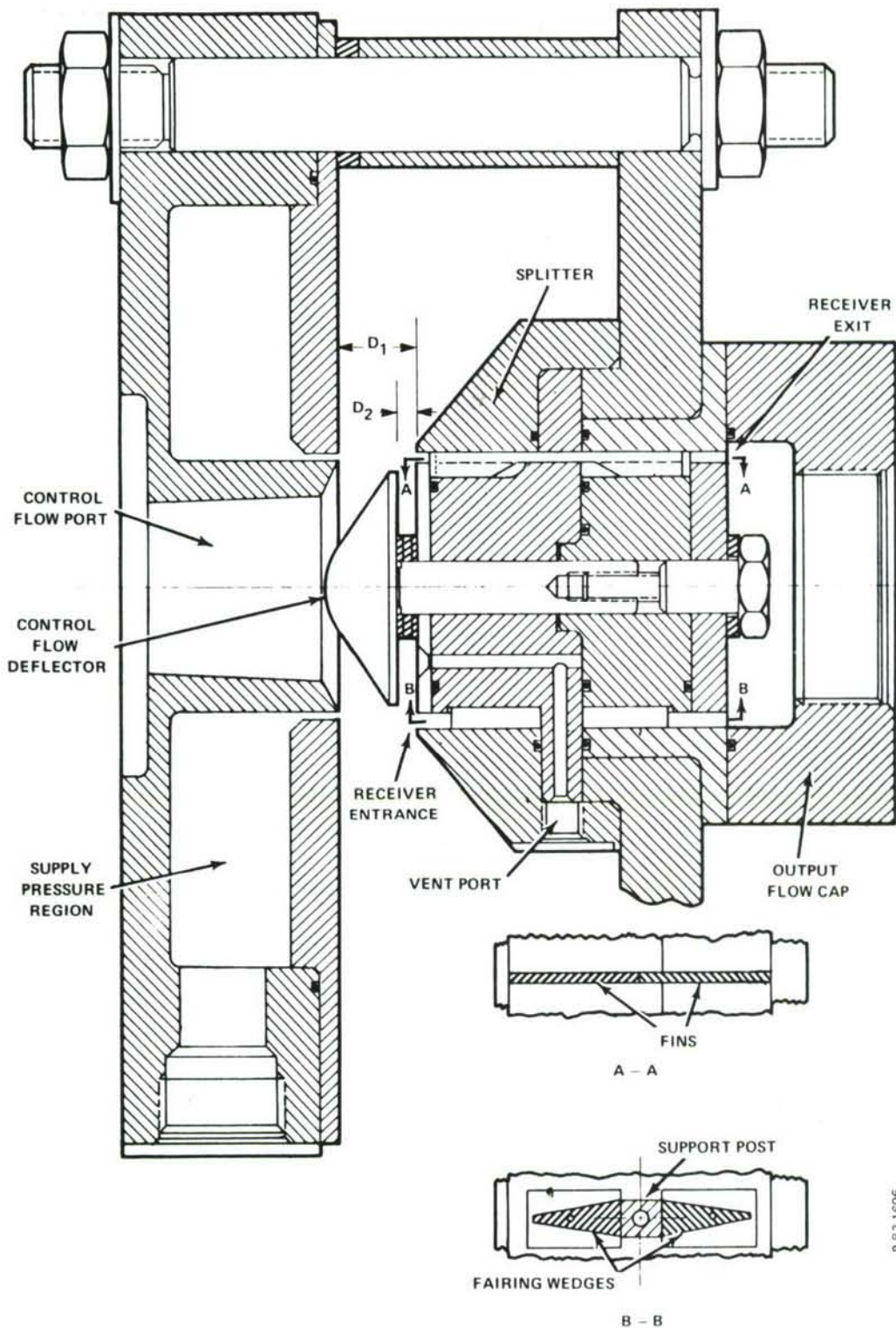


Figure 1 - Schematic Drawing of Annular Slot Jet Amplifier





P-83-1506

Figure 2 - Annular Slot Amplifier Model

on the dynamic control flow source. The receiver annulus basic dimensions are:

outer diameter	2.833 in
inner diameter	2.584 in
mean diameter	2.708 in
area	1.06 in <sup>2</sup>
slot width/mean diameter	0.046

The area of 1.06 in<sup>2</sup> is slightly larger than the receiver area of the straight slot model, which was 0.80 in<sup>2</sup>. The slot width-to-mean diameter ratio of roughly 5% is small enough that the jet deflection phenomena are largely two-dimensional rather than three-dimensional. This introduces the least amount of complexity in changing from a straight slot geometry to the annular slot geometry.

The power jet annulus basic dimensions are:

outer diameter	2.738 in
inner diameter	2.600 in
mean diameter	2.669 in
area	0.58 in <sup>2</sup>

The mean diameter of the power jet annulus is slightly smaller than the mean diameter of the receiver annulus to allow for an anticipated divergence of the cylindrical power jet stream.

The ratio of receiver slot width to power jet slot width is 1.8. Initially, the power jet was only half as wide, making the ratio of receiver slot width to power jet slot width twice as large, 3.6. The latter value was close to a value of 4.0 which was found to give good results in the straight slot model. However, after some initial testing, the power jet annular slot was widened to its present dimensions, and the amplifier performance was substantially improved. The exact reasons for the improvement are not known. It is suspected that the increase in momentum flux which could be modulated at the receiver entrance contributed to the higher gain and range of the amplifier. Also, better alignment of the power jet stream with the receiver annulus may have resulted when the power jet slot width was increased.



Two basic shapes of control flow deflector were tested: the one shown in Figure 2 and the other shown in Figure 3. Several variations were made on the base or maximum diameters of these control flow deflectors.

It is seen from Figure 2 that the receiver slot is formed by an outer group of parts or housing, and an inner cylinder group of parts. The inner cylinder group of parts is positioned by means of three equally spaced support posts. One of these is indicated in Section B-B of Figure 2. Fairing wedges are provided for streamlining purposes. In addition, six sets of fins are provided in the receiver slot to aid in flow straightening and to prevent any circumferential acoustic standing waves. One set of fins is shown in Section A-A of Figure 2.

Three vent paths were provided through the inner cylinder support posts. Their purpose was to make the pressure under the base of the control flow deflector essentially equal to atmospheric pressure. During the testing, it was found that the paths were too small to have any appreciable effect on the pressure in the region under the deflector base. The construction of the amplifier model parts did not allow the vent path areas to be enlarged significantly. Therefore, the amplifier model can be considered as having an essentially isolated region under the deflector base.

The output flow cap collects the receiver outlet gas. When a downstream load orifice or valve is connected to the output flow cap, the static characteristics of the amplifier model can be measured. The output flow cap has too much volume under compression for meaningful dynamic tests. Therefore, the output flow cap is replaced by a concentric tube load which is an extension of the receiver annulus. This will be discussed further in Section 4.

## 2.2 INITIAL TESTS AND ADJUSTMENTS

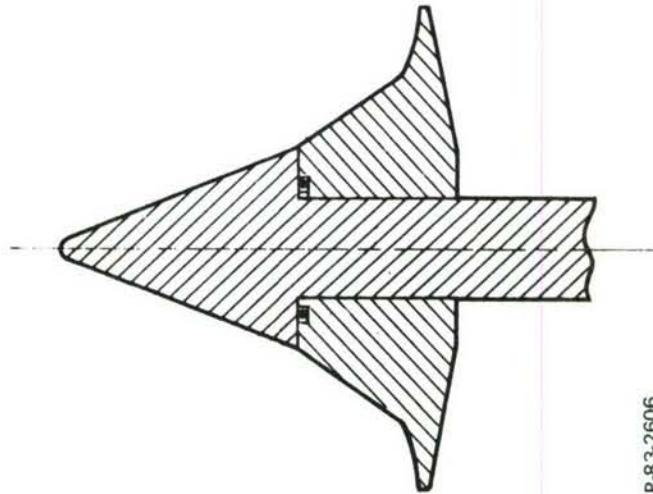
The first tests to be performed on the annular slot model were steady state tests to determine the shapes of the control flow deflector and the combinations of the  $D_1$  and  $D_2$  distances which gave the best output pressure versus control pressure characteristics. Amplifier geometries which were favorable from the viewpoint of the steady state pressure characteristics were then considered candidates for evaluation under dynamic conditions.

Figure 4 shows the results of typical tests. Here,

$P_{out}$  = output pressure (steady state)

$P_{cs}$  = static control pressure (steady state)

For the control pressure, the distinction is made between static pressure and total pressure. The static pressure is that measured at a tap in the wall of the duct approximately 4 inches upstream of the control port. The total pressure is that measured at a pitot probe in the control port and on the center line, pointed upstream. Because the



P-83-2606

Figure 3 - Alternate Control Flow Deflector



control port gas velocity reaches a Mach number of 0.06 maximum, averaged over the control port area, the corresponding difference between the static and total pressures is 0.04 psi maximum. This is 5% of the typical control pressure level of 0.8 psig. However, ununiform velocity distribution over the control port area could affect the instrumented total pressure substantially. Large discrepancies were, in fact, observed occasionally between control static and total pressures. For purposes of consistency, control static pressure has been used exclusively for the data in this report. A similar difference between the output static and total pressures prevails in the amplifier receiver. The difference can be as much as 10% of the output pressure level, with the loads used. Total output pressure was not instrumented during the testing, and the output pressure data reported should be understood to be static pressure. This is measured at a tap in the outer tube wall of the concentric tube load, 1.19 inches downstream of the receiver exit.

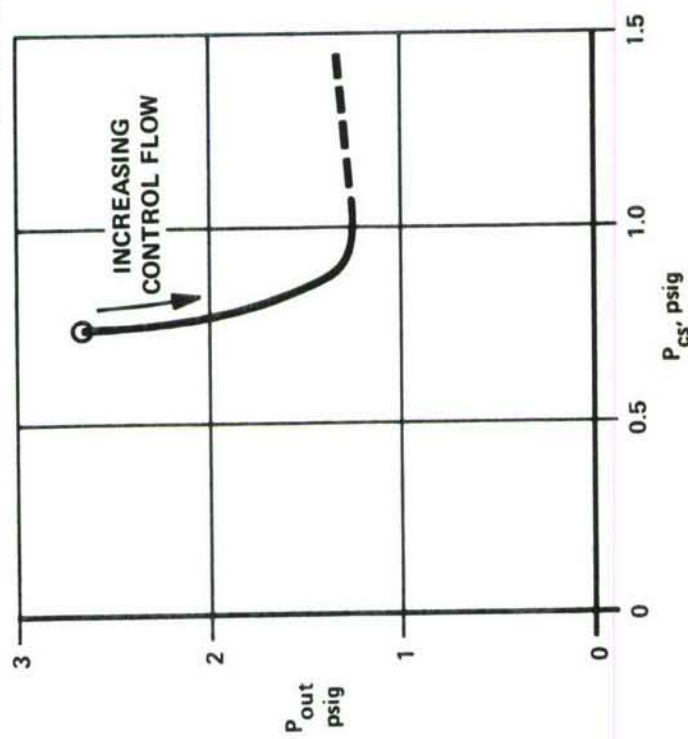
Desirable amplifier characteristics are high pressure gain (i.e., the steepness of the curves in Figure 4) and a large and nearly linear range of  $P_{out}$  variation. Testing showed that with either type of control flow deflector, best results were obtained with  $D_1 = 0.536$  in. and  $D_2 = 0$ . These results were evidenced by the linear range and slope of  $P_{out}$  versus  $P_{cs}$  plots obtained in numerous test runs in which the distances of  $D_1$  and  $D_2$  were varied. These plots always had the general form of those in Figure 4, but did not have as large a linear range of  $P_{out}$  variation, and in some cases did not have as steep a slope in the linear range, as the plots shown in Figure 4 for  $D_1 = 0.536$  in. and  $D_2 = 0$ . The sensitivity to the  $D_1$  dimension is not great, and a variation of  $\pm 0.020$  inch is tolerable. Such a variation yields about as much change in  $P_{out}$  versus  $P_{cs}$  plots as can be expected from the repeatability between runs with  $D_1$  fixed.

In Figure 4, the maximum  $P_{out}$  point corresponds to zero control flow, or a blocked control line. It is seen that a positive control pressure of approximately 0.75 psig results. This is due to a portion of the high velocity power jet spilling inward toward the centerline rather than outward to the atmospheric vent region, thereby pressurizing a blocked control line. The flattening-out of the curve at low values of  $P_{out}$  is due to the power jet being entirely diverted from the receiver by the control flow. We may observe in Figure 4 that the standard control flow deflector gives very high values of incremental pressure gain, while the alternate control flow deflector gives lower gain but better linearity. Both geometries were judged worthy of dynamic testing.

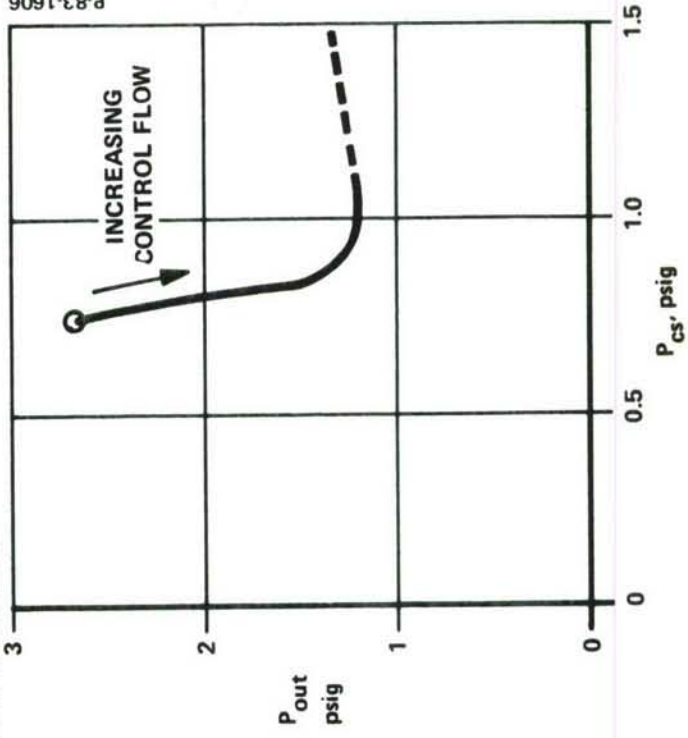
Dynamic testing (to be discussed in Section 4) was done using both the standard and alternate deflector geometries. The standard geometry deflector gave dynamic output pressures on the average 15% higher than those of the alternate geometry deflector under otherwise similar conditions. Therefore, most work was done with the standard geometry deflector, and all of the test data in the rest of this report pertains to the standard deflector.

The gains as evidenced in Figure 4 are considered unusually high for a jet amplifier. For the alternate deflector geometry, the pressure gain is 12.6, and the standard deflector yields a local incremental gain approaching infinity. Conventional planar jet proportional amplifiers under similar load conditions have pressure gains of approximately 3 to 5.

$P_S = 10$  PSIG,  $D_1 = 0.536$  IN  
50 FT. CONCENTRIC TUBE LOAD



(a) Standard Control Flow Deflector



(b) Alternate Control Flow Deflector

Figure 4 - Output Pressure Versus Control Static Pressure, Annular Slot Model



Another set of steady state tests was performed to obtain data for mapping the amplifier load and control characteristics. The schematics for these tests are shown in Figures 5 and 6.

To obtain the steady state characteristics, the load valve opening was varied while adjusting the control bias valve so as to maintain a constant control pressure. The variable load valve setting can be thought of as a means of setting load lines upon the characteristic curves of the amplifier. Knowing the flow-pressure relationships for the loads, the static characteristic curves of the amplifier can be determined for constant control pressure, or for constant control flow. Constant control pressure was selected for defining the characteristic curves of the amplifier.

### 2.3 LOAD LINES

Before proceeding to discuss the results, some general comments on load line techniques should be noted. Let us use an arbitrary set of characteristic curves as shown in Figure 7. The amplifier output flow, which is equal to the flow into the amplifier's external load, is plotted on the vertical axis. A characteristic curve is the locus of all combinations of output flow and load pressure for some specified, fixed internal condition of the amplifier, without regard to nature of the load. In the case illustrated in Figure 7, the fixed internal amplifier condition is the constant value of control pressure,  $P_{cs}$ . The curves are somewhat idealized (straight line sections are used) for ease of discussion. The plot can be divided into characteristic regions, i.e., those regions where the slopes of the curves are negative and those where the slopes are positive. In the region where the slopes are negative, the device is said to have an output impedance which is positive; i.e., and increase in load pressure (an increase in back pressure on the amplifier) causes a decrease in output flow. This effect is, of course, true for any passive resistive element (orifice, pipe, etc). Passive flow restrictors are by definition positive resistances. So it is, then, that in the region where the amplifier characteristic curves have negative slope, the output impedance is defined as being positive. Mathematically, the negative partial derivative of the load pressure with respect to the load flow defines the output resistance,  $r_o$ .

$$r_o = - \left. \frac{\partial P_L}{\partial W_L} \right|_{P_{cs} = \text{constant}}$$

Conversely the output conductance  $g_o$ , is given by:

$$g_o = - \left. \frac{\partial W_L}{\partial P_L} \right|_{P_{cs} = \text{constant}} = \frac{1}{r_o}$$



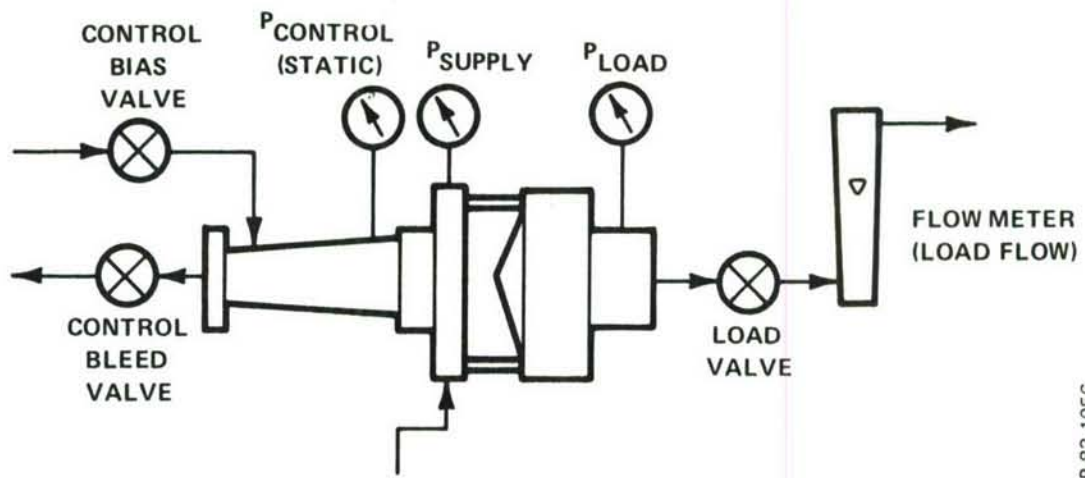


Figure 5 - Test Schematic for Load Characteristic Map

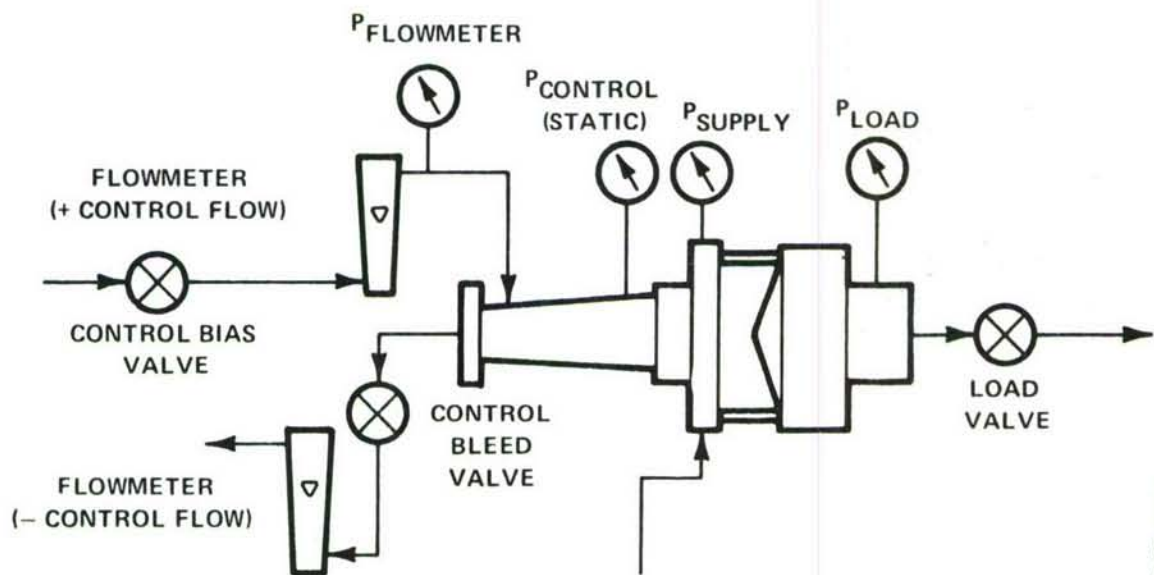


Figure 6 - Test Schematic for Control Characteristic Map

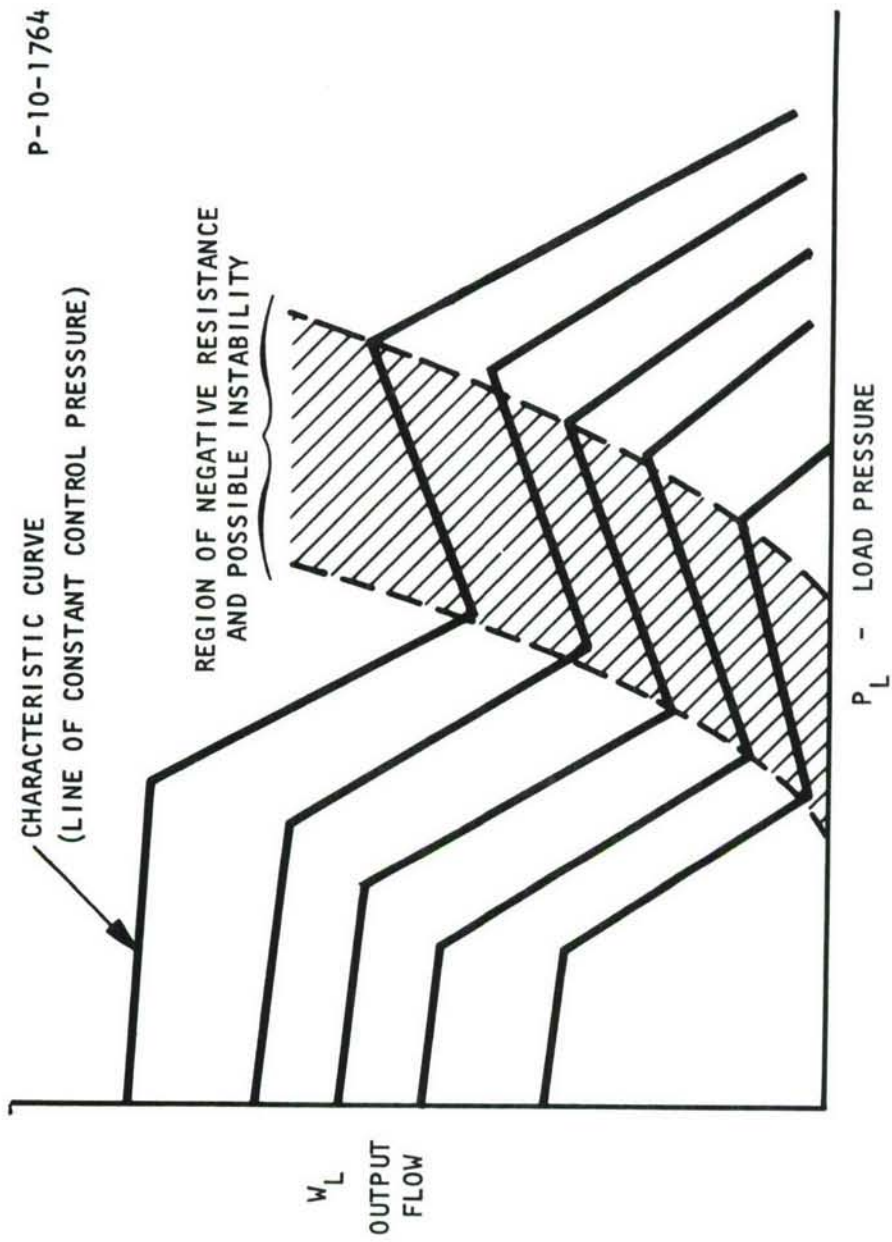


Figure 7 - Arbitrary Set of Characteristic Curves

In the region of the curves where the slopes are positive, the output resistance of the amplifier is negative. In this region the device behavior is contrary to that expected from passive resistances, i.e., an increase in back pressure causes an increase in flow. The effect is opposite to that of positive resistances, hence the device is characterized as having a negative output impedance. Physical reasons leading to the establishment of negative resistance will be discussed later.

Given the characteristic curves, load lines may be constructed across these curves so that the device output may be described for a given load. A load line is the locus of all combinations of output flow and load pressure for a fixed load condition, without regard to the nature of the amplifier. It can be seen that for a given value of  $P_{CS}$  and a given load condition, the resulting steady state values of  $W_L$  and  $P_L$  are defined by the intersection point of the relevant characteristic curve and load line.

Again for ease of discussion, a straight line relationship is assumed between flow and pressure drop for the load. (Physically, such a load could be realized by using laminar flow restrictors.) For a linear load:

$$W_L = \frac{P'_L - P_V}{R_L} = \frac{P_L}{R_L}$$

where:

$W_L$  = Flow rate, lb/sec

$P'_L$  = Output pressure of the amplifier, which is upstream pressure to the load, psia

$P_V$  = Back pressure on the load, held constant and for discussion here equal to atmospheric pressure, psia

$R_L$  = Load resistance, psi-sec/lb

$P_L$  = Gage pressure upstream of the load, psig

Load lines for various values of  $R_L$  are shown plotted over the characteristic curves in Figure 8. The greater the slope of the load line,  $\partial W_L / \partial P_L$ , the lower the resistance of the load.

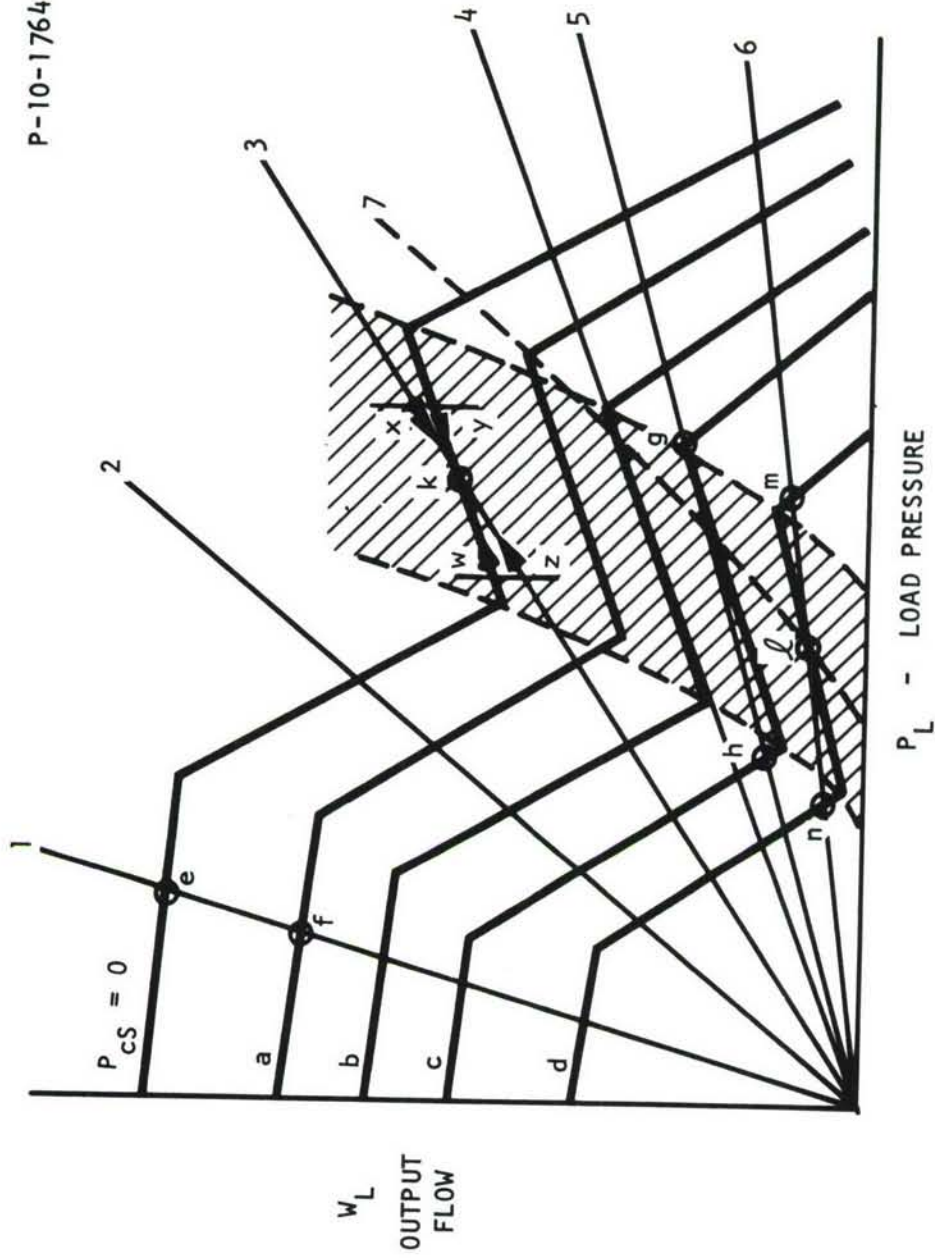


Figure 8 - Load Lines Superimposed on Characteristic Curves



Taking first the regions of positive output impedance, the operation of the amplifier with a load is easily followed from point to point while changing control pressure. For each control pressure there is a unique operating point found by the common point of crossing of the load line, and the characteristic curve for the control pressure used. Referring to Figure 8, if load line 1 is used, then, as the control pressure is increased from "o" to "a" the operating point moves from "e" to "f," and so on. Using the load line, transfer curves may be constructed showing output flow,  $W_L$ , as a function of  $P_{CS}$ ; or load pressure,  $P_L$ , as a function of  $P_{CS}$ .

A particularly interesting region of operation occurs for load line 4. As the control pressure is increased and the operating point enters the negative resistance region, the slightest change in control pressure causes a very large change in output pressure and flow. The gain is nearly infinite. Where the characteristic curve and load line are tangent the gain of the device is infinite. For load line 5, as control pressure is increased to a value "c" operating point "g" is obtained. A slight increase in control pressure beyond "c" causes the operating point to jump to point "h." If a plot of  $P_L$  versus  $P_{CS}$  were made, the plot would show hysteresis.

The discussion above relates to constructing transfer curves once the characteristic curves are known. Load lines may be used to find the characteristic curves as follows. Controlling by  $P_{CS}$  to successive constant values while varying the load line continuously from 1 to 6, the various characteristic curves can be traced out, with certain exceptions. These exceptions do not negate the presence of a continuous characteristic curve. Rather, changes in location of the load line and/or dynamic compensation are required to find the balance of the characteristic curves. These exceptions all occur in the negative resistance region.

Methods of obtaining the complete negative resistance sections of the characteristic curves can be discussed by considering load lines 3, 4, and 5 or 6. In the case of load line 3, there is a unique crossing point, "k", for the load line and the characteristic curve. This point can be realized experimentally providing the system is dynamically stable. To show whether the system is stable requires knowledge of the energy storages in the circuit under test. For the setup shown in Figure 5, usually a large volume exists between the amplifier and the load valve, so that the dominant energy storage device is capacitive. To examine whether an operating point is stable, one assumes a dynamic state of  $P_L$  at a value above or below that for point "k". Assume instantaneous values at point "x" for the load and point "y" for the amplifier, at a dynamically increased value of  $P_L$ . Since the flow through the load (point "x") is larger than the flow from the amplifier (point "y") the additional flow must be coming from the capacitance and the rate of change of load pressure must then be negative in sign. With a negative rate of change of load pressure, operating points "x" and "y" are moving toward



"k" as the arrows show. If we select points "w" and "z" as instantaneous operating points for a dynamically decreased value of  $P_L$ , then the flow leaving the amplifier (point "w") is larger than that flowing through the load (point "z") and the capacitance must be charging, and the rate of change of load pressure is positive. Therefore, points "w" and "z" will move towards point "k". Thus, point "k" is a stable operating point and can be measured experimentally.

The opposite is true for load line 6. Point "l" is an unstable operating point since selecting instantaneous values off of the point will yield rates of change of load pressure that drive the system to either point "m" or "n". To determine the characteristic curve in the negative resistance region between points "n" and "m", it is necessary to back-pressure the load orifice so that the load line passes from below and up through the negative resistance region, as depicted by load line 7. Using a back-pressured load now causes operating point "l" to be stable, and it can be measured experimentally.

Load line 4 presents an interesting situation, as mentioned earlier. Here a slight change in loading towards load line 5 causes a very rapid reduction in load pressure,  $P_L$ . The gain is very high. Operation of an amplifier of this type would use a load line which lies somewhere between 3 and 4 in order to obtain high gain while still having a stable amplifier.

In the test data to be shown below, some negative resistance regions were not mapped by using the necessary special load lines (like 7), as these regions would never be used in the final system. Reasonable estimates can be made, however, from knowing the locations of points like "n" and "m". The curve in the negative resistance region will be close to a straight line drawn between such points.

While on the subject of load lines, there is, of course, no doubt about their utility in deriving steady state characteristic curves. In operating the amplifier dynamically, it must be determined over what range of frequencies the characteristic curves and load lines are valid. Considering first the load line, if the loads used are taken as properly terminated transmission lines, then the load line representation is valid over all frequencies for which the load behaves like a transmission line. The only question left is, "are the characteristic curves valid for the same range of frequencies?" The answer to this question rests in how the amplifier is mathematically modeled, and in recognizing whether critical dimensions in the amplifier are shorter than, say, one-tenth of a wavelength at the highest frequency to be used.

In the case of dynamic modeling, all energy storage mechanisms at the input and receiver of the amplifier must be identified and modeled either as lumped or distributed systems, depending on the frequency. If these energy storages, inertances, capacitances, or sections of lines are all identified, then the portions of the amplifier left for analysis include only the jet interaction region. As long as the jet interaction region length is a small fraction of a wavelength, the static gain characteristics

of the amplifier will be preserved. The steady state characteristic curves can then be used to define amplifier gains and those portions of the amplifier input and output impedances related to the amplifier jet interaction region.

## 2.4 STATIC CHARACTERISTIC MAPS

In running the steady state tests, the standard control flow deflector was used, and the  $D_1$  and  $D_2$  distances were as cited previously. Figure 9 is the resulting load characteristic map. The individual curves are loci of constant static control pressure. These curves were faired in as the best smooth paths among many individual data points. The broken portions of the curves denote regions where instability and jumping between operating conditions was encountered, as discussed above. Thus, in the broken portions of the curves there is more uncertainty concerning the actual loci of operating points than in the solid portions of the curves. The solid dots on the curves denote points where there is no net inlet or outlet control flow, i.e., the control bias valve and control bleed valve of Figure 5 are both shut. These blocked control line points will sometimes be referred to as "self-bias" points.

The data was run using gaseous nitrogen as the working fluid. The standard control flow deflector was used, and  $D_1$  was 0.536 inch;  $D_2$  was 0.0.

It may be noted from Figure 9 that the self-bias point for a static control pressure of 0.75 psig corresponds to a load pressure of 3.1 psig. This is at variance with the data of Figure 4 where the self-bias point is 0.75 psig for static control pressure and 2.6 psig for load or output pressure. The variance is due to minor unavoidable changes in alignment which accompanied several disassembly and reassembly procedures. These minor alignment changes shifted the operating conditions. However, the conclusions drawn as to optimum setting remain unchanged.

Several interesting things can be seen in the annular slot model load characteristic map. First, in the range from about 2 to 3 psig load pressure, the curvatures are such that a tangent line will lie below the curve near the tangent point. In conventional planar jet proportional amplifiers, the curvatures are such that a tangent line will always lie above the characteristic curve. Figure 10 compares qualitatively the annular slot and the conventional planar amplifier. The load line represents a fixed flow rate versus pressure drop relationship for the part of the pneumatic circuit downstream of the amplifier receiver. The intersection of the load line with a solid curve corresponding to a fixed static control pressure defines the amplifier's steady state operating point. It can be seen that in the case of the annular slot amplifier, parts of the characteristic curves can be nearly parallel to the load line. This makes possible a much larger change in the load pressure for a given change in control pressure than in the case of the conventional planar amplifier. Thus, high values of pressure gain are to be expected of the annular slot amplifier if it is properly loaded.



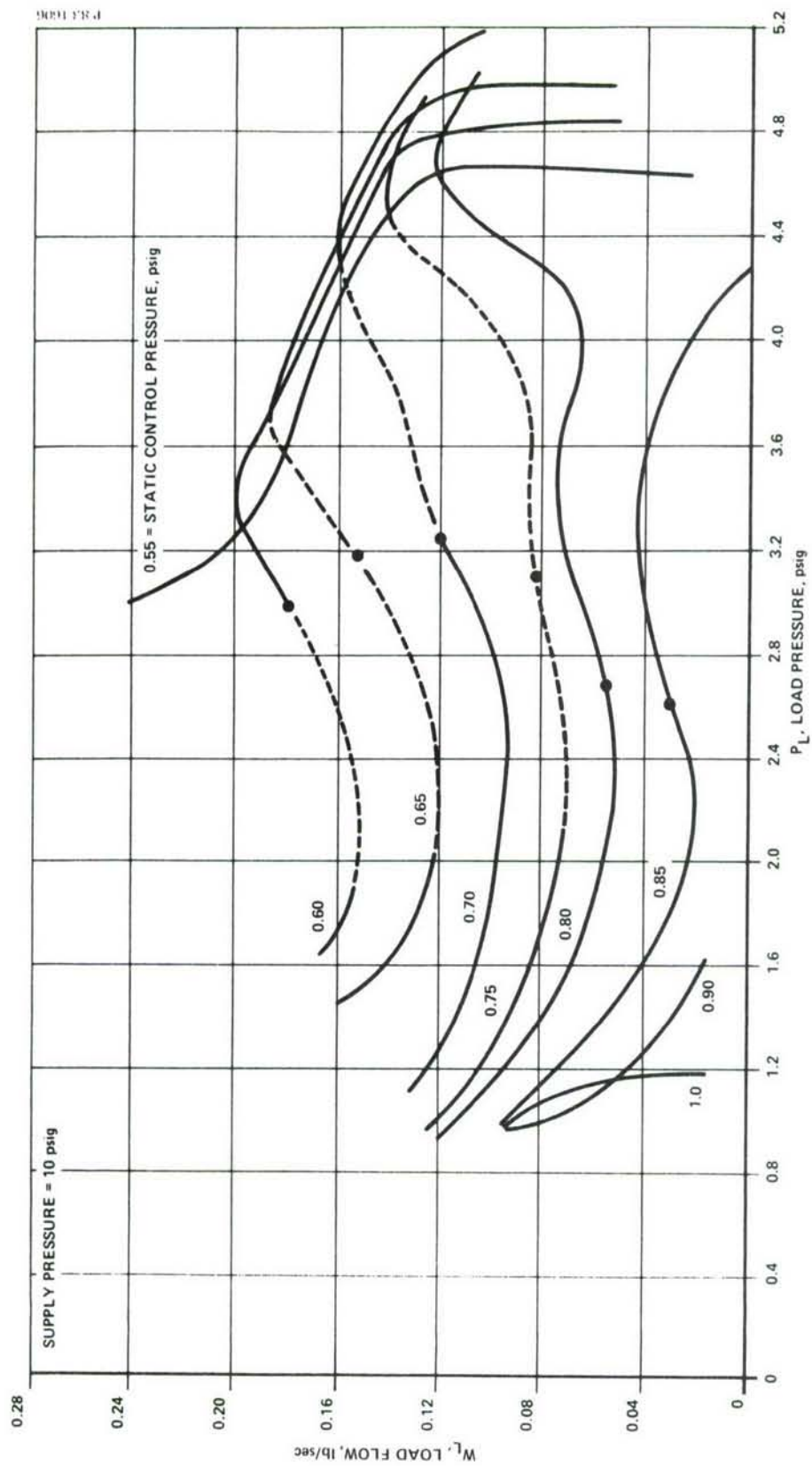


Figure 9 - Load Characteristic Map for Annular Slot Model



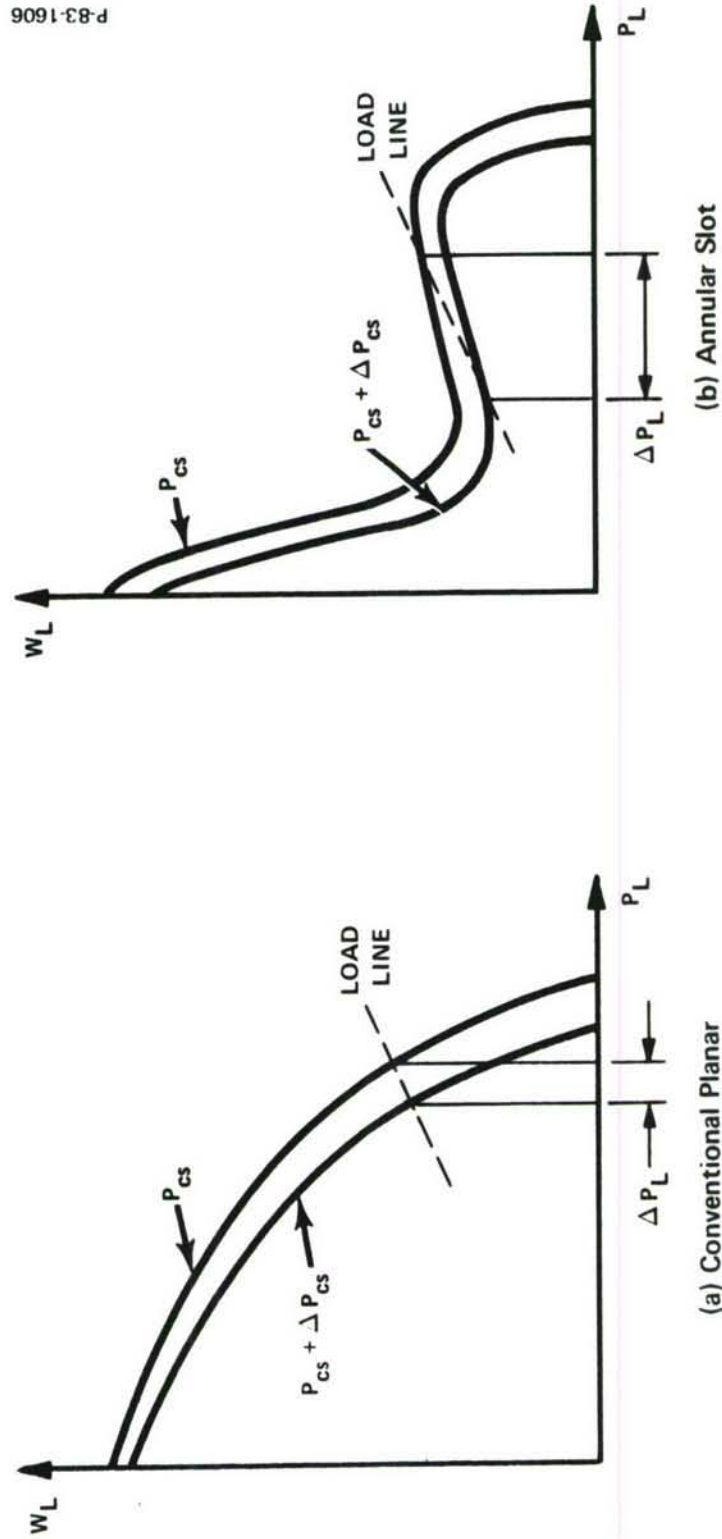


Figure 10 - Qualitative Comparison of Amplifier Types

A disadvantage of characteristic curves shaped as in the case of the annular slot amplifier is that operating points giving moderately high load flow and load pressure simultaneously are excluded. Thus, the annular slot amplifier cannot modulate as high a power into a load as can a conventional planar amplifier having the same power jet size and pressure. This appears to be the price paid for the high gain capability and is considered a favorable trade-off for at least the first stages of a sound generator system.

The annular slot model control characteristic map is shown in Figure 11. The zero flow horizontal axis is the locus of the self-bias points. It may be noted that there is a variance in the self-bias static control pressure and load pressure combination for Figure 4 and Figure 11. The reason is the same as for the variance cited previously in the case of Figures 4 and 9. It is seen in Figure 11 that the constant load pressure curves have positive slope in the left-hand part of the map, but negative slope in the right-hand part. In conventional planar amplifiers, the slopes are always positive.

We might point out here that the load and control characteristic maps can be used to find the input resistance of the amplifier for a given output load. First, a load line is drawn on the load characteristic map. Then points marking the excursion of the operating point along the load line with changes in control pressure are cross-plotted on the control characteristic map. The slope of the curve connecting the operating points on the control map defines the control port or input resistance. When we perform this procedure with the maps of Figures 9 and 11, we obtain the low frequency or d-c control port resistance. However, this, is not necessarily the same as the control port impedance at acoustic frequencies. Thus, a dynamic study of the amplifier characteristics is necessary.

The steady state test results described above generally define the nature of the annular slot amplifier. It differs markedly from the conventional planar proportional jet amplifier in the shapes of the curves of the characteristic maps. The physical reason for the difference has not been positively identified, but it is believed to be related to a regenerative feedback phenomenon in the vent region. By regenerative feedback, it is meant that some of the energy in the deflected power jet is, in effect, fed back to the control region. The phase relationship is such that as the power jet moves to increase the output pressure, the energy which is fed back causes increased movement of the power jet in the direction to further increase the output pressure.

In any case, the possibility of achieving a high gain makes the annular slot amplifier very attractive for the sound generator application. The next phase of the investigation concerned dynamic testing to see if the amplifier had good a.c. performance also. This will be covered in Section 4.

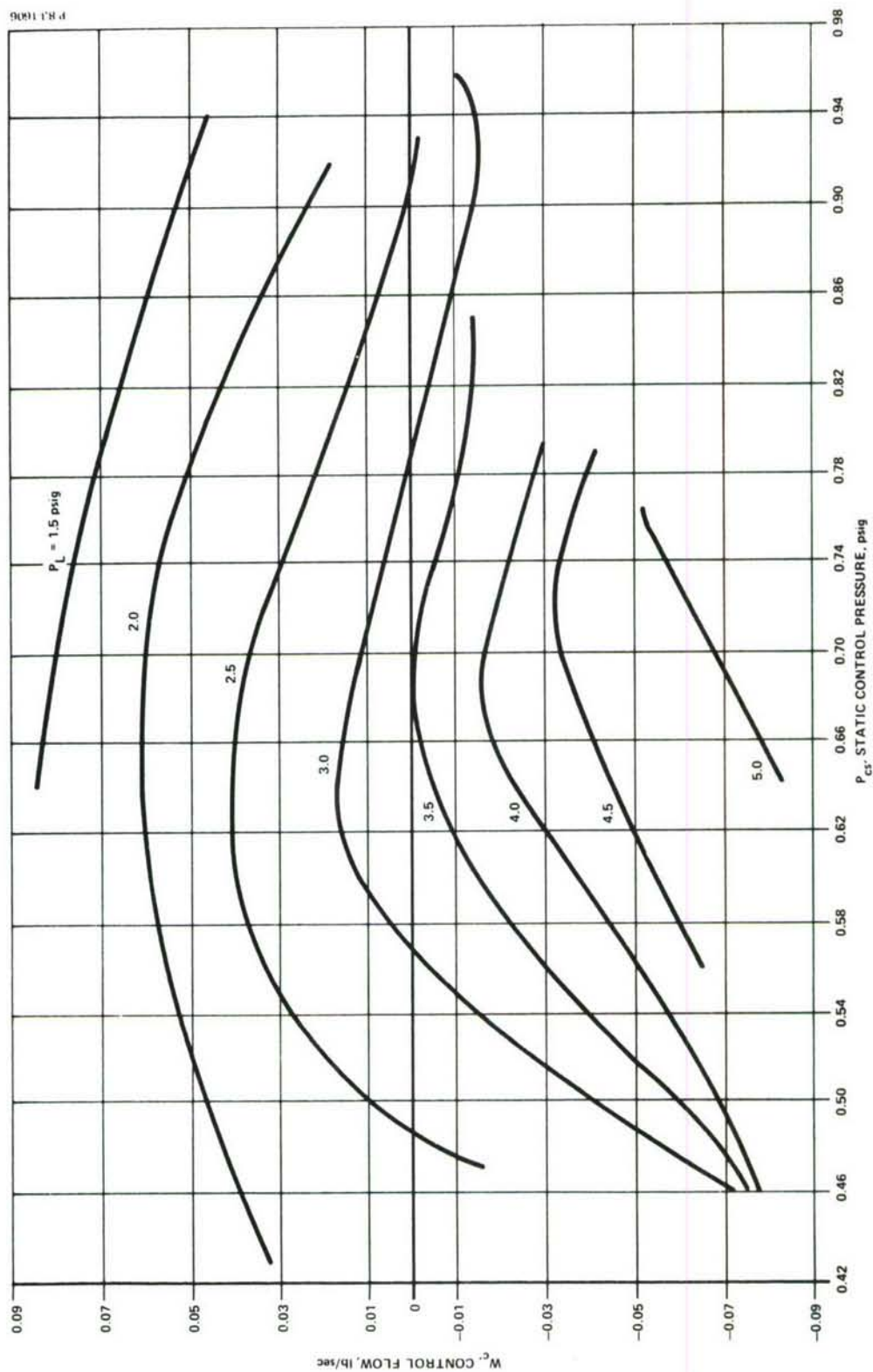


Figure 11 - Control Characteristic Map for Annular Slot Model



### SECTION 3

#### CONTROL FLOW SOURCE

An electric-to-pneumatic transducer is required as a signal source for the fluidic sound generator system. This signal source provides dynamically varying flow to the first-stage annular slot amplifier control port. Two approaches were considered. The first would use a commercial electrodynamic loudspeaker driver. The second would use a bank of piezo-electrically actuated flapper valves, each of which would in turn drive a planar proportional fluidic amplifier stage. The first approach using the commercial loudspeaker driver was selected. In this section, the considerations bearing on both approaches will be reviewed.

#### 3.1 ELECTRODYNAMIC DRIVER

The main advantage of this approach is that the transducer can be a commercially available component and hence relatively low in cost and short in delivery time. Its main disadvantage is its poor low-frequency response. The unit selected (Altec Lansing Model 290 E) has the following specifications:

Maximum electrical power input	100 watts
Frequency response	300 to 8,000 hz
Throat diameter	1.08 in.
Duct diameter at connection flange	1.40 in.

The driver has a voice coil impedance of 4 ohms, but is driven through a transformer and capacitor circuit. Looking into this circuit, the impedance is 50 ohms. A 6 db/octave roll-off is provided below 300 hertz to protect the voice coil and diaphragm from being driven beyond their travel limit.

Figure 12 is a frequency response taken of the driver loaded by 48 feet of aluminum tubing whose inner diameter matched the driver connection flange diameter. The pressure was measured by a dynamic pressure pickup installed in the tubing wall within 1 inch of the driver flange. The attenuation in the tubing was such that the standing wave amplitude was approximately 0.03 psi minimum to maximum. The peaks of the standing wave pattern were separated by approximately 13 hz intervals. Neglecting the small standing wave effect, the driver had an ideal acoustic load. (An ideal acoustic load is one which has the same dynamic pressure-flow characteristic as an infinitely long, rigid tube filled with air at standard pressure and temperature, and whose cross section area is equal to the port area at the driver flange.) The power for the driver is obtained from a commercial audio amplifier



(McIntosh Model MI-200B) rated at 200 watts maximum power. A constant-amplitude input signal was supplied to the amplifier. At 500 hz, this resulted in a 47-volt rms drive signal at the amplifier output. This drive signal varied with frequency approximately 5 volts rms minimum to maximum over the test frequency range.

From Figure 12 we can see that the amplifier and driver combination is essentially flat from about 800 to 2500 hz. The response is not flat below 800 hz, peaking about 5 db at 550 hz and being down 8 db at 300 hz.

The acoustic power being sent down the tubing can be calculated from the equation,

$$\mathcal{P} = a_1 \frac{p^2 A}{\rho c} \quad (3-1)$$

where

$\mathcal{P}$  = Power

$a_1$  = A constant to provide a consistent set of units

$p$  = rms pressure of acoustic signal

$\rho c$  = Characteristic acoustic impedance of the medium in the tubing

$A$  = Cross-section area of tubing

Using a specific system of units, and air at room temperature in the tube, equation (3-1) becomes

$$\mathcal{P} = 73.6 p^2 A \quad (3-1a)$$

where

$\mathcal{P}$  is in watts

$p$  is in psi (rms)

$A$  is in square inches

In the flat portion of the frequency response of Figure 12,

$p = 0.21$  psi (rms)

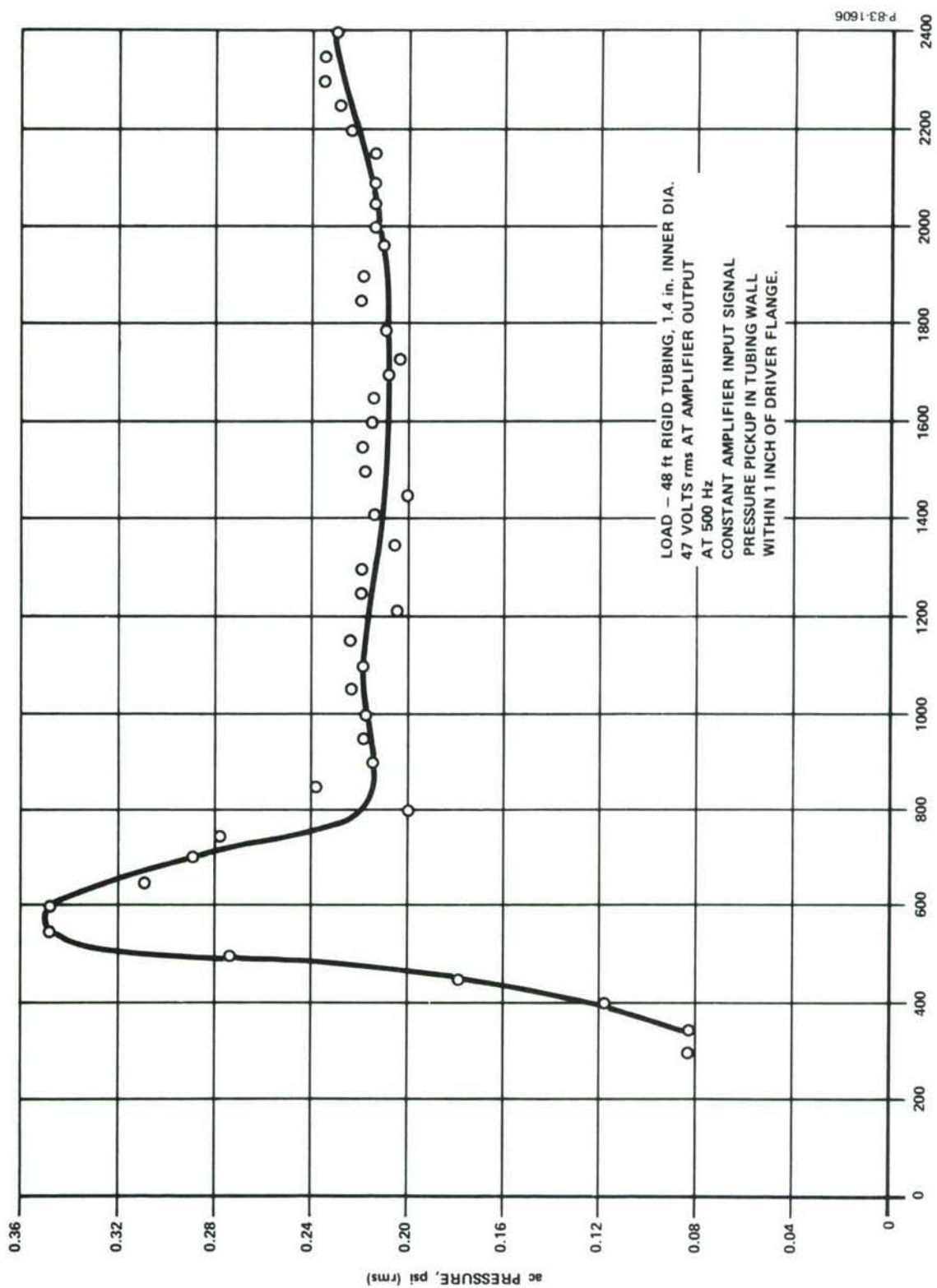


Figure 12 - Frequency Response of Loudspeaker Driver and Audio Amplifier

For the tubing used in the test,

$$A = 1.5 \text{ in}^2$$

Then from equation (3-1a),

$$P = 4.9 \text{ watts}$$

The dynamic variation of weight flow rate in the tube for small changes is given by:

$$w = \frac{gA}{c} p \quad (3-2)$$

where

$w$  = Weight flow rate, lb/sec

$g$  = 386 in/sec<sup>2</sup>

$c$  = Sound speed, in/sec

Other symbols are as used previously. Using equation (3-2) and changing from rms to single amplitude variations, the dynamic variation of weight flow in the test for the flat part of the frequency response was:

$$w = \pm 1.15 \times 10^{-2} \text{ lb/sec}$$

We should point out here that when the duct to which the electrodynamic driver is coupled is significantly different from an ideal acoustic load, then the dynamic pressure, weight flow rate and power will not generally be the values given above, even though the electronic amplifier input signal remains the same.

When the loudspeaker driver was used as a control flow source for the annular slot model, it was found that operation at the full rated electrical power of 100 watts resulted in rapid fatigue and failure of the voice coil and diaphragm assembly. This is because the annular slot model control line presents to the driver an acoustic impedance that is often far from ideal. It was found by experience that setting the drive signal for 47 volts rms at the audio amplifier output at 500 hz would give very long driver life. This corresponds to about 45 watts electrical power.

### 3.2 PIEZOELECTRIC VALVE

The piezoelectric valve concept is illustrated in Figure 13. Here, bars made of piezoelectric ceramic layers are cantilevered from supports. Voltage across the individual layers causes the bars to bend, thus increasing or decreasing the clearance between the free ends of the bars and the nozzle faces. The region in which the bars are located is pressurized, and bars' bending causes modulation of the gas flow through the nozzle passages.

The piezoelectric valve approach has the advantage of high frequency response capability with very little bulk. A disadvantage is that the valve constitutes a primarily capacitive electrical load, and draws high current at high frequencies. Although an inductance could be used to compensate for the capacitance around a given frequency, this is not consistent with a broad frequency band mode of operation.

A preliminary design investigation was conducted on the piezoelectric valve. Piezoelectric laminate bars were specified as follows:

material	lead zirconate titanate
overall dimensions	1.15 in. long by 0.317 in. wide by 0.084 in. thick
number of layers	six

The bars were constructed with thin metallic layers between the piezoelectric ceramic layers. The metallic layers extended beyond one end of the bar. Also, the exterior surface of each of the two exterior piezoceramic layers was plated with conducting material. Electrical connections can be made to the metallic layer extensions and the two plated exterior surfaces. For the module shown in Figure 13, the following parameters apply:

cantilevered length of bar beyond support	0.75 inch
maximum rated voltage magnitude between layers	210 volts
maximum deflection at tip of bar (calculated)	$\pm 7 \times 10^{-4}$ inches
natural frequency (calculated)	2900 hz
dynamic variation of nitrogen flow from valve module with 100 psia supply pressure (calculated)	$\pm 1.6 \times 10^{-3}$ lb/sec
electrical capacitance of valve module below resonant frequency (calculated)	0.25 microfarad



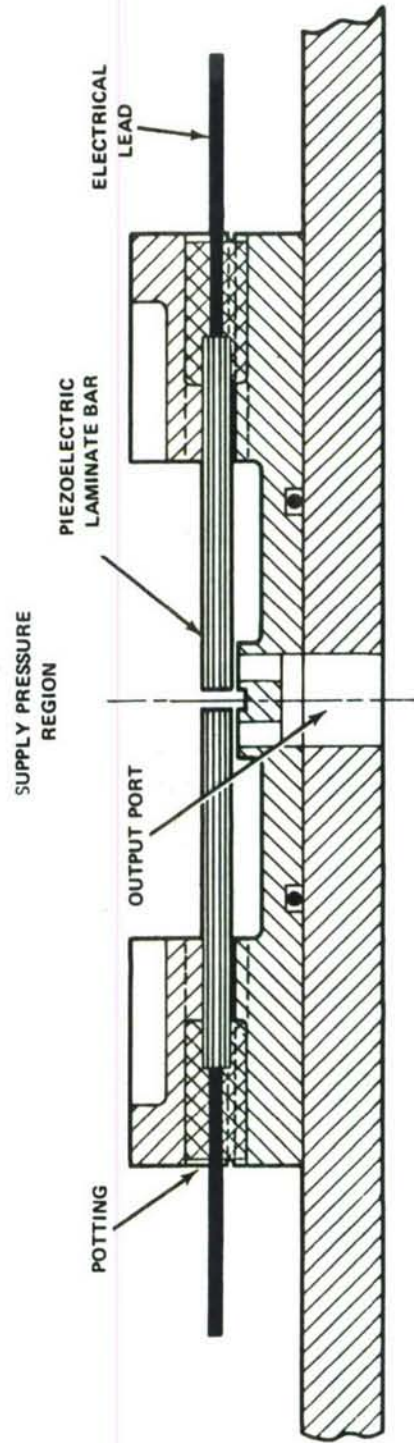
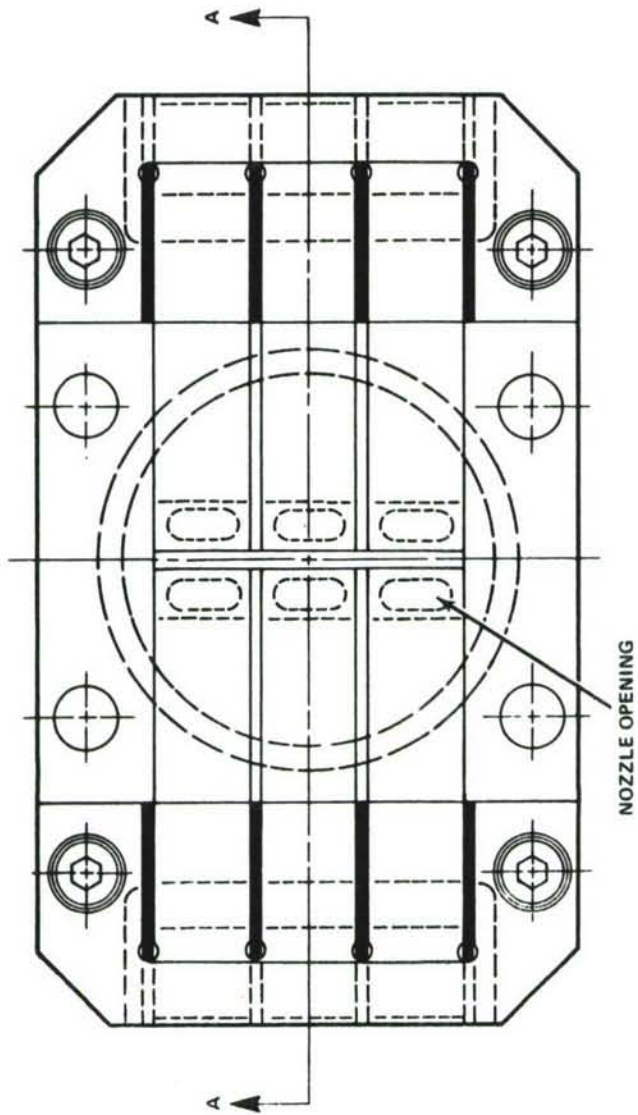


Figure 13 - Piezoelectric Valve Module

The results of the design study showed that five piezoelectric valve modules driven in parallel could be used advantageously. Each module would then drive a single-receiver fluidic amplifier of the conventional planar geometry. The outputs of the five fluidic amplifiers would then be coupled in parallel to the control line leading to the annular slot amplifier model. Such a combination of valve modules and planar amplifiers could be fabricated in a compact and convenient package.

Operation of the five valve modules at the upper end of the frequency range, 2000 hz, would require a peak a.c. current of 4.0 amperes under maximum output conditions. The peak a.c. voltage would be 210 volts, 90 degrees out of phase with the current. Electronic amplifiers to provide such an electrical drive signal are commercially available, although they are rather bulky and costly.

A quantity of the piezoelectric ceramic laminate bars was ordered from a manufacturer preparatory to fabricating the valve modules. However, the bars proved to be very difficult to manufacture. Only a small number were produced over an extended period of time. Because of these manufacturing difficulties, and also because of the electric drive complications, the piezoelectric valve approach for the control flow source was dropped. Instead, the electrodynamic loudspeaker driver approach was adopted.

### 3.3 CONTROL FLOW SOURCE STATUS

The electrodynamic driver currently used has been a reliable and repeatable control flow source when operated at a derated power level. If the driver could be operated continuously at its full rating, the dynamic control pressure amplitude would be about 50 percent higher than at present. However, the present level is sufficiently high to make meaningful experimental measurements. For an operational sound generator, a higher power control flow source would be desirable.

Another limitation of the current electrodynamic driver is its frequency range. Although its frequency response is not flat below 800 hz, it may be possible to compensate the electronic drive circuit to yield a frequency response flat down to 300 hz, still maintaining a significant power level.

By using other types of electrodynamic drivers, the frequency response could possibly be extended down to the desired 20 hz. However, it may be necessary to utilize two different control flow sources to cover the entire frequency range of 20 to 200 hz. One would be for the low frequencies, and the other for the middle and high frequencies. An electronic crossover network would also be necessary.



## SECTION 4

### GENERATOR DYNAMICS

#### 4.1 GENERAL

In analyzing the dynamic performance of the fluidic sound generator, several quantities must be examined. These include the fluidic amplifier input or control port impedance, the output or receiver impedance, the gain, and the coupling by which the amplifier load impedance effects the input impedance. These quantities are to be evaluated at the a.c. frequencies of interest, in contrast to low-frequency, quasi-steady state conditions. If the generator is to consist of more than one amplifier stage, interstage coupling approaches must be examined also.

A fundamental consideration in the analysis and design of the sound generator is that the dimensions of the fluidic amplifiers can be comparable to the wavelength of sound at the a.c. frequencies of interest. This appears to be unavoidable if the acoustic power capability of an amplifier is to be of the order of hundreds of watts or higher, and if the supply pressures available are of the order of 10 to 20 psig. Therefore, in analysis, design and evaluation of experimental results it was necessary to include possible distributed parameter or long line effects.

The purpose of the analysis which follows is twofold; first, to gain an insight as to the expected behavior of the amplifier stage, and second, to identify those parameters which could be manipulated to improve the performance once the stage is built. Because the amplifier form is new (annular slot configuration) it was not possible to provide an analysis prior to building the stage; rather the stage was built, and the analysis was used to interpret the data and to provide for redesign where possible.

Measured static characteristic curves for the stage indicated that the amplifier had an inherent regenerative feedback mechanism which gave very high stage gains (Section 4.2.1). This discovery would have negated any previous analysis which might have been undertaken.

With the static data at hand, an equivalent circuit for the amplifier stage was generated, as shown in Figure 14, and theoretical computations were then carried out to derive the stage input admittance and output admittance, as presented in Figure 17. Knowing these admittances, it was possible to make predictions as to the dynamic behavior of stage when long control and receiver ducts were attached to the stage. (These long connections could not be avoided, because transformer connections were necessary to achieve the best possible degree of impedance matching between stages.)

One very important conclusion to be drawn from Figure 17, is that for the amplifier geometry chosen the inlet control duct could not be

properly terminated to avoid reflection. From this, the design technique which had to be pursued was to try and match the output impedance of the electrodynamic driver to the input end of the control line duct so as to avoid a second reflection and thus establish a flat frequency response at the exit of the control line duct. This is treated in Section 4.6, and the result is expressed by equation (4-36). Since the output impedance of the driver was known to be higher than the characteristic impedance of the duct (Figure 19), it would appear to be a simple matter to introduce a shunt acoustic path to lower the apparent output impedance of the driver. With this design concept in mind, experimental frequency response tests were first run, as discussed in Section 4.3. In these tests, there was no shunt acoustic path at the driver end of the control line duct. A flat frequency response was not obtained, as was expected. Therefore, the shunt path was tried next in order to obtain a flat frequency response. This technique did not produce the required result, which led to the conclusion that the feedback mechanism in the amplifier stage must be distributed, (occurring because of a long feedback path). Additional frequency response measurements were made to establish the experimental input admittance to the stage and to identify the frequency response of the stage with its inherent feedback mechanism but not including the reflection effects in the control line duct. This is discussed in Section 4.4.

Additional analysis was then undertaken to see if a better transformer configuration could be found to connect the driver and stage control port to further flatten the frequency response. Section 4.7 treats this approach. The transformer in use was found to be near optimum, so no further design changes seemed possible short of a major redesign of the stage (Figure 28). The design and fabrication of the second-stage amplifier was then undertaken, as described in Section 5.

## 4.2 AMPLIFIER GAIN

### 4.2.1 Static Gain

From static gain measurements, it was concluded that the annular slot amplifier possibly has an inherent regenerative feedback loop, since the measured gains were higher than could be expected from conventional planar jet-on-jet amplifier practice. Static output impedance curves confirmed the presence of regenerative feedback. In regions of this data, the amplifier actually showed negative output impedance. A negative output impedance could only be substantiated on the basis of a relatively strong positive feedback mechanism.

The presence of a feedback mechanism, either positive or negative, will influence the input and output impedances of the amplifier, as will be shown below. Such effects must be recognized in making connections to the amplifier stage.

Where the feedback mechanism takes place via a signal path which is as long as even a quarter wavelength, impedances and amplifier stage gains can be expected to be frequency-variant.

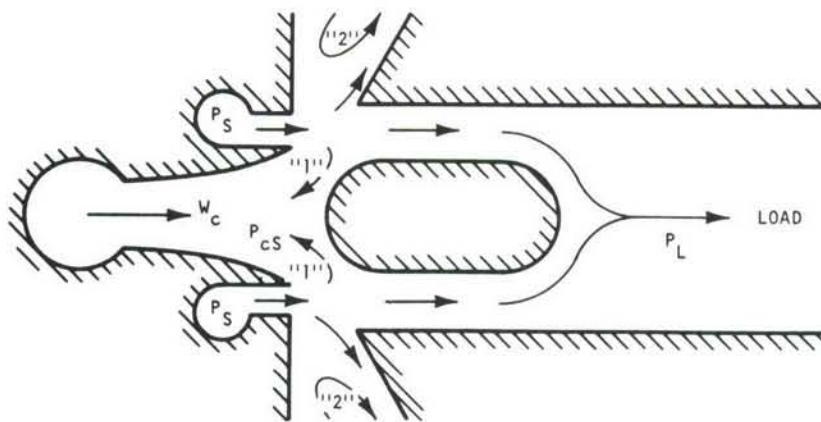


#### 4.2.2 A Lumped Parameter Small Signal Steady State Analysis

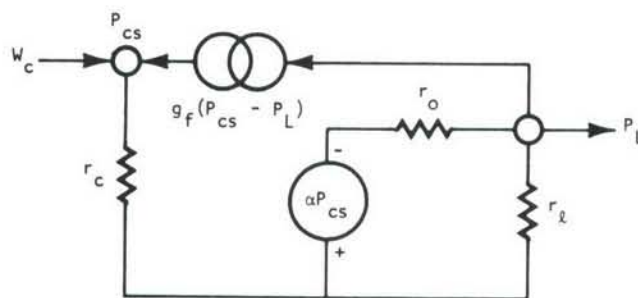
In an effort to identify the effects of regenerative feedback and to provide a starting point for further dynamic analysis, a simple static lumped parameter analysis was first carried out for the annular slot amplifier. The regenerative feedback mechanism must be identified or at least hypothesized if a satisfactory analytical model is to be found. There are two possible locations for this feedback mechanism. One is inside the annular power jet and is set up because of spilled flow at the receiver which flows back into the control port. This source of feedback is denoted by the flow arrows marked "1" in Figure 14. This feedback appears at first to be negative, as the spilled flow would tend to force the power jet out thus reducing the load pressure and in turn the amount of fluid returned to the control passage. However, in referring to the measured control port characteristics, Figure 11, a contradiction is noted as to whether the feedback is positive or negative. For values of  $P_{CS}$  less than 0.6 psig the input curves have positive slopes and magnitude increases in  $P_L$  cause increases in  $P_{CS}$  for a given  $W_C$ . However, at pressures above  $P_{CS} = 0.6$  psig the characteristic curves have negative slopes and magnitude decreases in  $P_L$  cause increases in  $P_{CS}$  for a given  $W_C$ . It can only be concluded that the sensitivity of the change in spilled flow "1" with changes in  $P_{CS}$  is highly nonlinear, and that above  $P_{CS} = 0.6$  psig, the jet flow geometry is such that regenerative feedback takes place. Feedback is here interpreted as the change in  $P_{CS}$  caused by a  $P_L$  change, for constant values of control flow,  $W_C$ .

The second mechanism of regenerative feedback can be identified by considering the effect of the spilled flow passing out the vent of the amplifier. It is known that vent flow sets up a vortex flow field in the vent region as described by the flow arrows "2" in Figure 14. The vent flow pattern acts as an aspiration pump in the vicinity of the power jet, reducing the pressure around the outside of the jet and causing it to move outward. Outward movement of the power jet increases the vent flow aspiration pumping which, in turn, further increases the outward motion of the jet. This is, of course, a regenerative mechanism. For purposes of modeling, a reduced pressure at the outside of the power jet is equivalent to an increase in pressure,  $P_{CS}$ , internal to the power jet. Making use of this substitution yields a very simple equivalent circuit for the amplifier as shown in Figure 14(b) which is general in that the circuit will account for either or both cases cited as the cause of regenerative feedback.

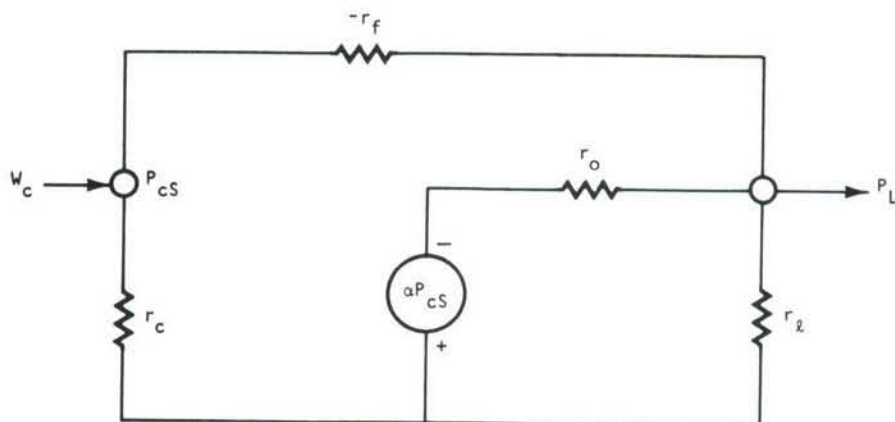
To represent the feedback mechanism, an equivalent flow source,  $g_f (P_{CS} - P_L)$ , is postulated. A more general flow source would utilize different coefficients on  $P_{CS}$  and  $P_L$ , but for purposes of simplicity a single coefficient,  $g_f$ , is used. As noted in Figure 14(b), that flow which is removed from the load pressure node,  $P_L$ , is in turn added to the  $P_{CS}$  node thus identifying a feedback path. The flow passes through a control port resistance,  $r_c$ , thus causing a change in  $P_{CS}$  as the feedback flow changes. This control port resistance,  $r_c$ , is a coupling resistance which couples the effects of the feedback flow and control flow



(a) PHYSICAL MODEL



(b) EQUIVALENT CIRCUIT



(c) CIRCUIT WITH NEGATIVE FEEDBACK RESISTANCE  
REPLACING FLOW SOURCE

Figure 14 - Lumped Parameter Equivalent Circuit

P-10-1764



to set up the control pressure  $P_{CS}$ . This simple coupling may not be entirely accurate, but the circuit analysis is simple and certainly feedback effects can be examined on a qualitative basis.

The feedback flow source can be replaced by a negative resistance between nodes  $P_{CS}$  and  $P_L$  as shown in Figure 14(c).<sup>\*</sup> To prove the substitution, the flow in the feedback branch is equated to the spilled flow source; i.e.

$$\frac{(P_{CS} - P_L)}{-r_f} = g_f (P_{CS} - P_L)$$

If  $r_f$  were positive the flow directions in the feedback path of Figure 14(c) would be opposite to that of the feedback flow source in Figure 14(b). Of course, a negative resistance,  $r_f$ , is consistent with regenerative feedback. The pressure source,  $\alpha P_{CS}$ , used in Figures 14(b) and 14(c) represents the stagnation pressure change which would be observed if the load port were blocked. The load receiver of the amplifier will cause some loss and therefore its impedance is described as  $r_o$ . The load resistance is given as  $r_\ell$ .

Observations of the control line self-bias pressure show that as load pressure is increased - through decrease of the external load resistance,  $r_\ell$  - the self-bias pressure decreases. This is indicated in the right-hand portion of the plot in Figure 11. The circuit in Figure 14(c) provides this relationship. The circuit is converted for nodal analysis in Figure 15. The pressure source generator,  $\alpha P_{CS}$ , becomes a flow source  $g_o \alpha P_{CS}$  and resistances are now shown as their reciprocal conductances.

A flow source  $W'_L$ , not normally present, has been added at the load terminal. Its sole use is in deriving the output impedance of the amplifier. We will make the substitution,  $g_L = g_o + g_\ell$ . The flow equations are then given by the matrix set, equations (4-1).

$$\begin{vmatrix} W_C \\ W'_L \end{vmatrix} = \begin{vmatrix} g_C - g_f & g_f \\ g_f + \alpha g_o & g_L - g_f \end{vmatrix} \begin{vmatrix} P_{CS} \\ P_L \end{vmatrix} \quad (4-1)$$

It should be noted that in Figures 14 and 15, and in equation (4-1), all flows and pressures are taken to be small changes about quiescent values in the actual fluidic amplifier.

<sup>\*</sup>For a further treatment of this form of fluidic circuit analysis, see Reference 2, pp. 27-35.



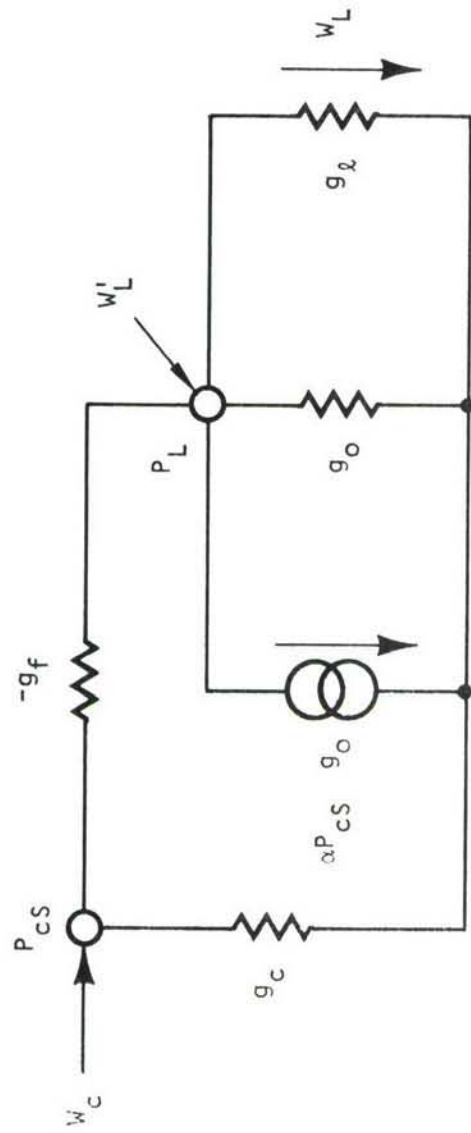


Figure 15 - Equivalent Circuit (Nodal Analysis)

Solving the set for  $P_{cs}/W_c$  and inverting, the input admittance is given by equation (4-2).

$$\frac{W_c}{P_{cs}} = Y_c = g_c - \frac{\alpha g_o g_f + g_f g_L}{g_L - g_f} \quad (4-2)$$

It will be noted that  $Y_c$  can be negative, zero, or positive depending on the magnitudes of  $g_L$  and  $g_f$ . Before determining possible ranges of values for these parameters, the matrix set (4-1) is solved for the expressions  $P_L/P_{cs}$  and  $W'_L/P_L$ . These are:

$$\frac{P_L}{P_{cs}} = - \frac{(g_f + \alpha g_o)}{g_L - g_f} \quad \text{for } W'_L = 0 \quad (4-3)$$

$$\frac{W'_L}{P_L} = g_o + g_\ell - \frac{g_f (g_c + \alpha g_o)}{g_c - g_f} \quad \text{for } W_c = 0 \quad (4-4)$$

We know that changes in  $P_L$  are opposite in sign to changes in  $P_{cs}$ . Therefore, from the pressure gain expression, equation (4-3), we know that

$$g_L = g_o + g_\ell > g_f.$$

Having noted this result, we see from equation (4-2) for the input admittance that

$$Y_c < g_c$$

In terms of the actual load flow,  $W_L$ , the output admittance is found from equation (4-4) by letting  $g_\ell = 0$ . Also, we must multiply the left-hand side of equation (4-4) by  $(-1)$  since the slope of the output characteristic curves is by definition the negative of the output admittance.

Static measurements of the load or output characteristics of the amplifier model were shown in Figure 9. Thus,

$$Y_{out} = - \frac{W_L}{P_L} = g_o - \frac{g_f (g_c + \alpha g_o)}{g_c - g_f} \quad (4-4a)$$

It is advantageous to operate in the region where the characteristic curves have positive slope, i.e., in the negative output admittance region, in order to achieve high gain. In this region  $W_L$  increases as  $P_L$  increases, or,

$$Y_{out} < 0.$$

Therefore, in equation (4-4a),

$$g_c > g_f$$

Also,

$$\frac{g_f (g_c + \alpha g_o)}{g_c - g_f} > g_o \quad (4-5)$$

It should be remembered that a very simple equivalent circuit has been selected, and also that in the real amplifier all of the conductances are nonlinear and dependent upon quiescent operating levels.

#### 4.2.3 Control Port Input Conductance ( $g_c$ )

The input conductance of the control port can be estimated on the basis of the normalized input conductance of other jet-type fluidic amplifiers. The annular slot amplifier can be visualized as one-half of a planar amplifier rotated through 360 degrees to sweep out a three-dimensional geometry. A representative planar amplifier, Bendix model 10PA19A, was tested to determine its control port conductance. This amplifier has two right and two left control ports. For the purposes of the tests, the control ports on either side were connected in parallel, and the amplifier was operated as though it had just one



right and one left control port. Figure 16 shows the test data. The amplifier was operated single-ended, with the various ports in the conditions noted on Figure 16, to match the condition of the annular slot amplifier. In a manner similar to that of the annular slot amplifier, this test amplifier also self-biased, as shown by the zero control flow intercepts along the control pressure axis in Figure 16.

Taking slopes at these intercepts, the amplifier control port conductances are found to be inversely proportional to the square root of the gage supply pressures used. Also, compressible flow theory states that flows are proportional to orifice areas. Therefore, the input conductance is related to these parameters as given by,

$$g_c = \frac{\Delta W_c}{\Delta P_{cs}} \sim \frac{A_c}{\sqrt{P_s}}$$

where

$A_c$  = Control port area, in<sup>2</sup>

$P_s$  = Supply pressure, psig

A normalized form of the input conductance may be obtained by multiplying the numerator and the denominator of the above expression by the left and right sides respectively of the following expression for supply nozzle flow:

$$W_s \sim A_s \sqrt{P_s}$$

That is:

$$g_c = \frac{\Delta W_c}{\Delta P_{cs}} \sim \frac{A_c}{A_s} \frac{W_s}{P_s}$$

where

$W_s$  = Supply flow, lb/sec.

$A_s$  = Power jet nozzle area, in<sup>2</sup>

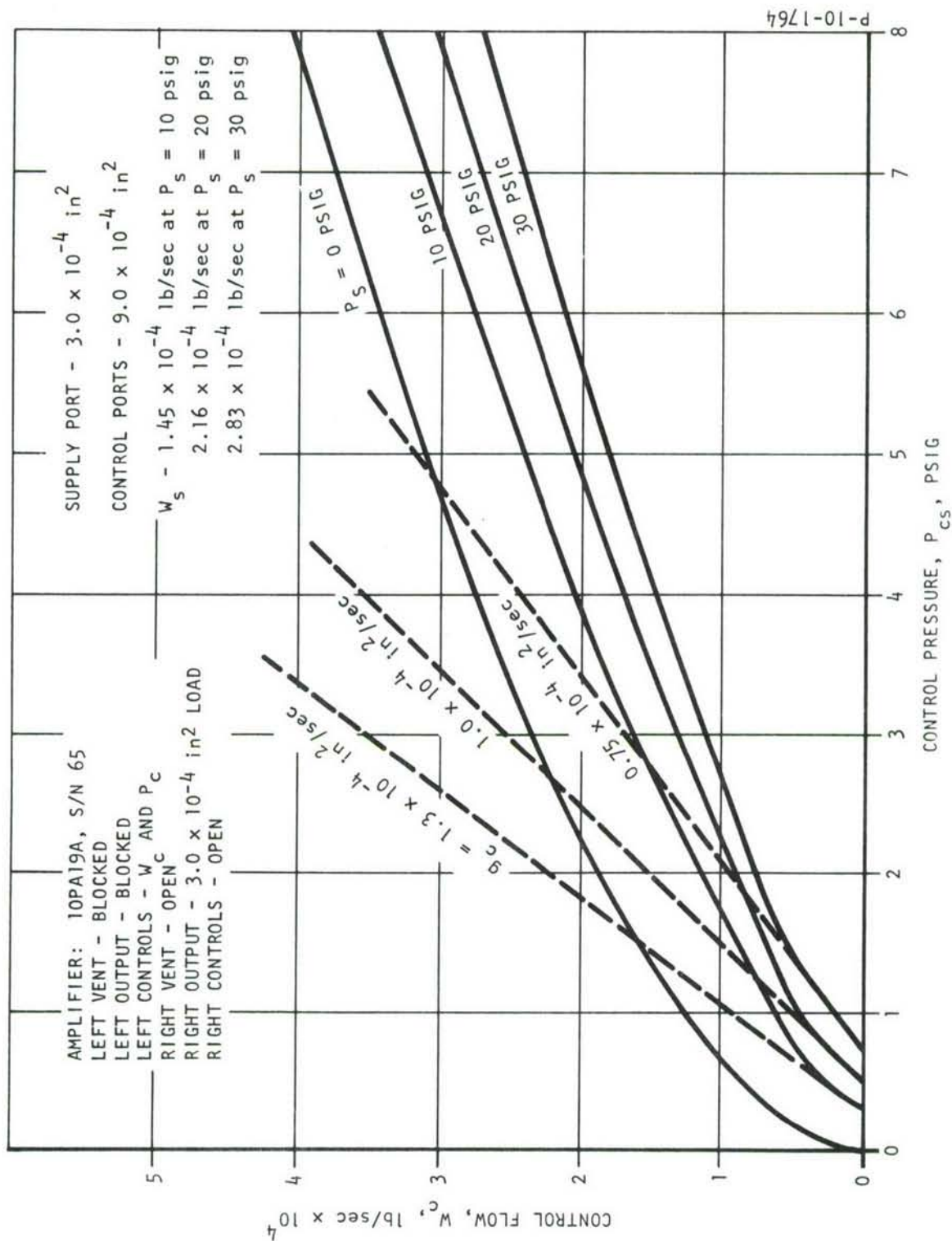


Figure 16 - Input Characteristic Curves for Planar Proportional Jet Amplifier in Single-Ended Configuration

Here, we have assumed that the flow through the supply nozzle is in the subsonic regime, which is the case for our annular slot amplifier.

The expression for input conductance that we will use is obtained by rewriting the one above:

$$g_c = \frac{g_{nc} A_c W_s}{A_s P_s} \quad (4-6)$$

where

$g_{nc}$  = Normalized control port conductance, dimensionless

The normalized conductance from the data of Figure 16 is approximately 3.0. For the annular slot amplifier model:

$$A_c \approx 3 \text{ in}^2$$

$$A_s \approx 0.6 \text{ in}^2$$

$$W_s \approx 0.315 \text{ lb/sec}$$

$$P_s = 10 \text{ psig}$$

Using equation (4-6),

$$g_c = \frac{(3) (3) (.315)}{(0.6) (10)} = 0.47 \text{ in}^2/\text{sec} \quad (4-7)$$

At this point, we will note that the annular slot amplifier has an unusually large vent region as compared with conventional fluid amplifiers. To account for this, we will arbitrarily double the value of  $g_{nc}$ . It will be seen later that experimental data on the annular slot model justifies the larger value of  $g_{nc}$ . Thus, we will take,

$$g_c = 1 \text{ in}^2/\text{sec} \quad (4-8)$$



#### 4.2.4 Receiver Output Conductance ( $g_o$ )

The receiver output conductance,  $g_o$ , can be found by assuming the receiver acts as an orifice having an area equal to the entrance area of the receiver. The small signal conductance of an orifice can be estimated\* by taking total differentials of the Fliegner orifice flow formula\* given by equation (4-9).

$$W = \frac{2 c_1 c_d A \sqrt{P_d} \sqrt{P_u - P_d}}{\sqrt{T}} \quad (4-9)$$

where:

$c_1$  = Gas flow constant,  $^{\circ}R^{1/2}/\text{sec}$

$c_d$  = Discharge coefficient, dimensionless

$A$  = Orifice area,  $\text{in}^2$

$P_d$  = Downstream pressure, psia

$P_u$  = Upstream pressure, psia

$T$  = Gas temperature,  $^{\circ}R$

Linearizing equation (4-9),

$$\Delta W = \frac{W_o (\Delta P_u - \Delta P_d)}{2 (P_{uo} - P_{do})} + \frac{W_o (\Delta P_d)}{2 (P_{do})} \quad (4-10)$$

---

\*

Reference 3, p. 302.

where subscript zeros denote quiescent values of the variables.

The term  $W_o \Delta P_d / 2 P_{do}$  in equation (4-10) is small compared to the first term on the right-hand side of equation (4-10), as  $P_{do} \gg P_{uo} - P_{do}$ . Neglecting this term, the conductance of the orifice or amplifier receiver is given as:\*

$$g_o = \frac{\Delta W}{\Delta (P_u - P_d)} = \frac{W_o}{2 (P_{uo} - P_{do})} \quad (4-11)$$

For the amplifier model,  $P_{uo}$  is the measured upstream stagnation pressure taken when the receiver is blocked. Measurements of  $P_{uo}$  gave approximately 5 psig (20 psia). For the amplifier load used,  $P_{do}$  is approximately 3 psig (18 psia). The flow  $W_o$  was measured at about 0.08 lb/sec. Using equation (4-11),  $g_o$  is then:

$$g_o = \frac{0.08}{2 (2)} = 0.02 \text{ in}^2/\text{sec} \quad (4-12)$$

#### 4.2.5 Load Conductance ( $g_\ell$ )

For purposes of testing the annular slot amplifier model to high frequencies, a 50-foot concentric tube assembly was used to load the amplifier stage. This tube assembly was mounted to form an extension of the amplifier's annular receiver passage. Sound waves making the 100 foot round trip from the receiver to the end of the duct and back to the receiver were attenuated significantly. The acoustic admittance of such a duct, sufficiently long to prevent reflections, is given by equation (4-13).

$$g_\ell = \frac{gA}{c} \quad (4-13)$$

where:

$$g = 386 \text{ in}/\text{sec}^2$$

$c$  = Speed of sound, in/sec

$A$  = Duct area, in<sup>2</sup>

\*

Reference 2, pp.27-35

For nitrogen or air at normal temperatures,

$$g_{\ell} \approx \frac{A}{34} \quad (4-13a)$$

The receiver area and hence load area is approximately 1.06 in<sup>2</sup>. Therefore:

$$g_{\ell} = \frac{1.06}{34} = 0.0312 \frac{\text{in}^2}{\text{sec}} \quad (4-14)$$

#### 4.2.6 Amplification Factor ( $\alpha$ )

Because of the unique design of the amplifier, an annular slot source and receiver and a control port whose width is much more than that of the power jet port, it was difficult to estimate accurately the amplification factor  $\alpha$ . Initial static tests showed pressure gains, with the amplifier loaded, of nominally 15, and it was thought that  $\alpha$  must then be quite large, perhaps 20. However, the discovery of the regenerative feedback changed this opinion and subsequently  $\alpha$  is known to be smaller, in the range of 6 to 10. It must be remembered that the  $\alpha$  under discussion here is defined by the simplified equivalent circuits of Figures 14 and 15. The value for  $\alpha$  determined from these circuits is likely to be only loosely related to the actual blocked pressure gain of the amplifier. However, we are evaluating only the trends in parameters and so other amplifier parameters were computed based on,

$$\frac{P_L}{P_{cs}} = -15$$

under low-frequency or steady state conditions.

#### 4.2.7 Determination of Amplifier Parameters

Solving equation (4-3) for  $g_f$  in terms of  $\alpha$ :

$$g_f = 0.048 - 0.00125\alpha \quad (4-15)$$



From equation (4-4a), the output admittance is given by:

$$Y_{out} = g_o - \frac{g_f (g_c + \alpha g_o)}{g_c - g_f} \quad (4-16)$$

Using parameter values obtained previously,

$$Y_{out} = 0.02 - \frac{g_f (1 + 0.02\alpha)}{1 - g_f} \quad (4-17)$$

Values of  $g_f$  and  $y_o$  are plotted in Figure 17 for various values of  $\alpha$ . The input admittance to the amplifier is given by equation (4-2):

$$Y_c = g_c - \frac{\alpha g_o g_f + g_f g_L}{g_L - g_f} \quad (4-18)$$

Again using parameter values obtained previously,

$$Y_c = 1 - \frac{g_f (0.02\alpha + 0.0512)}{0.0512 - g_f} \quad (4-18a)$$

Values of  $Y_c$  are also plotted in Figure 17 for various values of  $\alpha$ .

From the calculations results presented in Figure 17, it is noted that the output admittance of the amplifier is negative with a nominal value of  $-0.025 \text{ in}^2/\text{sec}$ . This compares with values from the static measurements of Figure 9 which are in the neighborhood of  $-0.03 \text{ in}^2/\text{sec}$ .

Since the quantity  $g_c$  is included in equation (4-16) for the output admittance, and since the calculated and the experimentally derived values of output admittance are reasonably close, we can conclude that the value

$$g_c = 1 \text{ in}^2/\text{sec}$$

given by equation (4-8) must be a good approximation.

We see from equation (4-16) that when  $g_c$  is relatively large compared to  $\alpha g_o$  and  $g_f$ , and when  $g_o$  and  $g_f$  are of the same order of magnitude, then  $Y_{out}$  is influenced strongly by  $g_f$ . That is the present case.

The input admittance,  $Y_c$ , lies between  $1/3$  and  $1/2$  of the input conductance  $g_c$ .

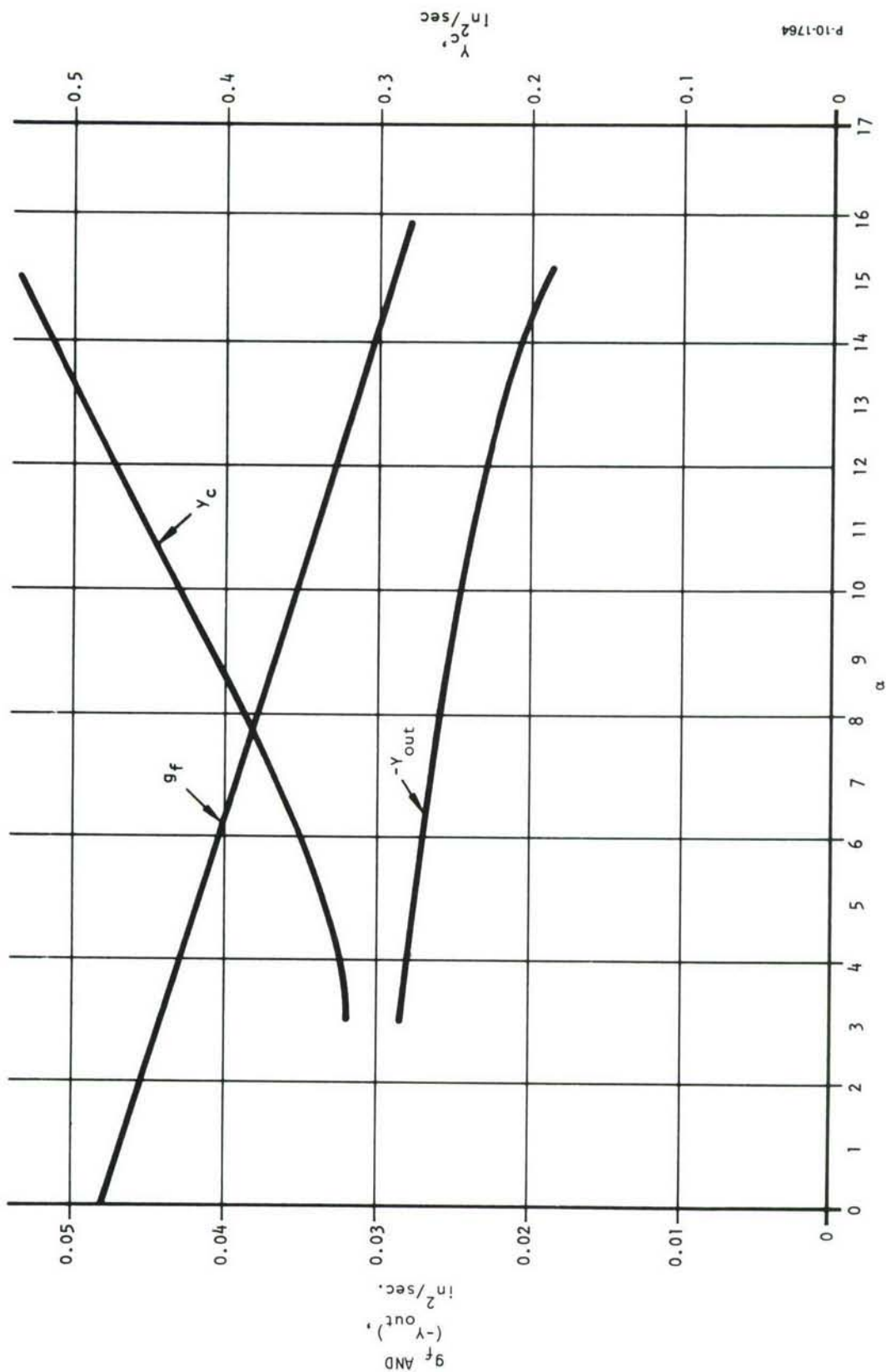


Figure 17 - Plot of Equivalent Circuit Parameters

Taking the area of control port, approximately 3 in<sup>2</sup>, the ideal acoustic admittance of the duct leading to the control port is, by equation (4-13a), approximately 3/34 or 0.09 in<sup>2</sup>/sec. Figure 17 shows the control port admittance,  $Y_c$ , is 3 to 5 times greater than this ideal acoustic admittance value. Therefore, an acoustic mismatch at the control port is indicated. Since it is not possible to design the amplifier so the distance from the driver to the control port is less than 1/10 of a wavelength at the highest operating frequencies, reflections and standing wave effects in the control line are to be expected.

#### 4.3 INITIAL FREQUENCY RESPONSE TESTS

The analysis given in the previous section was conducted with the view towards obtaining insight into trends of behavior of the annular slot amplifier model. Frequency response tests were conducted to see if reflections were present at the input and also to evaluate the overall response of the amplifier.

In these tests, the electrodynamic driver control flow source was driven by an electronic audio amplifier, as described in Section 3. The input signal to the electronic audio amplifier was a constant amplitude, variable frequency sine wave signal. The electronic amplifier gain was adjusted to give 47 volts rms at the electronic amplifier output at 500 hz. This was the standard frequency response procedure used in this program.

As described previously, the frequency response tests were run with a 50-foot concentric tube load attached to the outlet of the fluidic amplifier to avoid reflections in the fluidic output load circuit. Input and output dynamic pressure data were then taken using dynamic pressure pickups located as near to the control port and receiver exit of the fluidic amplifier as possible.

A typical installation of a pressure pickup is shown in Figure 18. The hole in the brass fitting is 0.090 inch in diameter. The fluid resistance and the volume under compression in this installation are sufficiently small so that dynamic errors in pressure measurements are negligibly small over the frequency range of interest. This type of pressure pickup installation has proven to be very convenient for measurements in thin-walled ducts.

The electrical signals from the piezoelectric pressure pickups were amplified by charge amplifiers and the output signals from the charge amplifiers were then recorded. Most of the frequency response data in this report was taken using a tracking filter between the charge amplifier output and the input terminal of the recorder. This served to suppress noise and harmonics in the measured quantities. A Princeton Applied Research lock-in amplifier Model No. HR-8 with a type-A preamplifier was used for this function.



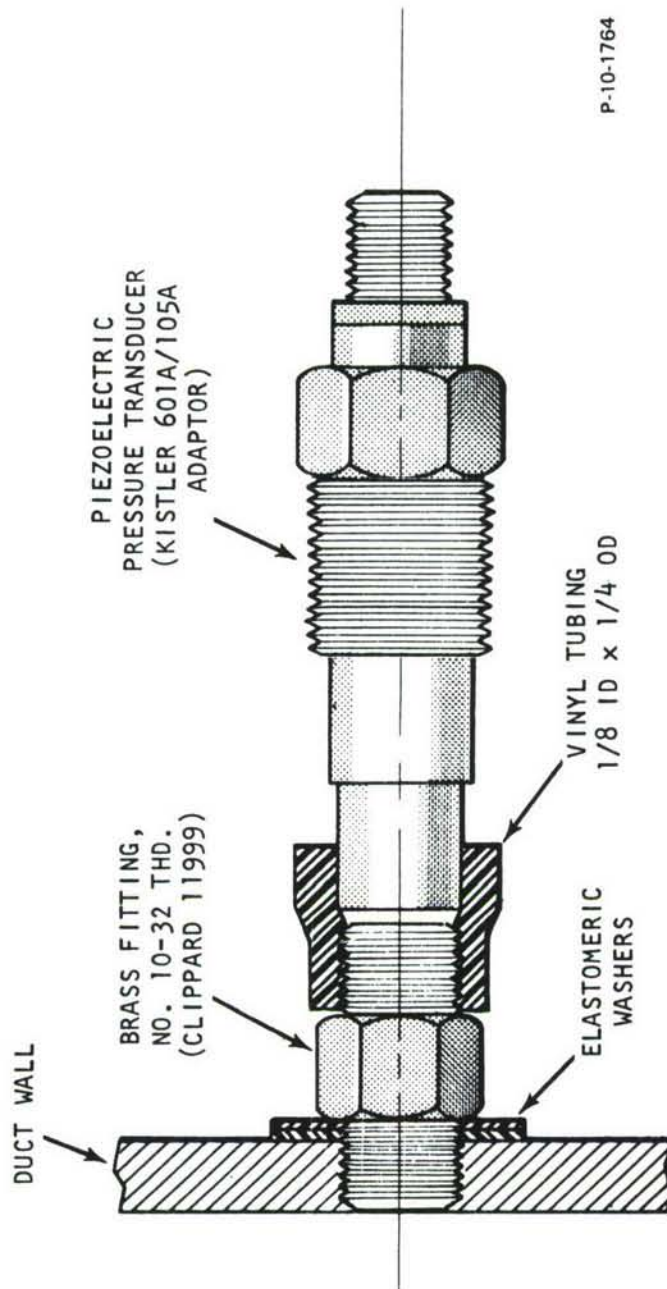


Figure 18 - Pressure Transducer Installation

For all test results given in this report, the power jet supply pressure was 10 psig unless otherwise specified.

If the conclusions drawn from the simplified analysis in the previous section were even close to correct, it was expected that the input frequency response curves would show reflections and a standing wave of a.c. pressure amplitude should be evident. The reason for the reflections is, again, that the relatively long control line duct (approximately 11 inches long) acts as a transmission line which is terminated in an impedance that is approximately 1/3 of the control port acoustic characteristic impedance.

The control line duct employed with the annular slot amplifier model begins with a 0.91 in<sup>2</sup> initial area within the electrodynamic driver. The area increases gradually with distance until, after 11 inches, it is 2.99 in<sup>2</sup> at the control port. The duct is formed by sections having conical shapes. The cutoff frequency corresponding to an exponential duct shape giving the same area change in the same length is 160 hz. Therefore, we conclude that the duct acts as a reasonably good acoustic connector down to the lowest driver frequency, 300 hz.

An acoustic connector of this kind transforms acoustic impedances\*. To show the effect of the transformation let,

$Z'_r$  = Impedance evaluated at the large or control port end of the duct, sec/in<sup>2</sup>

$A_r$  = Area at the large or control port end of the duct, in<sup>2</sup>

$A_s$  = Area at the small or input end of the duct, in<sup>2</sup>

$R = A_r/A_s$ , dimensionless

Then, the effect of  $Z'_r$  as felt at the input end is as though the duct continued on at the constant area  $A_s$ , but was terminated in an impedance of value  $R Z'_r$ .

To illustrate the result of this transformation, let  $Z'_r$  be expressed in terms of the characteristic acoustic impedance at the control port end of the duct. Thus,

$$Z'_r = (m + j n) \frac{c}{g A_r}$$

---

\*Reference 7, pp. 112-4

where,

m = Normalized resistive component, dimensionless

n = Normalized reactive component, dimensionless

$$j = \sqrt{-1}$$

c = Sound speed, in/sec

$$g = 386 \text{ in/sec}^2$$

Then, at the input end of the duct,  $Z_r$  is seen as,

$$Z_r'' = Z_r R = (m + j n) \frac{c}{g A_s}$$

where

$$Z_r'' = \text{Transformed control port impedance, sec/in}^2$$

We note that  $Z_r''$  is given by the duct characteristic impedance evaluated at the input end, multiplied by the same normalizing factor  $(m + j n)$  as was used at the control port end.

The result can be summarized in a general form as follows. When a tapered duct has a cutoff frequency well below the operating frequency range of interest, the duct can be treated as an equivalent constant-area duct. To do so we,

- (a) Select any convenient area A as a reference area, and define a duct characteristic impedance  $Z_o$  on the basis of that area, so that

$$Z_o = \frac{c}{g A}$$

- (b) Set the termination impedance  $Z_r$  of the constant-area duct equal to the normalizing factor prevailing at the actual duct termination times  $Z_o$ . Thus,

$$\begin{aligned} Z_r &= Z_r' \frac{g A_r}{c} Z_o \\ &= Z_r' \frac{A_r}{A} \end{aligned}$$



- (c) If any generator impedance  $Z'_g$  is connected to the input end of the actual duct, set the generator impedance  $Z_g$  of the constant-area duct equal to the normalizing factor prevailing at the actual duct input times  $Z_o$ . This is an exactly similar procedure as that used for the termination impedance. Thus,

$$\begin{aligned} Z_g &= Z'_g \frac{g A_s}{c} Z_o \\ &= Z'_g \frac{A_s}{A} \end{aligned}$$

We will treat the control line duct as an equivalent constant-area duct so that we can use existing transmission line analysis techniques. The consequences of impedance mismatches can then be readily seen. The fact that the control port impedance is approximately 1/3 of the acoustic characteristic impedance causes the input impedance to the duct to vary with frequency. The duct input impedance is some 3 times the characteristic impedance at odd quarter wavelengths, and about one-third the characteristic impedance at half wavelengths. This can be shown as follows.

The input or sending end impedance of a transmission line is given by,\*

$$Z_s = Z_o \frac{Z_r + Z_o \tanh \gamma L}{Z_o + Z_r \tanh \gamma L}$$

where

$Z_s$  = Line input impedance,  $\text{sec/in}^2$

$Z_o$  = Line characteristic impedance,  $\text{sec/in}^2$

$Z_r$  = Line termination impedance,  $\text{sec/in}^2$

$\gamma$  = Propagation constant,  $\text{in}^{-1}$

$L$  = Line length, in.

---

\* Reference 4, p. 105.

The propagation constant is expressed as,

$$\gamma = \alpha_t + j \beta_t = \alpha_t + j \frac{2\pi f}{v}$$

where

$$\alpha_t = \text{Attenuation constant, in}^{-1}$$

$$\beta_t = \text{Phase constant, in}^{-1}$$

$$j = \sqrt{-1}$$

$$f = \text{Frequency, hz}$$

$$v = \text{Phase velocity of wave, in/sec}$$

For the duct dimensions and frequency range with which we are concerned, we can make the following simplifying assumptions:

$$\alpha_t \approx 0$$

$$v \approx c \text{ (ordinary speed of sound)}$$

$$\gamma \approx \frac{2\pi f}{c} = j \frac{2\pi}{\lambda}$$

where

$$\lambda = \text{Wavelength, in}$$

The duct input impedance expression then becomes,

$$Z_s = Z_o \frac{Z_r + j Z_o \tan (2\pi L/\lambda)}{Z_o + j Z_r \tan (2\pi L/\lambda)}$$

Under the same simplifying assumptions as above, the duct characteristic impedance is,

$$Z_o = \frac{c}{gA}$$

where

$c$  = Speed of sound, in/sec

$g$  = 386 in/sec<sup>2</sup>

$A$  = Duct area, in<sup>2</sup>

It will be noted that this is the reciprocal of equation (4-13), the admittance of a very long duct.

Examining the above equation for duct input impedance, we see that,

$$\text{as } \frac{L}{\lambda} \rightarrow \frac{1}{2}, 1, \frac{3}{2}, \text{ etc.},$$

$$\tan (2\pi L/\lambda) \rightarrow 0$$

Because  $Z_r \approx 1/3 Z_o$ ,

$$Z_s \rightarrow Z_r \approx \frac{1}{3} Z_o$$

Also,

$$\text{as } \frac{L}{\lambda} \rightarrow \frac{1}{4}, \frac{3}{4}, \frac{5}{4}, \text{ etc.},$$

$$\tan (2\pi L/\lambda) \rightarrow \pm \infty$$

and

$$Z_s \rightarrow Z_o^2 / Z_r \approx 9 Z_r \approx 3 Z_o$$

The effect of this variable impedance presented to the control line driver is to cause mismatching and therefore reduction of the power which can be introduced into the control line duct. The magnitude of the power input at the odd quarter wavelength and the half wavelength frequencies depends upon the output impedance of the driver.

The output impedance of the driver, that is, the acoustical impedance looking upstream into the exit port of the driver, is usually considerably larger than the characteristic impedance for the exit port because of inherent losses in the driver. Assuming a driver efficiency of 10 percent, i.e., the ratio of acoustic power out to input electric power, then the output impedance of the driver can be shown to be equal to  $9 Z_o$ . Consider the Thévenin equivalent circuit for the driver and load as shown in Figure 19. Here,



$E$  = rms open-circuit pressure of equivalent generator, psi

The power delivered to the ideal or design load is,

$$P_1 = \frac{1}{100} \frac{E^2}{Z_o}$$

The total power converted or dissipated in the circuit is,

$$P_2 = \frac{1}{10} \frac{E^2}{Z_o}$$

The efficiency is,

$$\left( P_1 / P_2 \right) \times 100 = 10 \text{ percent}$$

Thus, a driver output impedance of  $9 Z_o$  is consistent with a driver efficiency of 10 percent. This efficiency value is considered representative of a driver with a proper acoustic load.

With a driver output impedance of  $9 Z_o$ , and a control line duct termination impedance of  $1/3 Z_o$ , we conclude that the power delivered to the duct at half wavelength frequencies is very low, since,

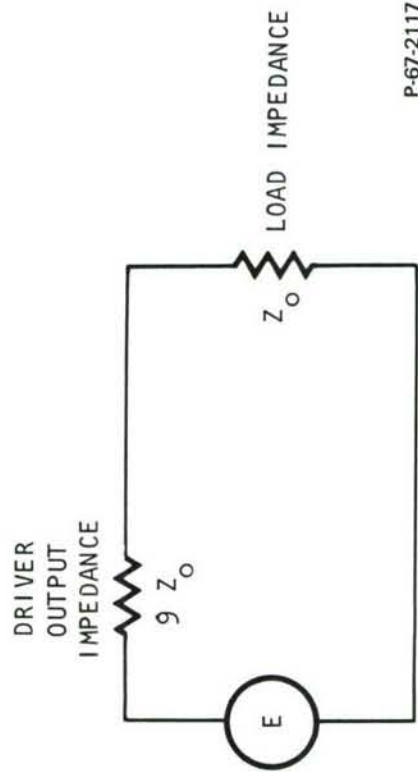
$$Z_s \approx 1/3 Z_o$$

and this is in series with  $Z_g = 9 Z_o$ .

Conversely, at odd quarter wavelength frequencies the power delivered to the duct is substantially larger, since,

$$Z_s \approx 3 Z_o$$

and is in series with, again,  $Z_g = 9 Z_o$ .



P-67-2117

Figure 19 - Thevenin Equivalent Circuit for 10 Percent Efficient Driver  
With Design Load Value

For the control duct length of 11 inches, the duct operates at multiple half wavelengths for frequencies of approximately 600, 1200, 1800 etc., hz. A valley or low pressure amplitude response should be expected at the output of the amplifier at these frequencies.

The input or control line response test results are shown in Figure 20(a) and the output response results are shown in Figure 20(b). During the test runs, the steady state control line and output pressures,  $P_{CS}$  and  $P_L$ , ranged from 0.75 to 0.76 psig and from 2.48 to 2.58 psig respectively. A tracking filter amplifier was used to obtain the frequency response with noise and harmonic distortion removed. As noted from the output data, a definite valley in pressure response occurs at 1200 hz. but no similar valley is evident at 600 hz. There is a valley at 600 hz. but the value of the pressure amplitude is considerably higher than at 1200 hz. The control line pressure response (Figure 20(a)) also shows a valley at 1200 hz. However, interpretation of the control line response data is difficult because the pressure pickup location is not at the amplifier control port. It is located as close as possible to the port, but is still approximately 4 inches from the control port. Because of the low input power at 1200 hz., a valley would be expected at this frequency anywhere in the control line duct.

The lack of a prominent valley at 600 hz. for the output and input responses can be explained, at least partially, by the resonant response of the driver as evidenced in Figure 12.

As discussed previously, the driver output impedance does not match the characteristic impedance of the duct. Therefore, it was reasoned that some distortion of a simple standing wave pattern could be expected due to reflections at the sending end of the duct. Knowing that the driver output impedance would be higher than that of the duct, an acoustic load was connected in parallel at the driver end by opening a gap between the driver and the duct. Various gap sizes were tried but no appreciable change in the shape of the control line pressure frequency response curve was noted. We conclude from these results that there was no change in the hypothesized standing wave pattern.

Another purpose of the tests described above was as follows. If the driver output impedance with its shunt load could be made to match the duct, then reflected waves from the control port would be absorbed. Although there would still be a standing wave pattern in the duct, the pressure amplitude at the control port would be constant with frequency (except for the 600 hz driver resonance). This will be demonstrated analytically in Section 4.6. Therefore, a flat frequency response curve should be obtained if reflections at the control port were the only problem. However, no acoustic shunt at the driver end could be found that came even close to providing the desired result.

It was, then, decided to attempt to achieve an impedance match at the control port end of the duct by reducing the admittance of the



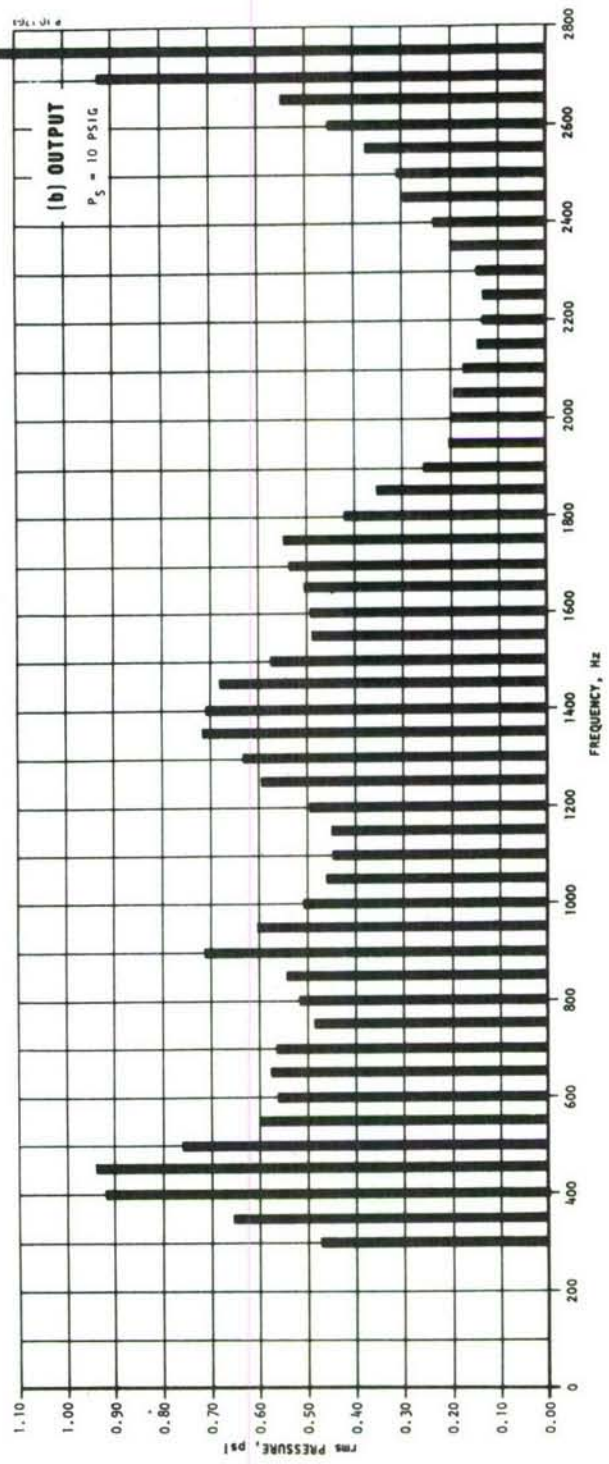
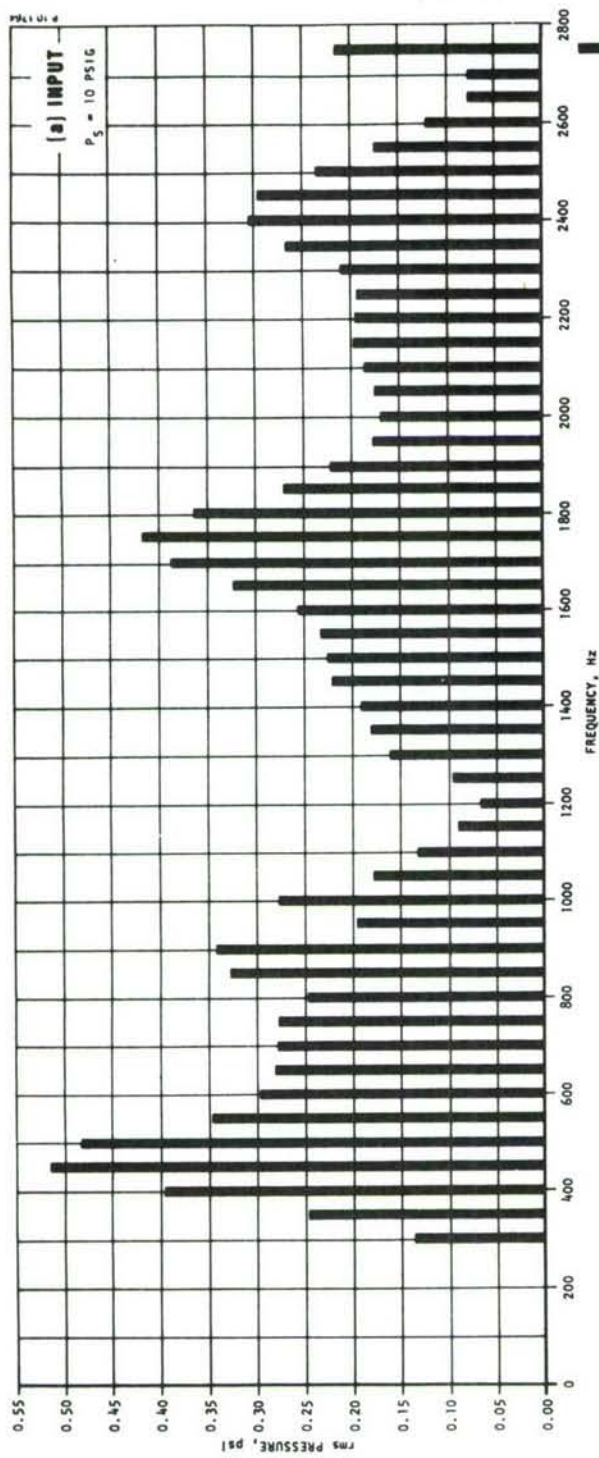


Figure 20 - Frequency Response of Annular Slot Model

control port. Since the valley in response occurred at 1200 hz. as expected, the port admittance was known to be too large. It was possible to reduce  $g_c$  by moving the control flow deflector towards the duct. In doing so the gain of the amplifier could also be expected to decrease since less control port area would be available to act on the power jet. Even so, the control flow deflector was moved forward by placing shims under its base so that the control port area was reduced in successive steps from 100 percent to 80 percent to 60 percent to 40 percent of the full value. The reduction in area to 80 percent was accomplished with 0.10 inch shim, 60 percent with a 0.20 inch shim, and finally 40 percent with a 0.30 inch shim.

The input frequency response test results for each of these reduced control port areas are shown in Figures 21(a), 22(a), and 23(a). Corresponding output response curves are shown in Figures 21(b), 22(b) and 23(b). For the data taken, the response for the 60 percent port area is perhaps the best in that a marked reduction in standing wave ratio has taken place. The response, however, is by no means flat. Also, the overall stage gain suffered markedly by the reduction in the control port area. The gain is essentially one-half of that possible with the full control port. In looking at the output response data, it is apparent that there is a strong enhancement of gain in the vicinity of 1400 to 1500 hertz, which changed very little with changes in control port area.

It was concluded that other distributed phenomena must be present, i.e., another signal path length exists which must be causing some of the variation in stage gain with frequency. A set of tests were then undertaken to determine the a.c. input admittance of the control port and also to isolate the variation in stage gain as a function of frequency. By isolating both control port and load distributed effects, it was reasoned that any other distributed paths could be more readily identified. These tests and the results are discussed in Section 4.4.

#### 4.4 A.C. IMPEDANCE AND GAIN MEASUREMENT TESTS

To determine experimentally the control port a.c. characteristics, the pressure standing wave method was used. A 25-foot length of uniform area aluminum tubing was adapted to run from the electrodynamic driver to the amplifier model control port. The tubing area was 2.64 in<sup>2</sup>. From the end of the tubing, the control line passage tapered smoothly outward along a 1.87 inch length to the physical control port itself, which is 2.99 in<sup>2</sup> in area. The physical control port is defined as the point along the control line passage where the area begins to flare out rapidly. (See Figure 2)

The construction of the amplifier prevents installation of a pressure pickup in the immediate vicinity of the control port. However, beginning 3.00 inches from the end of the aluminum tubing, pressure pickup taps were situated at 0.25 inch intervals for a length of 9.50 inches, and at 0.50 inch intervals for an additional length of 7.00 inches. The 25-foot



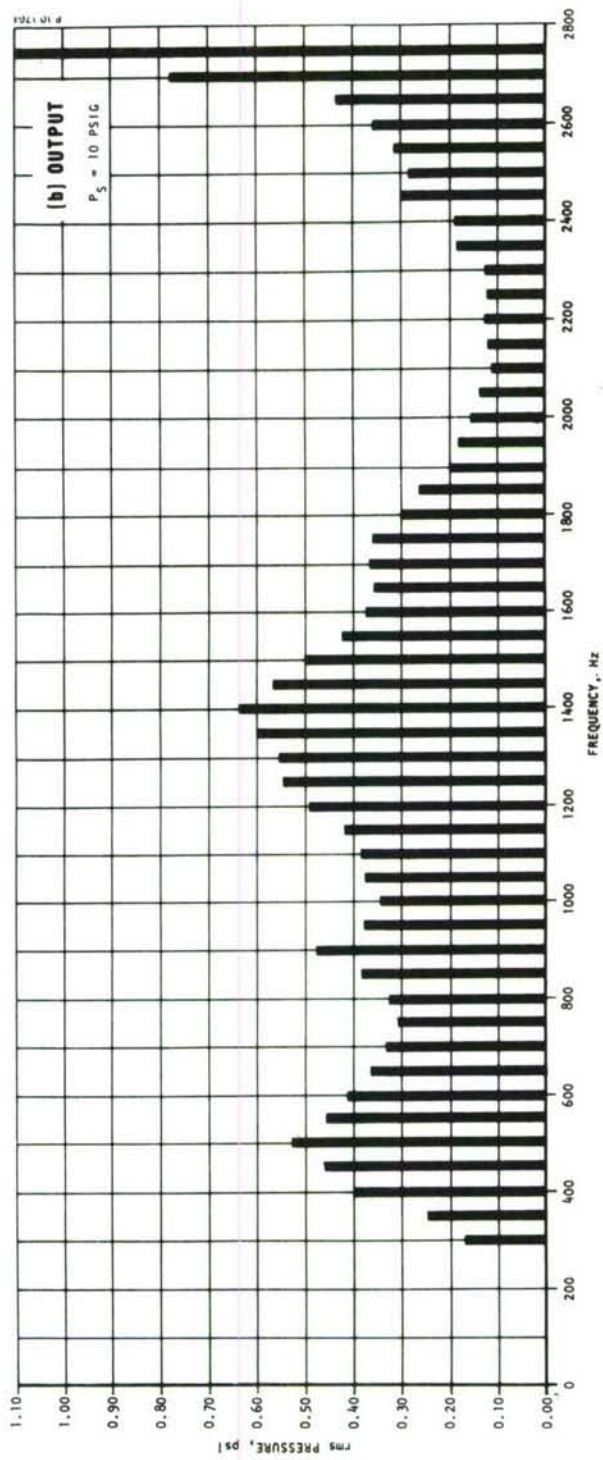
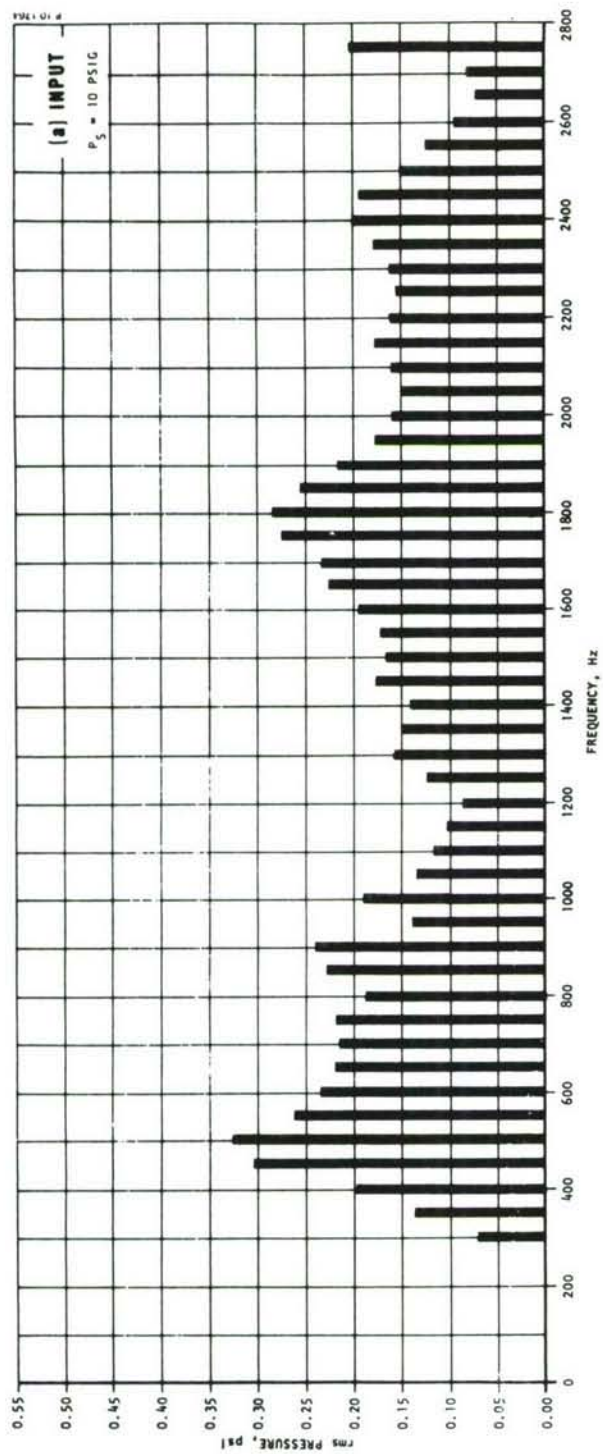


Figure 21 - Frequency Response (80 Percent Control Port Area)



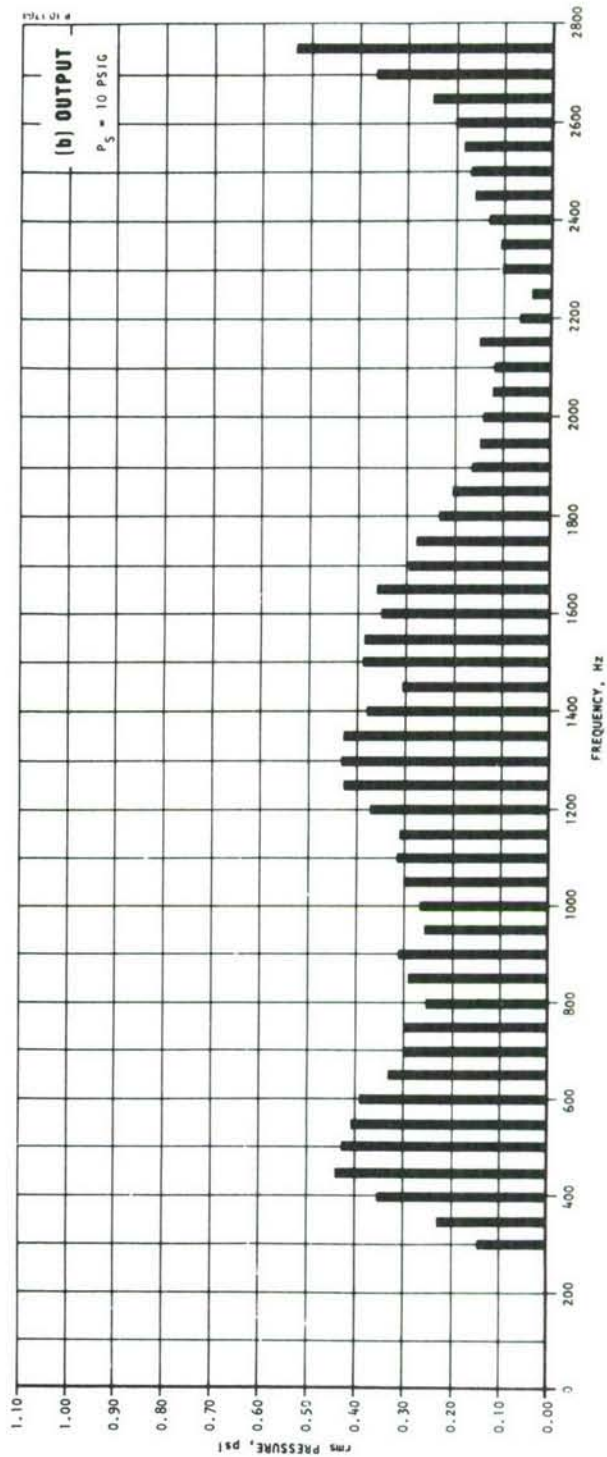
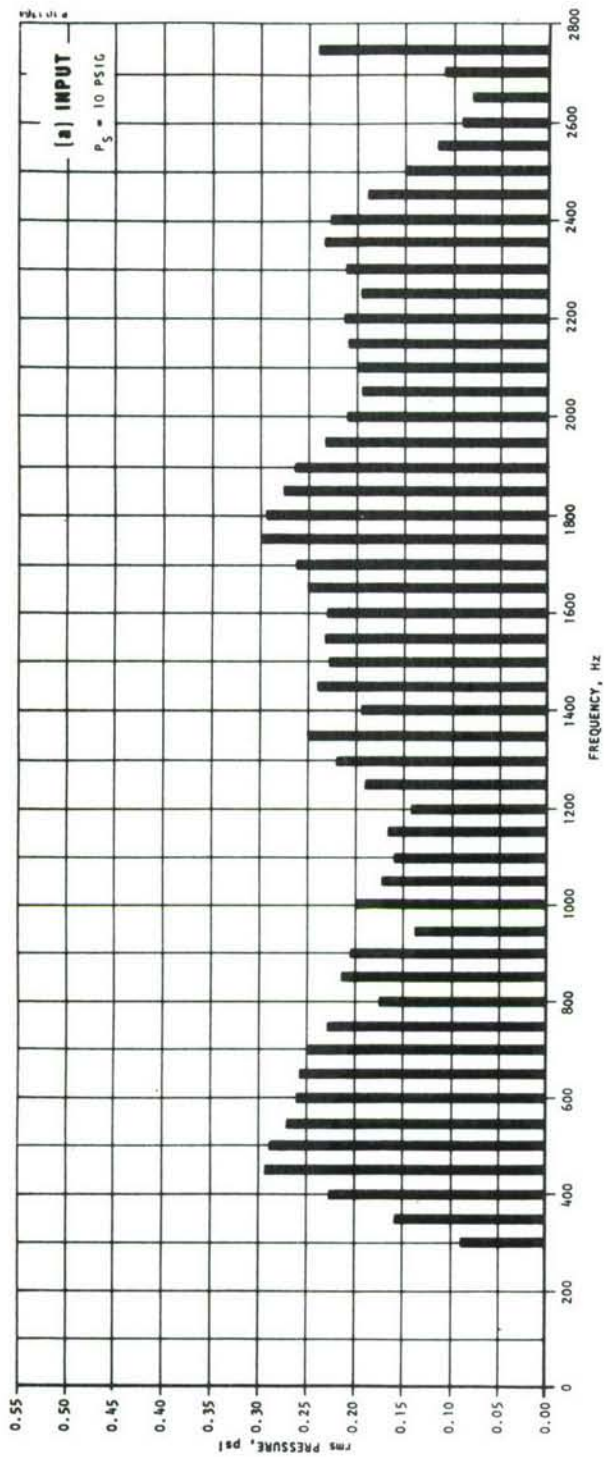


Figure 22 - Frequency Response (60 Percent Control Port Area)

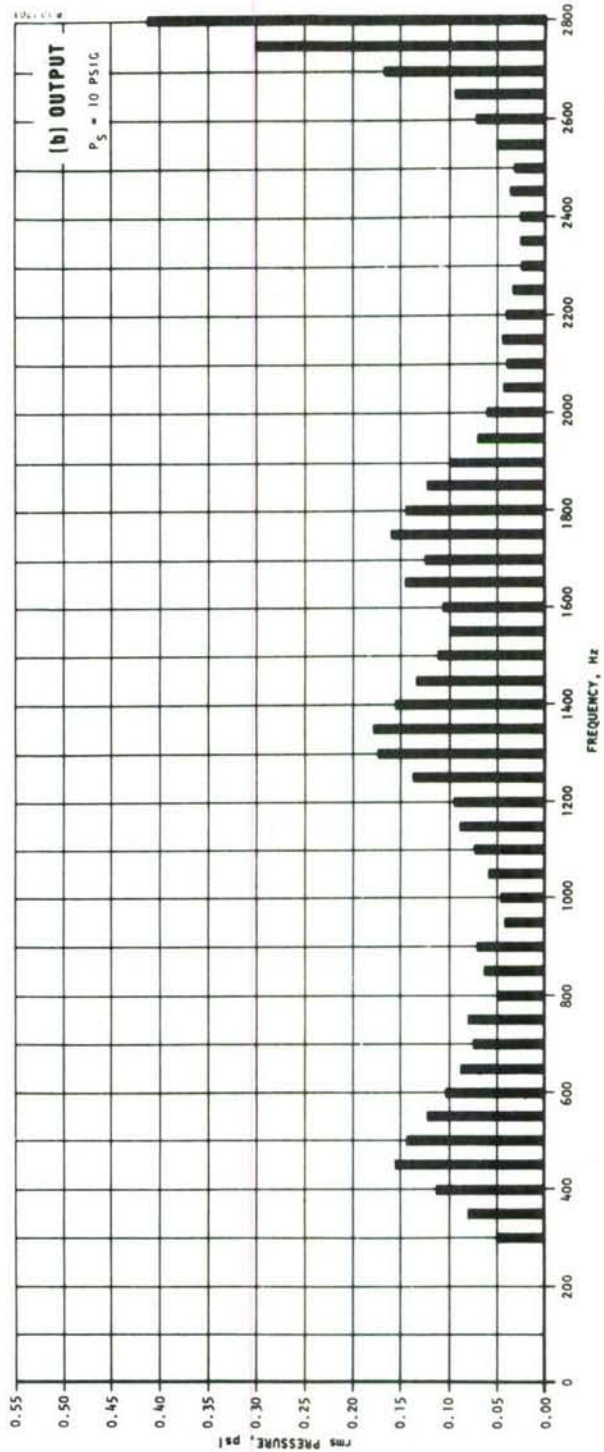
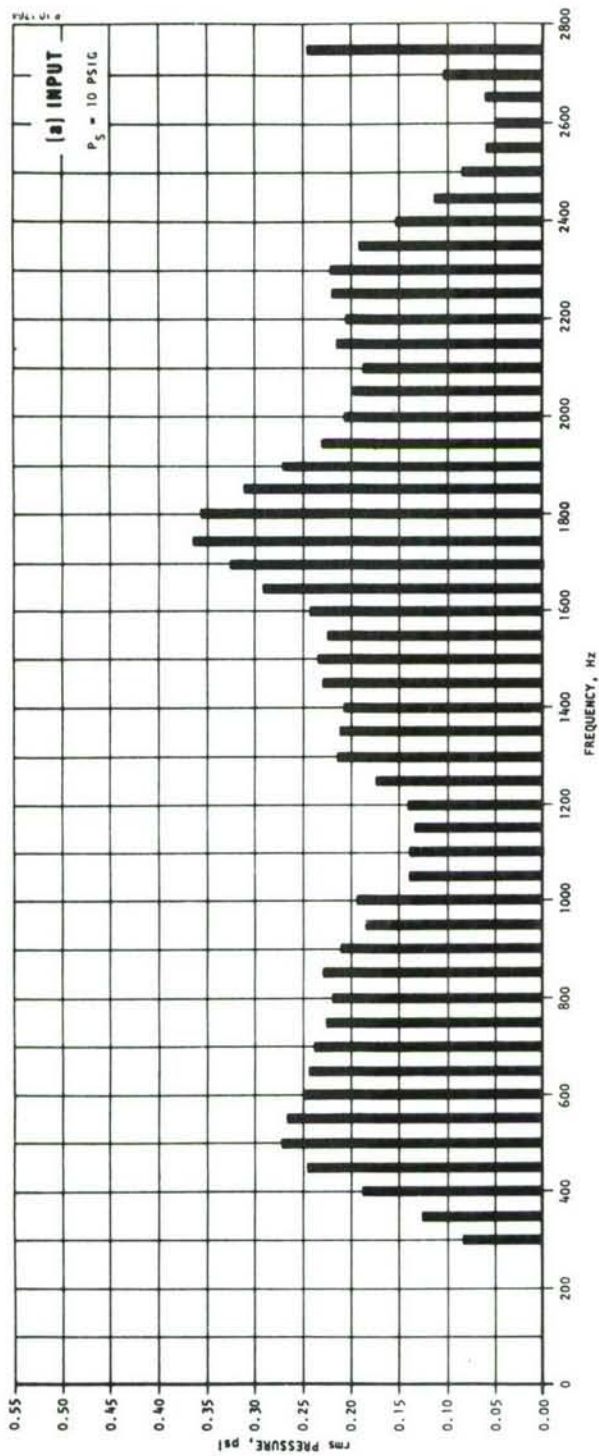


Figure 23 - Frequency Response (40 Percent Control Port Area)

length from the electrodynamic driver to the control port provided attenuation of pressure waves reflected from the control port and traveling back to the electrodynamic driver and then forward to the control port again. The output load on the fluidic amplifier was the long concentric tube assembly described previously.

The test procedure was to drive the annular slot amplifier model at a fixed frequency and amplitude, and move a dynamic pressure pickup from tap to tap. By plotting the a.c. pressure amplitude versus distance, the standing wave pattern can be obtained for that particular frequency. Figure 24 shows a typical plot. From similar plots for other frequencies, the ratio of pressure amplitude maximum and minimum, and the distance from the control port to the first pressure minimum can be found for each frequency. The control port impedance as a function of frequency can then be found using the techniques of electrical transmission line engineering. Either a Smith chart\* can be employed, or the following formula can be used:\*\*

$$Z_c = \frac{c}{g A} \left[ \frac{1 - jr \tan (2\pi d_m / \lambda)}{r - j \tan (2\pi d_m / \lambda)} \right] \quad (4-19)$$

where:

$Z_c$  = Impedance of control port,  $\text{sec/in}^2$

$g = 386 \text{ in/sec}^2$

$c$  = Sound speed in the gas,  $\text{in/sec}$

$A$  = Tube cross section area,  $\text{in}^2$

$j$  = Square root of  $(-1)$ , dimensionless

$r$  = Standing wave ratio, maximum pressure amplitude/  
minimum pressure amplitude, dimensionless

$d_m$  = Distance from control port to first pressure  
minimum of the standing wave pattern,  $\text{in.}$

$\lambda$  = Wave length at the test frequency,  $\text{in.}$

---

\* Reference 4, pp. 126-143; Reference 5, pp. 8, 92-8.

\*\* Reference 4, p. 177.



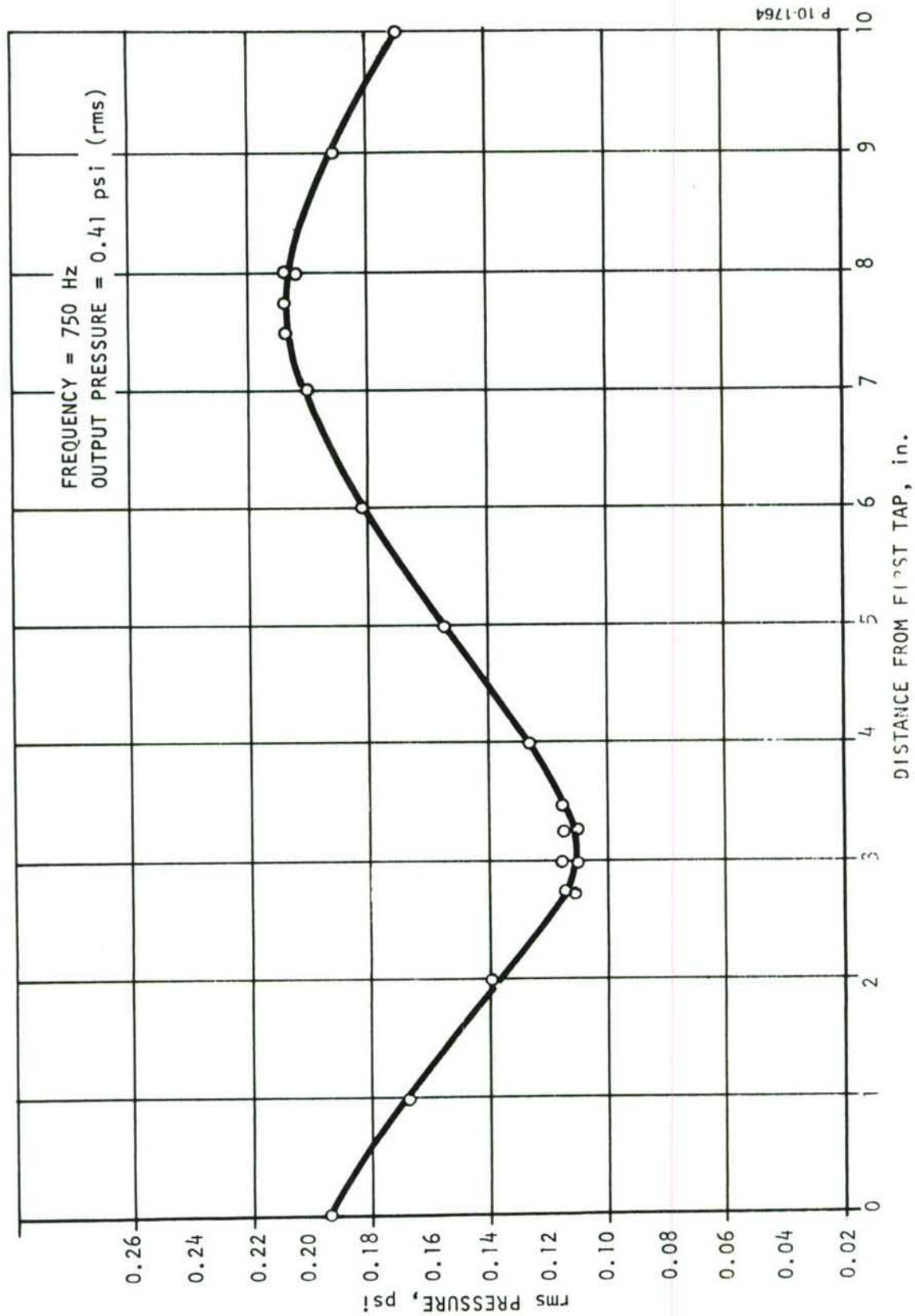


Figure 24 - Typical Standing Wave Plot

It is assumed in equation (4-19) that attenuation over 2 or 3 wave lengths can be ignored. Figure 25 is a Smith chart showing the test data points.

At this point, we should point out that the distance from the pressure amplitude minimum to the control port is not the distance measured to the physical control port. Instead, the distance to an effective control port location gives a more symmetrical distribution of data points for varying frequency. The best effective control port location was found to be that corresponding to the crown of the control flow deflector. Also, because the actual control port area of the annular slot amplifier is uncertain, we use the tube cross section area as a standard basis.

Also at this point, we introduce the use of the lower case letter symbol for variables to denote the a.c. component of pressure. This will help to distinguish it from the steady-state pressures and pressure variations derived from linearized static models, which will still be denoted by the upper case letter symbol. We will follow the same practice for the letter symbols denoting a.c. and steady-state components of weight flow. For the a.c. component of the effective control port pressure, we will drop the subscript s. Thus, the steady-state and the a.c. components of this pressure are denoted by  $P_{CS}$  and  $P_c$  respectively.

From the standing wave data, the pressure amplitude at the effective control port can be deduced. Either a simple construction on the Smith chart or the following formula can be used:

$$P_c = \frac{P_{\min}}{(1 - K_r)} \sqrt{\left[1 - K_r \cos(4\pi d_m/\lambda)\right]^2 + K_r^2 \sin^2(4\pi d_m/\lambda)} \quad (4-20)$$

where:

$$K_r = \frac{r - 1}{r + 1} \quad (4-21)$$

and

$p_c$  = Amplitude of the a.c. pressure at the effective control port, lb/in<sup>2</sup>

$p_{\min}$  = Amplitude of the a.c. pressure at the standing wave minimum, lb/in<sup>2</sup>

$K_r$  = Reflection coefficient magnitude, dimensionless



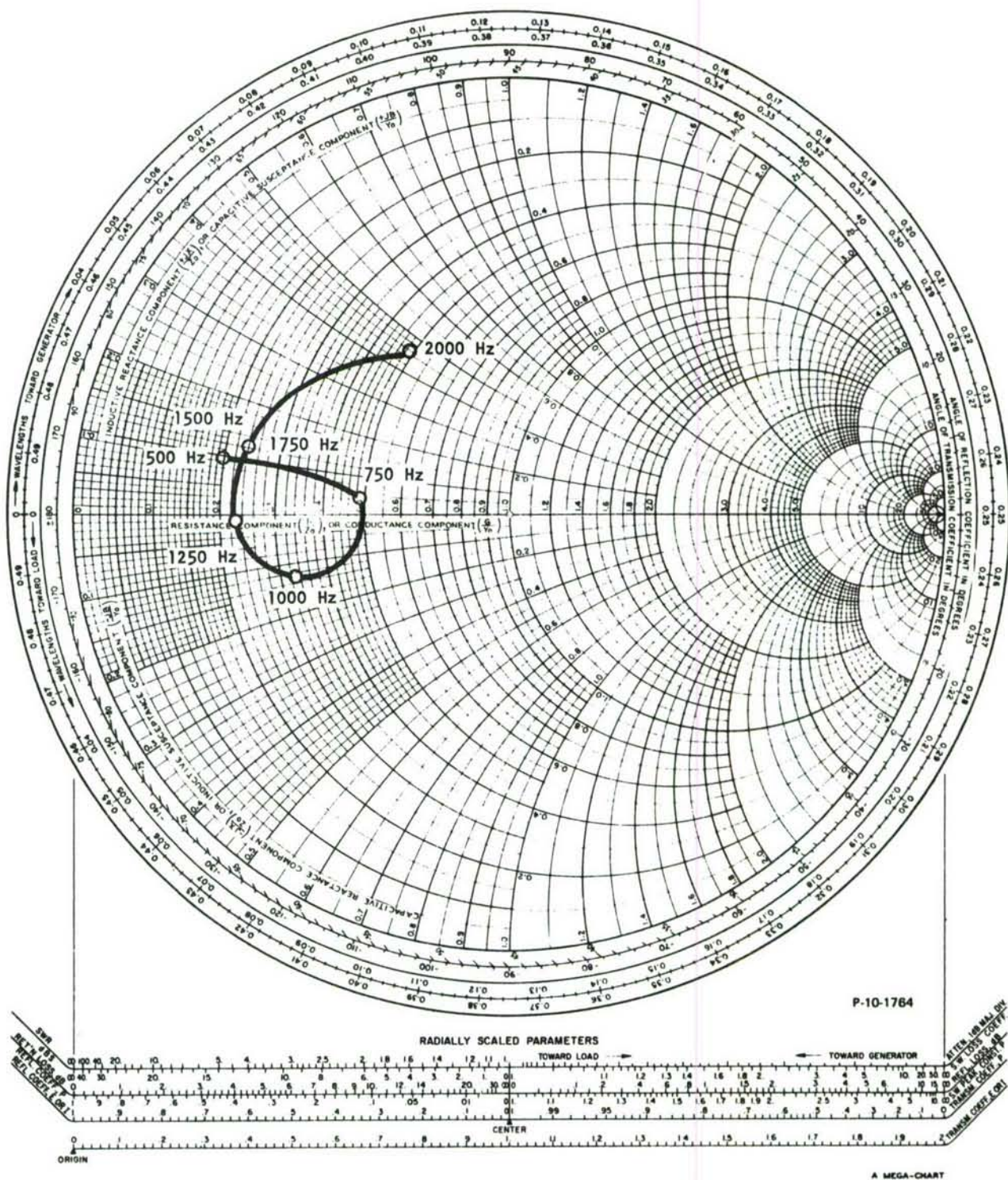


Figure 25 - Smith Chart of Control Port Impedance Obtained From Standing Wave Data



All other symbols are as used in equation (4-19).

The a.c. pressure gain of the annular slot amplifier model is found by dividing the output pressure amplitude by the effective control port pressure amplitude,  $P_c$ . Thus,

$$G = \text{pressure gain} = \frac{P_{\text{out}}}{P_c}$$

Note that this is not the gain value obtained from the ratio of the a.c. output pressure to the a.c. control line pressure. The a.c. control line pressure is that recorded as the input in frequency response tests such as that shown in Figure 20. The a.c. control line pressure can differ from the a.c. effective control port pressure,  $p_c$ , because of standing wave effects. In treating the dynamic behavior of the basic amplifier, the effective control port pressure is the more meaningful quantity. As mentioned previously, the physical construction of the amplifier prevents direct instrumentation of  $p_c$ , the a.c. effective control port pressure.

The control port impedance may be expressed in terms of the normalized resistance and reactance components, as follows:

$$Z_c = \frac{c}{g A} \sqrt{(R')^2 + (X')^2} \quad (4-22)$$

where,

$R'$  = Normalized resistance, dimensionless

$X'$  = Normalized reactance, dimensionless

Figure 26 shows the results of the tests. It is seen that the control port reactance is small compared to the resistance, except at 2000 hz. However, at this frequency the wave length is relatively short and the effect of system errors can be magnified. From 500 to 1750 hz,

$$\sqrt{(R')^2 + (X')^2} \approx 0.3$$

Thus, the control port is an acoustic mismatch to the control line duct, having an impedance too low by a factor of approximately 3. This is in

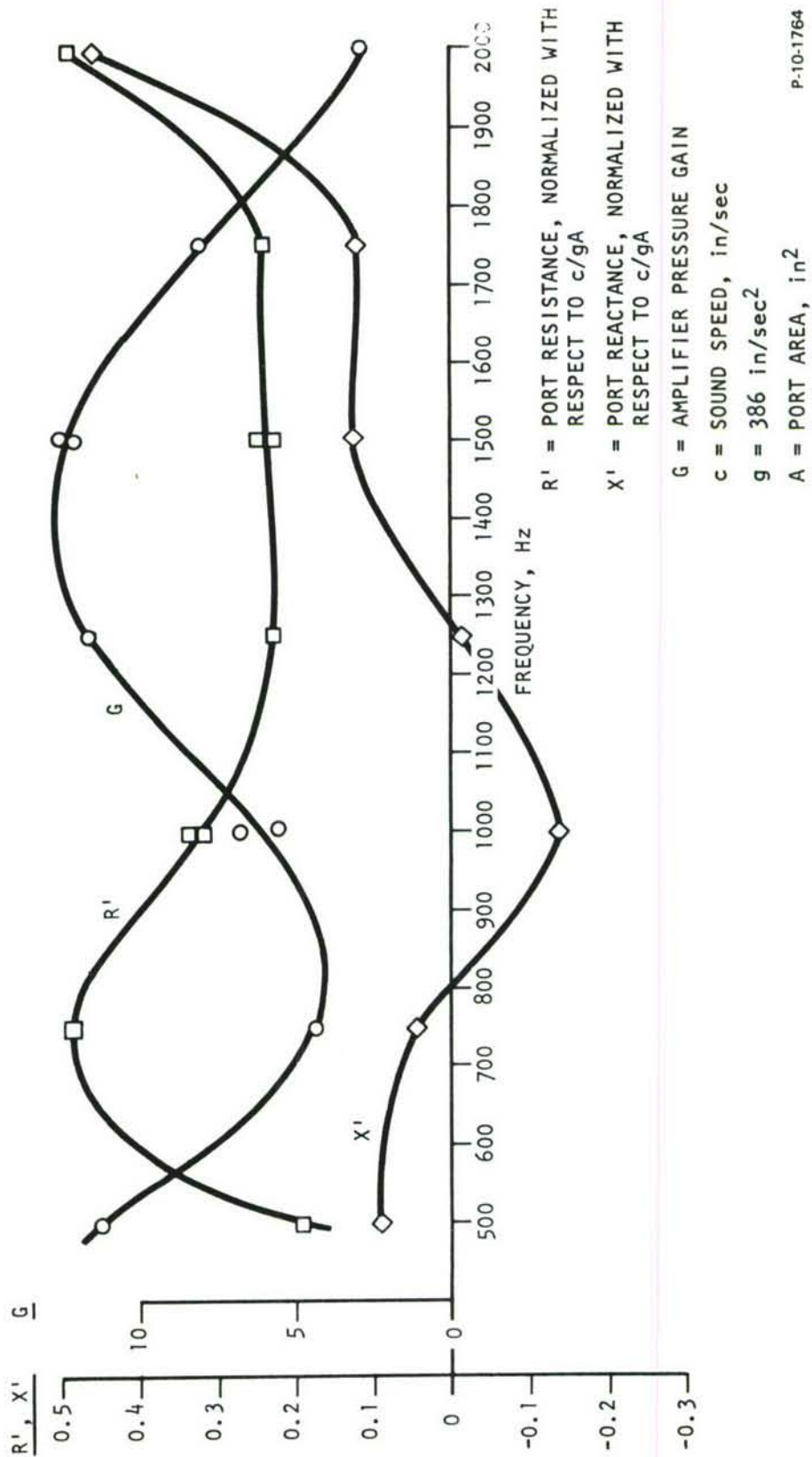


Figure 26 - Control Port Dynamic Characteristics

agreement with the conclusions of Section 4.2.7, where the control port admittance,  $Y_c$ , (the inverse of  $Z_c$ ) was stated to be too high by a factor of from 3 to 5.

Very significant is the variation in pressure gain with frequency. The average value of gain, approximately 8, is still quite high compared with conventional planar jet amplifier experience. As noted in Section 2, conventional planar jet amplifiers under similar load conditions have pressure gains of approximately 3 to 5. The gain variation with frequency for the annular slot amplifier cannot be explained on the basis of the simple lumped parameter equivalent circuits of Figures 14 and 15. This fact supports the conclusion that another distributed signal path exists in the amplifier.

#### 4.5 THE ADDITIONAL DISTRIBUTED SIGNAL PATH

From the gain and impedance data presented in Figure 26 it must be concluded that additional distributed signal paths exist in the amplifier structure apart from those associated with the inlet control duct and amplifier receiver passages.

There are two possibilities which can be considered; one, that the vent region acts like a short finite horn which reflects, and two, that the regenerative feedback path in the amplifier is distributed.

In analyzing the data in Figure 26, and particularly the cyclic behavior of the amplifier gain, i.e., a peak in gain at 1400 hertz and minimum gains at 700 and 2100 hertz, one immediately looks for a reflection path of some 4.7 inches. This is because 4.7 inches represents a quarter wavelength at 700 hz. The radial dimension of the vent region from the power jet to the exit plane of the vents measures 4.5 inches. Therefore, a possibility exists that the vent region is acting as a finite horn, poorly terminated, in the range of frequencies from 300 to 2000 hz. The minimum dimension of the vent region at the exit plane is 2.5 inches, which is 0.38 of a wavelength at 2000 hz. This means that reasonably good radiation should exist at 2000 hz., depending on the cutoff frequency of the effective horn. The vent region was designed, however, to provide a very rapid flare-out of area so that acoustically, the cutoff frequency is high (above 3000 hz). With a high cutoff frequency the impedance presented to the power jet would be low. If the vent were the source of trouble, one would expect a cyclic gain variation but with the peak gains at the higher frequencies being successively lower. This is not the case as shown in Figure 26.

The evidence, then, for the data at hand leads to the conclusion that the distributed path involved in causing the cyclic gain variation must be in the regenerative feedback mechanism. It should be noted, however, before proceeding with the case for the distributed feedback, that the acoustic effects in the vent are not fully understood as yet. In particular, there is vortex flow in the vent region caused by a deflected portion of the power jet flowing along the downstream conical



surface of the vent region. The interaction of the vortex flow pattern with an acoustic field could change the acoustic behavior of the vent considerably over what might be expected otherwise.

To analyze the postulated distributed feedback case, the equivalent circuit developed in Section 4.2.2, Figure 14(b), can be converted to nodal form and expanded to include this path, as shown in Figure 27. The spilled flow source is as before, with the exception that the effect of  $p_L$  in the source is delayed by  $h$  seconds.\* This time delay  $h$  represents the time for a  $p_L$  signal to propagate along the feedback path before being summed with the  $p_c$  signal in the jet interaction region. The quantity  $h$  is equal to the feedback path length divided by the propagation velocity in the feedback path.

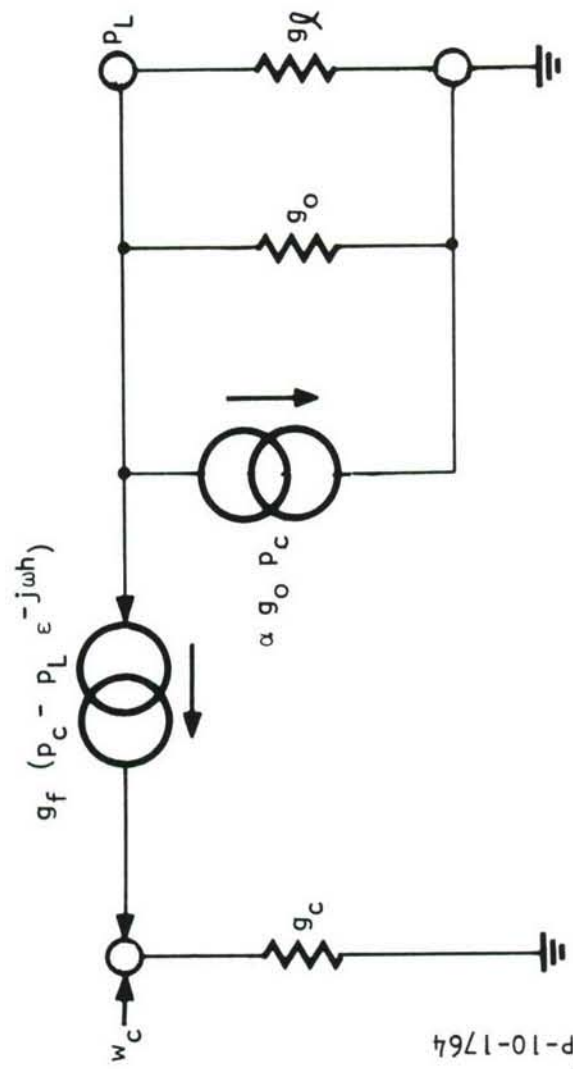
The physical location of the distributed feedback path is as yet to be identified. Its most probable location is in the vent region of the amplifier. There is, of course, some question as to the validity of the circuit shown in Figure 27, but it will serve to explain why a distributed feedback path of some kind could cause cyclic variations in the amplifier gain.

To analyze the circuit in Figure 27, the following Euler expansion of  $\epsilon^{-j\omega h}$  will be used:

$$\begin{aligned}\epsilon^{-j\omega h} &= \cos \omega h - j \sin \omega h \\ &= \cos \frac{\omega \ell}{v_r} - j \sin \frac{\omega \ell}{v_r} \\ &= \cos \frac{\pi f}{2 f_o} - j \sin \frac{\pi f}{2 f_o}\end{aligned}\tag{4-22}$$

---

\* The theory for representing a transport lag or time delay of sinusoidal signals in the manner shown in Figure 27 is given in standard control systems texts. See, for example, Reference 6, pp. 4, 47.



P-10-1764

Figure 27 - Simplified Circuit with Distributed Feedback

where:

$\omega$  = angular frequency =  $2\pi f$ , rad/sec

$f$  = frequency, hz.

$f_o = \frac{v_r}{4\ell}$ , quarter wavelength resonant frequency of feedback path, hz.

$v_r$  = propagation velocity, in/sec.

$\ell$  = path length, in.

We note that if the feedback is acoustic, the propagation velocity is the speed of sound, or

$$v_r = c$$

If the feedback is by the convection of vortex flow patterns,  $v_r$  is the convection velocity. It is believed that acoustic feedback is the more probable case.

Summing flows at the  $P_L$  node in Figure 27,

$$-\alpha g_o p_c - g_f \left[ p_c - p_L \epsilon^{-j\omega h} \right] = (g_o + g_\ell) p_L. \quad (4-23)$$

Solving for  $p_L/p_c$ ,

$$\frac{p_L}{p_c} = \frac{-(\alpha g_o + g_f)}{g_o + g_\ell - g_f \epsilon^{-j\omega h}} \quad (4-24)$$

Using equation (4-22),

$$\frac{p_L}{p_c} = \frac{-(\alpha g_o + g_f)}{g_o + g_\ell - g_f \left[ \cos \frac{\pi}{2} \frac{f}{f_o} - j \sin \frac{\pi}{2} \frac{f}{f_o} \right]} \quad (4-25)$$



Equation (4-25) may be put into the familiar transfer function form for feedback systems:

$$\frac{P_L}{P_C} = \frac{K_1}{1 + K_2 \beta} \quad (4-26)$$

where

$$K_1 = - (\alpha g_o + g_f) / (g_o + g_\ell)$$

$$K_2 = g_f / (g_o + g_\ell)$$

$$\beta = - \left[ \cos \frac{\pi}{2} \frac{f}{f_o} - j \sin \frac{\pi}{2} \frac{f}{f_o} \right]$$

From equation (4-26), it is noted that gain is a maximum when  $f/f_o$  is 0, 4, 8, etc., and the gain is minimum when  $f/f_o$  is 2, 6, 10, etc. The gain is high at zero frequency and is not high again until the feedback path is a full wavelength. From the test data, this next peak in gain occurred at 1400 hz. Therefore, the length of the acoustic feedback path is:

$$\ell = \frac{c}{f} = \frac{13,200}{1400} = 9.4 \text{ inches} \quad (4-27)$$

This path length is so large that it must be concluded that the feedback takes place in the external vent region of the amplifier. The characteristic frequency  $f_o$  for the amplifier is 350 hz. A valley in gain is expected for the amplifier at 700 hz. and 2100 hz., as has been observed.

#### 4.6 AMPLIFIER NOMINAL GAIN (NO FEEDBACK)

Equation (4-26) expresses the amplifier gain in the form of a feedback system transfer function. The quantity  $\beta$  changes with frequency such that the feedback is alternately regenerative and degenerative. An estimate of the nominal non-feedback gain  $K_1$  can be found by evaluating equation (4-26) in its two extremum forms.

For regenerative feedback,

$$\beta = -1$$

From Figure 26,

$$\text{Maximum Gain} = 12.5$$

Then,

$$\frac{K_1}{1 - K_2} = 12.5 \quad (4-28)$$

For degenerative feedback,

$$\beta = 1$$

From Figure 26,

$$\text{Minimum Gain} = 4.0$$

Then,

$$\frac{K_1}{1 + K_2} = 4.0 \quad (4-29)$$

Solving equations (4-28) and (4-29) simultaneously, the nominal amplifier gain  $K_1$  is 6. Since the feedback is positive (regenerative) at low frequencies, a very interesting experiment would be to add a parallel acoustic feedback circuit 9.4 inches in length which is negative at low frequencies. If our distributed feedback model is correct, the frequency-variant gain could be eliminated and a flat response gain of 6 achieved. Unfortunately, such a modification of the experimental annular slot amplifier was beyond the scope of the program.

Let us assume that a satisfactory correction can be found for cancelling the effects of the distributed regenerative feedback path discussed above. (This might be done by means of compensating distributed negative feedback, for example.) Then maintaining a frequency-invariant output pressure response will still require eliminating the cyclic variation of the effective control port pressure amplitude with frequency. As discussed earlier, the cyclic frequency variation of the effective control port pressure amplitude is caused by impedance mismatches at the sending and receiving ends of the control line duct, the duct length being comparable to a wavelength at the operating frequencies. If the control flow source (driver) could be designed so that its output impedance matched the duct characteristic impedance at the sending end, then reflections forward from the driver would be eliminated. A standing wave would still exist along the control line duct, but cyclic variation with frequency would be eliminated for the duct receiving end pressure amplitude. (The duct receiving end pressure is, of course, the effective control port pressure,  $p_c$ .)

To demonstrate this fact, consider the case where a generator or driver, having an output impedance  $Z_o$ , is connected to a duct whose characteristic impedance is also  $Z_o$ . For simplicity in this example, we will assume the duct terminating load is a resistance,  $r_c$ . The pressure at the line sending end is given by,

$$p_s = p_g \frac{Z_{in}}{Z_o + Z_{in}} = p_g \frac{1}{Z_o/Z_{in} + 1} \quad (4-30)$$

where

$Z_{in}$  = Input impedance of the duct,  $\text{sec/in}^2$

$Z_o$  = Characteristic impedance,  $\text{sec/in}^2$

$p_g$  = Open-circuit a.c. pressure of generator (rms), psi

$p_s$  = Input or sending end a.c. pressure (rms), psi



The a.c. pressure at the duct termination or control port is derived by using the duct transfer impedance:\*

$$p_c = p_s \frac{r_c}{Z_T} \quad (4-31)$$

The transfer impedance,  $Z_T$ , is given by

$$Z_T = r_c \cosh \gamma L + Z_o \sinh \gamma L = \frac{p_s}{w_r} \quad (4-32)$$

where

$\gamma$  = Propagation constant,  $\text{in}^{-1}$

$L$  = Duct length, in

$w_r$  = a.c. weight flow at receiving end (rms), lb/sec

The propagation constant  $\gamma$  is the same quantity that was introduced in Section 4.3.

From equations (4-31) and (4-32),

$$p_c = p_s \frac{1}{\cosh \gamma L + (Z_o/r_c) \sinh \gamma L} \quad (4-33)$$

The input impedance to the duct is given by,\*\*

$$Z_{in} = Z_o \frac{r_c \cosh \gamma L + Z_o \sinh \gamma L}{Z_o \cosh \gamma L + r_c \sinh \gamma L} \quad (4-34)$$

---

\* Reference 4, pp. 93, 105

\*\*  
Reference 4, p. 105

From equations (4-30), (4-33) and (4-34), we obtain,

$$\frac{p_c}{p_g} = \frac{r_c}{(r_c + Z_o)} \frac{1}{(\cosh \gamma L + \sinh \gamma L)} \quad (4-35)$$

Following the procedure used in Section 4.3, we make the approximation that the duct is lossless. Then,

$$\gamma = j \frac{2\pi f}{c} = j \frac{2\pi}{\lambda}$$

Under a similar approximation,  $Z_o$  remains constant with frequency and has no imaginary part.

Using the mathematical identities:

$$\cosh jx = \cos x,$$

$$\sinh jx = j \sin x$$

We then obtain,

$$\begin{aligned} \frac{p_c}{p_g} &= \frac{r_o}{(r_c + Z_o)} \frac{1}{\left[ \cos (2\pi L/\lambda) + j \sin (2\pi L/\lambda) \right]} \\ &= \frac{r_c}{r_c + Z_o} e^{-j (2\pi L/\lambda)} \end{aligned} \quad (4-36)$$

The factor

$$e^{-j (2\pi L/\lambda)} = e^{-j (2\pi f L/c)}$$

is a phasor. It is of constant magnitude and sets the phase relationship between  $p_c$  and  $p_g$ . Thus, equation (4-36) shows that if the magnitude of the generator pressure  $p_g$  stays constant with frequency, the

magnitude of the effective control port pressure  $p_c$  also stays constant with frequency, as long as the driver output impedance matches the duct characteristic impedance  $Z_o$ . The value of the terminating control port resistance  $r_c$  does not affect this result.

The type of operation described here, in which the driver output impedance is matched to that of the duct, does not necessarily allow the driver and duct to deliver the maximum power to the control port. What it does do is eliminate the cyclic variation of power with frequency, in spite of a mismatch between the duct and the terminating control port.

It may prove possible in future designs to obtain an impedance match between the control line duct and the control port of the amplifier if a complete understanding of the feedback mechanism can be found. Knowing its physical nature, adjustments in the feedback gain may be possible which will, in turn, affect the control port impedance. By adjusting the feedback gain an impedance match may be possible.

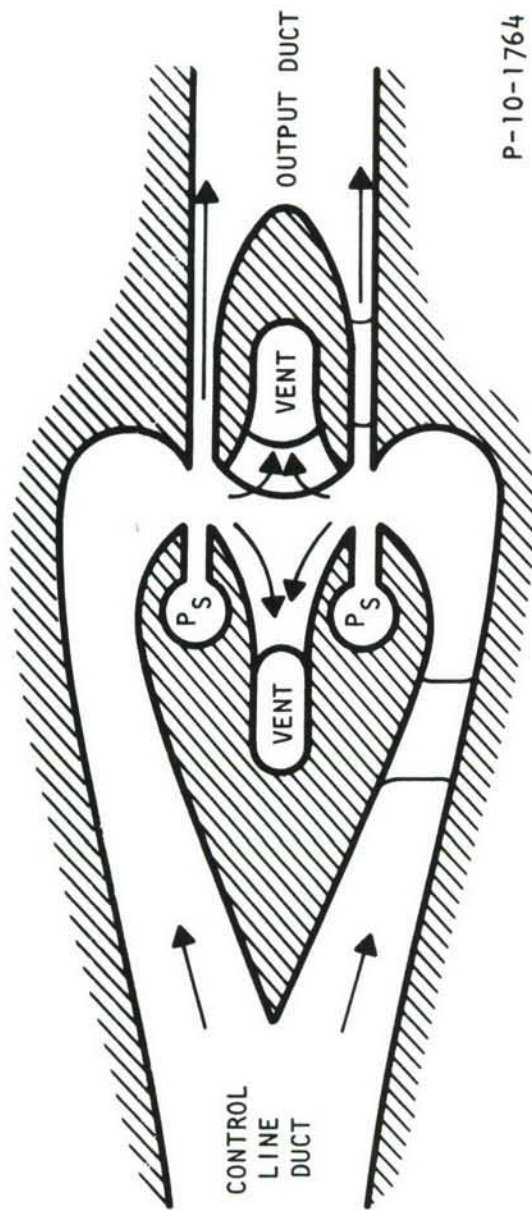
It was found that the control port impedance is less than the duct characteristic impedance, by roughly a factor of 3. This was discussed in Section 4.4. The duct characteristic impedance is given by,

$$Z_o = \frac{c}{g A}$$

Therefore, increasing the duct area with respect to the control port area is in the direction toward a better match. The presence of the power jet boundaries around the central axis of the annular slot amplifier prevents bringing a duct passage along the central axis and up close to the control port, if the duct area is substantially greater than the control port area. If the large area duct is not brought up close to the control port, the passage length between the control port and the area discontinuity will cause undesirable reflection effects. A solution to this problem could possibly be provided by the configuration shown in Figure 28. Here, the design is turned inside-out. The large area control line duct is brought around the outside of the power jet boundaries, and the vent regions are along the control axis. The control port is an annular slot around the outside of the free power jet. This configuration allows space for a large area control line duct to be brought up close to a smaller area control port. However, such a redesign may radically change the regenerative feedback mechanism. In that case, not only a complete redesign is required but a complete reevaluation of all impedances and gains would be required.

It must be noted that a number of avenues are open for further improving the performance of annular slot amplifier sound generator stages. Let us return to a brief consideration of one of the possible distributed signal paths which could cause cyclic frequency variation of the stage gain. This is the case where the external vent region is





P-10-1764

Figure 28 - Inside-Out Configuration with Large Control Line Duct Area

radially tuned, such that the external vent region acts as a short horn. If this effect were the real cause of the gain variation, then corrections to the vent design would yield an amplifier with a stage gain that takes on the measured peak value of 12.5 at all frequencies. One possible correction to be tried is to further increase the flare-out of vent area as shown by the line drawing in Figure 29. If the vent is acting as a horn, considerable changes should then be noted in overall stage response.

#### 4.7 COMPENSATION OF OUTPUT RESPONSE CURVES BY SELECTION OF CONTROL LINE PARAMETERS

It was not possible in this program to evaluate the parallel negative distributed feedback approach discussed previously, or the geometry modifications described in Figures 28 and 29. However, one possible approach aimed at reducing the overall variation in frequency response was studied analytically. This approach uses a control line duct whose total length and variation of area with length are chosen to compensate as much of the frequency-variant gain of the basic amplifier as possible.

The control line duct (and the interstage coupling duct, in the case of a two-stage sound generator) is, in the general case, an acoustic transformer. The duct area varies gradually and smoothly with length. Within a well-defined frequency range, the duct transforms the impedances connected at the ends of the duct, the transformer ratio being the duct area ratio. This was discussed in Section 4.3. In the compensation approach considered, the duct is still allowed to reflect, due to the impedance mismatches at the control port end and the driver end. The peaks and valleys of the duct response are then used to partially offset the cyclic gain variation with frequency of the amplifier proper. The spacing of the duct frequency response peaks and valleys in the frequency regime is determined by the duct total length.

Up to this point, we have analyzed the varying-area control line duct as an equivalent constant-area duct. We will now treat the control line duct as a transformer. The equivalent circuit is given in Figure 30. The electrodynamic driver is modeled as a controllable source of sinusoidally-varying pressure, of rms amplitude  $p_g$ , in series with a generator output impedance  $Z_g'$ . The quantity  $Z_g'$  is taken to be considerably larger than the characteristic impedance at the throat of the driver. The justification for this assumption was discussed in Section 4.3.

The quantity  $Z_{oc}$  is the characteristic impedance at the control port or receiving end of the duct. That is,

$$Z_{oc} = \frac{c}{g A_r}$$

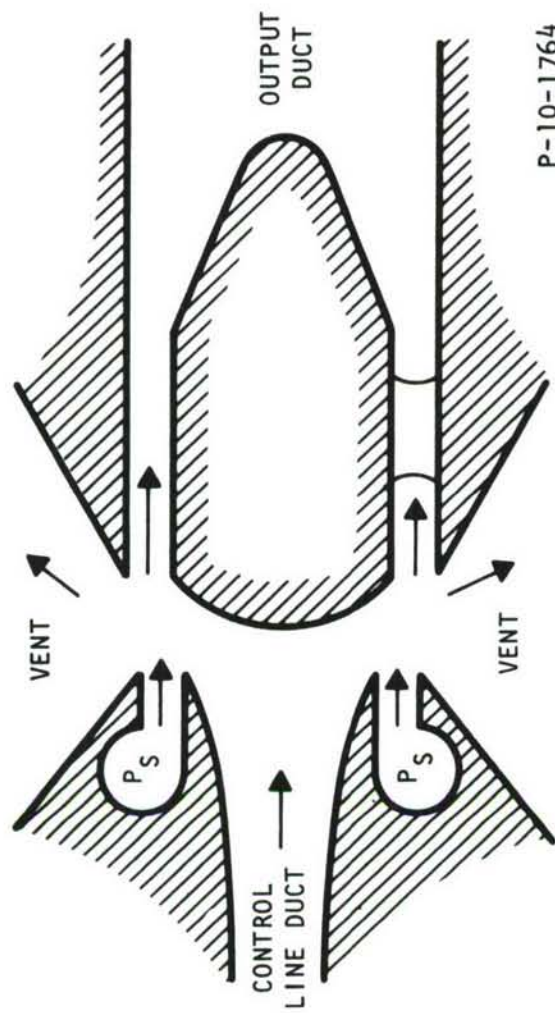
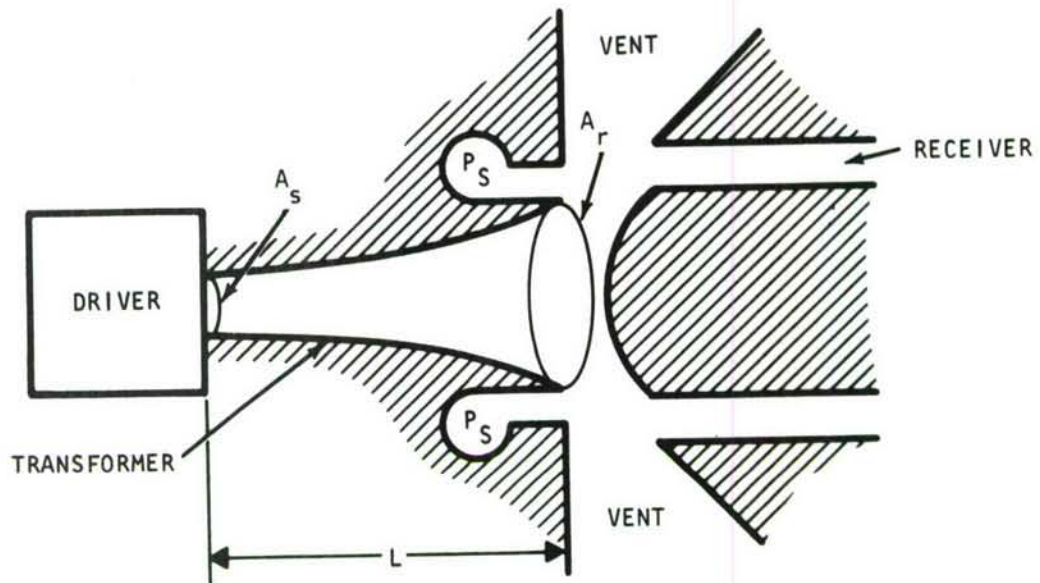
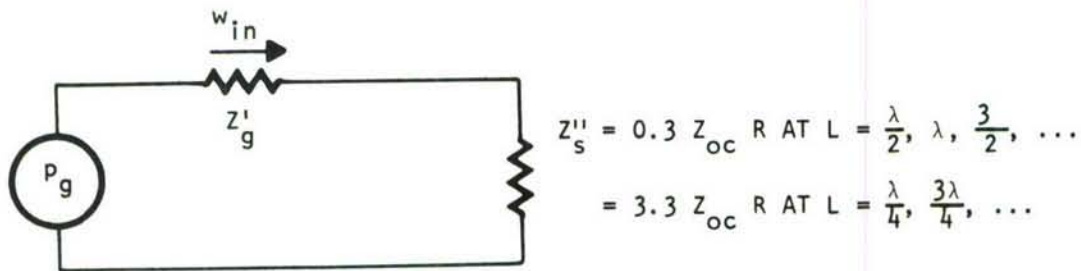
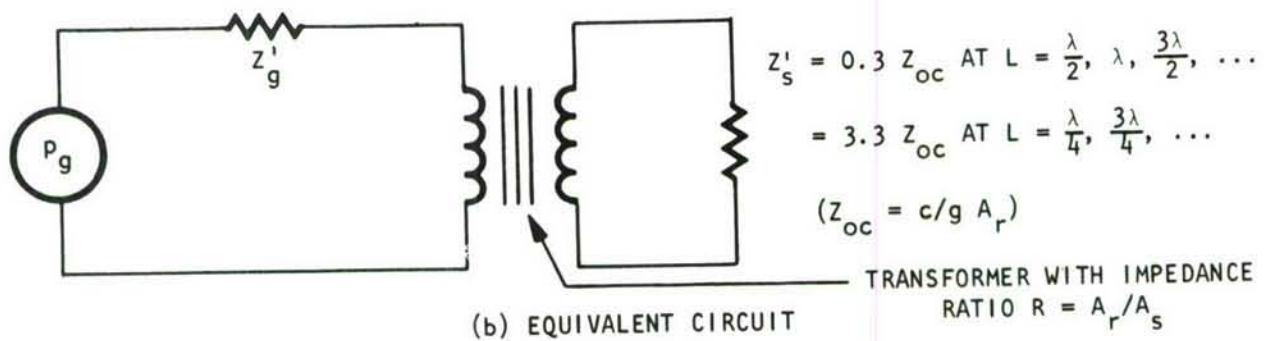


Figure 29 - Amplifier Configuration with Large, Flared Ducts





(a) PHYSICAL MODEL



(c) MODIFIED EQUIVALENT CIRCUIT

Figure 30 - Driver and Transformer Circuit

where,

$A_r$  = Area at the control port end of the duct, in<sup>2</sup>

From the circuit given in Figure 30, expressions may be derived for the control pressure at the end of the duct attached to the driver. From experimental results discussed in Section 4.4, the termination at the control port end of the duct is approximately  $0.3 Z_{oc}$ . The taper of the control line duct is so gradual that the duct may be viewed as a nearly perfect transformer at all frequencies of interest. A ratio,  $R$ , denotes the impedance transformation ratio. The quantity  $R$  is given by the ratio of the duct exit area to that at the entrance. Impedances at the control port end of the duct are then increased in size by the ratio  $R$  when presented to the driver.

The impedance presented to the driver varies depending on the frequency. It is a minimum when the duct is an even number of quarter wave lengths long, and equals  $0.3 R Z_{oc}$ . When the duct is an odd number of quarter wave lengths long, the impedance presented to the driver is a maximum and is equal to  $3.3 R Z_{oc}$ . The magnitude of the a.c. component of weight flow rate at the duct entrance, when duct length is one-half-wavelength, is:

$$(w_{in})_{\lambda/2} = \frac{p_g}{Z'_g + 0.3 Z_{oc} R} \quad (4-37)$$

The pressure at the duct entrance under these conditions is:

$$\begin{aligned} (p_{in})_{\lambda/2} &= (w_{in})_{\lambda/2} (0.3 Z_{oc} R) \\ &= \frac{p_g (0.3) Z_{oc} R}{Z'_g + 0.3 Z_{oc} R} \end{aligned} \quad (4-38)$$

The pressure at the duct exit, i.e., the control port, is the entrance pressure transformed by the ratio  $\sqrt{R}$ . Thus:

$$(p_c)_{\lambda/2} = \frac{0.3 Z_{oc} \sqrt{R} p_g}{Z'_g + 0.3 Z_{oc} R} \quad (4-39)$$

By the same approach, we can derive the following relationships for the case where the duct length is one-quarter-wavelength:

$$(w_{in})_{\lambda/4} = \frac{p_g}{Z'_g + 3.3 Z_{oc} R} \quad (4-40)$$

$$(p_{in})_{\lambda/4} = \frac{p_g (3.3) Z_{oc} R}{Z'_g + 3.3 Z_{oc} R} \quad (4-41)$$

$$(p_c)_{\lambda/4} = \frac{p_g Z_{oc} \sqrt{R}}{Z'_g + 3.3 Z_{oc} R} \quad (4-42)$$

For the quarter-wavelength case, the pressure at the control port is reduced by two factors, first by the  $\sqrt{R}$  due to transforming, and then by the standing wave ratio for the duct. The latter factor is 3.3 for the termination  $0.3 Z_{oc}$ . It will be interesting to examine the ratio:

$$\left[ (p_c)_{\lambda/4} \right] / \left[ (p_c)_{\lambda/2} \right]$$

This represents the peak-to-valley variation of the control pressure as frequency is changed. From equations (4-39) and (4-42),

$$\left[ (p_c)_{\lambda/4} \right] / \left[ (p_c)_{\lambda/2} \right] = \frac{1 + 0.3 Z_{oc} R/Z'_g}{0.3 + Z_{oc} R/Z'_g} \quad (4-43)$$

This ratio is plotted in Figure 31 versus the parameter  $Z_{oc} R/Z'_g$ .

For the compensation approach under consideration, the duct length or the transformer ratio  $R$  or both would be varied to achieve an amplifier frequency response with a minimum peak-to-valley excursion. Changing the duct length would be a straightforward procedure. Changing the transformer ratio would be accomplished by keeping the control port area  $A_r$  fixed, but increasing or decreasing the initial or inlet duct area  $A_s$ . This would involve machining out the part of the duct that is internal to the driver, or inserting a plug of the proper dimensions. It is assumed that changing  $A_s$  would not change the value of the generator impedance  $Z'_g$  appreciably.



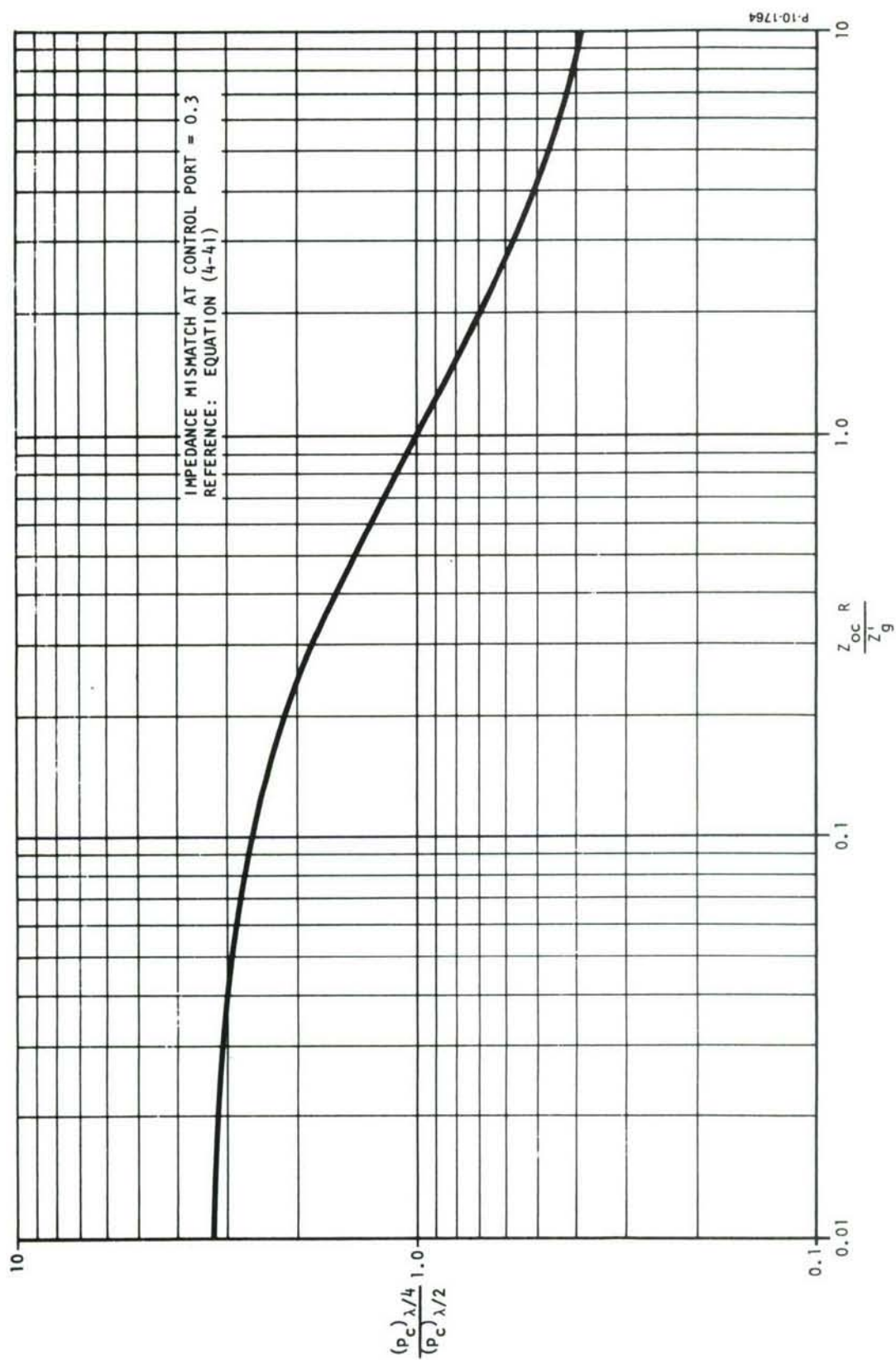


Figure 31 - Standing Wave Ratio Versus Impedance and Transformer Ratio Parameter

In Section 4.6, we saw that if there were a match between the duct input impedance and the driver output impedance, the frequency response  $p_c/p_g$  would be flat. In the case under discussion, the condition for such a match is,

$$Z_{oc} R = Z'_g$$

However, since the amplifier gain varies with frequency, a better approach is to select a transformer ratio and length so that some of the amplifier gain variation can be offset by the use of the standing wave effect in the control line duct. A number of trial and error calculations were made in which the duct length and pressure standing wave ratio were varied. A duct length of 11 inches and a duct pressure standing wave ratio between 2.0 and 2.5 appeared to be about the best combination.

A duct length of 11 inches gives a control pressure valley at 0, 600, 1200 and 1800 hz and a pressure peak at 300, 900, 1500 and 2100 hz. Two different standing wave ratio values were used, 2.0 and 2.5, and a composite gain curve was calculated using the gain as given in Figure 26. The absolute magnitude of  $p_c$  was tailored to match the experimental output pressure of the amplifier at 1200 hz. The results are plotted in Figure 32. Curve A is the measured output pressure response. Curve B is the calculated output pressure response for a standing wave ratio of 2.0 while Curve C is for a standing wave ratio of 2.5. Curve C matches the actual response reasonably well below 1300 hz, but is too high in the region from 1300 to 1700 hz. The large peaks resulting from the calculations are to a large extent the result of not including losses in the calculations. Curve B exhibits more peak-to-valley excursion in the region of frequencies below 1300 hz. Using a larger standing wave ratio would cause a large dip in response at 750 hz; therefore, a good standing wave ratio to use as a design goal is 2.5.

The calculated curves in Figure 32 were plotted assuming a driver output impedance that is nine times the characteristic throat impedance of the driver. This assumption corresponds to a driver efficiency of 10%. It was shown in Section 4.3 that for a 10% driver efficiency,

$$Z'_g = 9 \frac{c}{g A_s}$$

where

$$A_s = \text{Area at the driver or sending end of the duct, in}^2$$

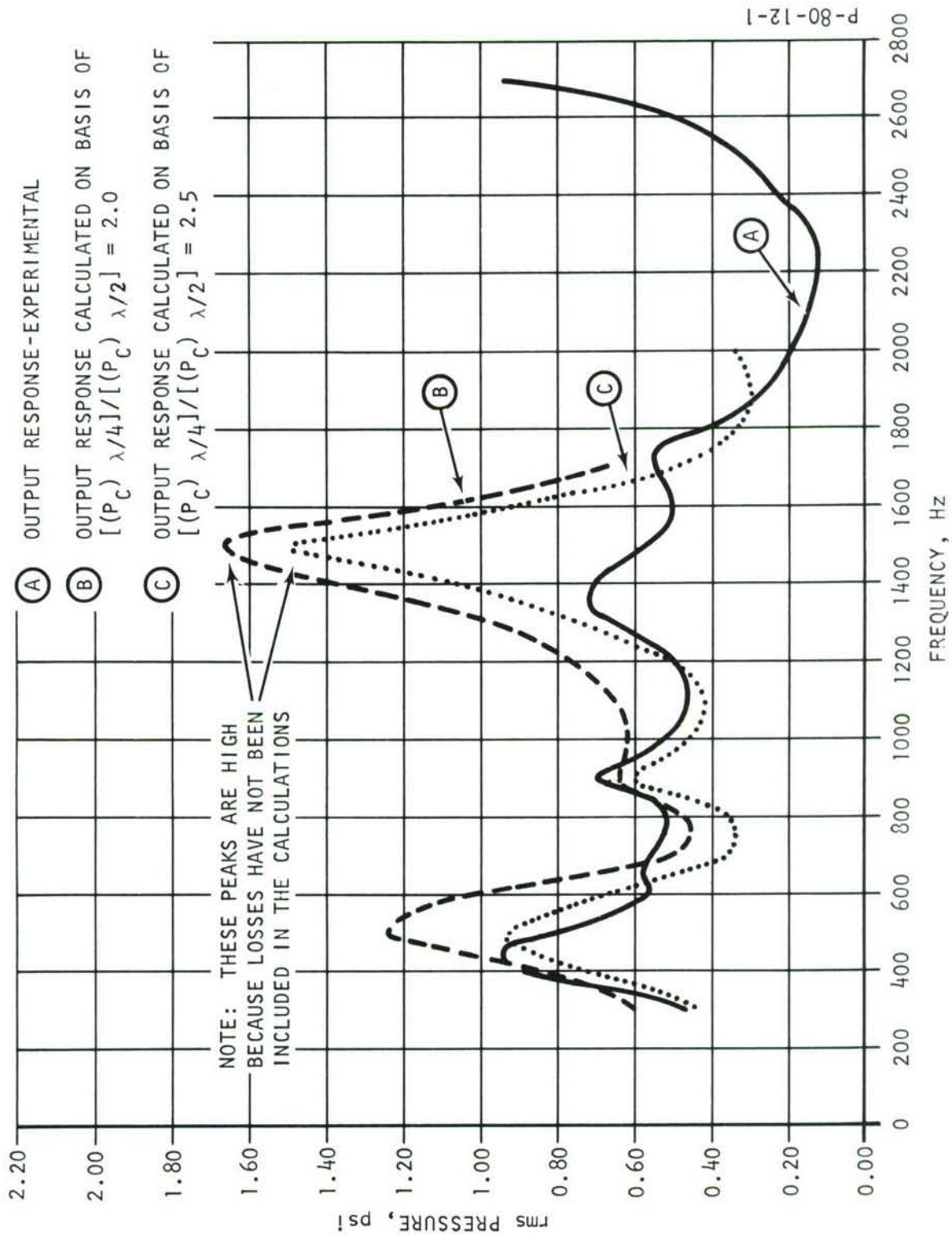


Figure 32 - Calculated Versus Measured Output Response



From Figure 31, a standing wave ratio of 2.5 yields,

$$\frac{Z_{oc}^R}{Z_g'} = 0.11$$

An approximate value of the amplifier control port area is,

$$A_r \approx 3 \text{ in}^2$$

The characteristic acoustic impedance is given by the inverse of equation (4-13a) in Section 4.2.5.

$$Z_{oc} = \frac{c}{g A_r} \approx \frac{34}{A_r}$$

for the pound (force)-inch-second system of units. Therefore, for our case,

$$Z_{oc} \approx 11 \text{ sec/in}^2$$

The electrodynamic driver output impedance is estimated to be about nine times the characteristic acoustic impedance at the driver throat. The throat area is,

$$A_s \approx 0.91 \text{ in}^2$$

Therefore,

$$\begin{aligned} Z_g' &\approx 9 \times \frac{34}{0.91} \\ &\approx 336 \text{ sec/in}^2 \end{aligned}$$

From these values,

$$\begin{aligned} R &= 0.11 \frac{Z_g'}{Z_{oc}} \\ &\approx 3.4 \end{aligned}$$

The actual transformation or area ratio of the tapered control line duct used in the annular slot amplifier model is 3.3. It is seen that this is quite close to the optimum value of 3.4 calculated above. Also, the actual control line duct length is 11 inches, which corresponds to the value used in calculating curve B and C in Figure 32. Therefore, a near optimum transformer has been used to connect the electrodynamic driver to the annular slot amplifier model.

#### 4.8 NOISE

In addition to the frequency response tests and the a.c. impedance and gain measurement tests, an output noise test of the annular slot amplifier model was also performed. To run this test, no electrical signal was provided to the control flow source and 10 psig supply pressure was applied. The load on the annular slot model was a 25-foot concentric tube assembly. The signal from the dynamic pressure transducer at the fluidic amplifier output was transmitted to a charge amplifier and from there to a Kay Vibralyzer. This instrument performs a frequency spectrum analysis of the signal. Figure 33 shows the output record of the instrument. The traces labeled "frequency calibration" were made by recording the electrical output signal from a variable-frequency electronic signal generator, the frequency being set successively to the values indicated along the horizontal axes. It is seen that in the frequency range of interest, the predominant noise peaks are at approximately 300, 600, and 1500 hertz. Also, the noise power density seems to increase steadily above 3500 hertz. The bandwidth of the analyzer used for Figure 33 is 20 hertz. The vertical scale is in arbitrary units.

Another evaluation of the noise was made by connecting a bandpass filter to the charge amplifier output, and measuring the filter output with a voltmeter. The bandpass settings were 20 hertz low cutoff and 3000 hertz high cutoff. The voltmeter used was of the vacuum tube type and was calibrated to read rms values for sinusoidal waveforms. The error resulting from measuring the random waveform is not expected to be substantial. The noise value obtained was 0.225 psi (rms). Referring to Figure 20(b), we see that this output noise pressure is lower than the signal pressure by more than a factor of 2 throughout most of the frequency range of interest.

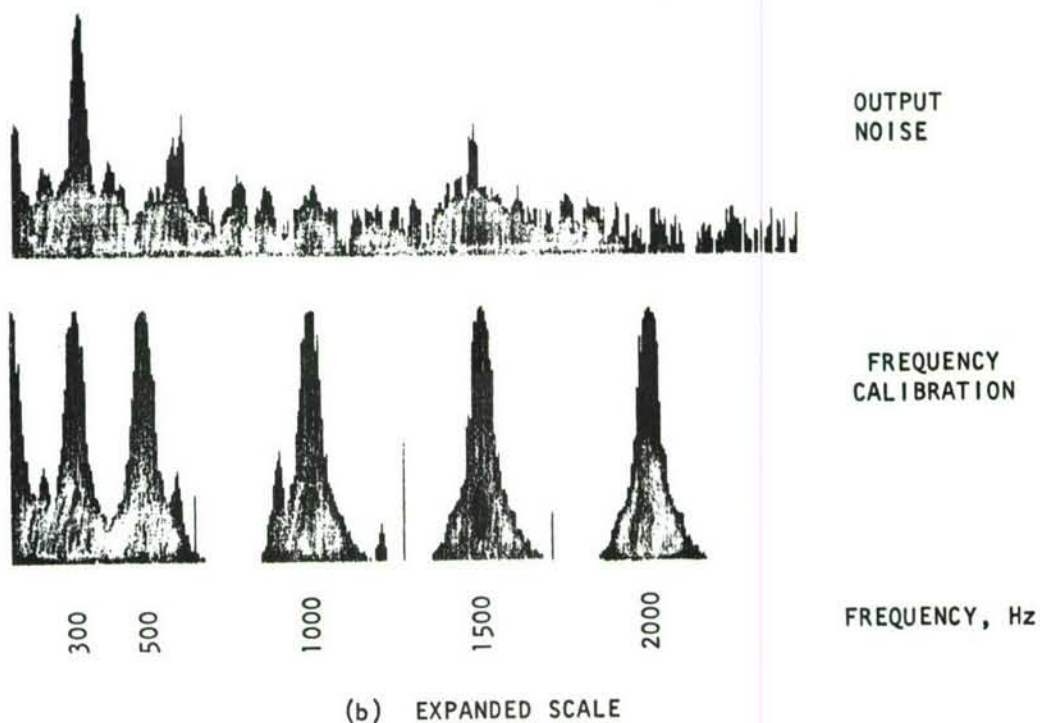
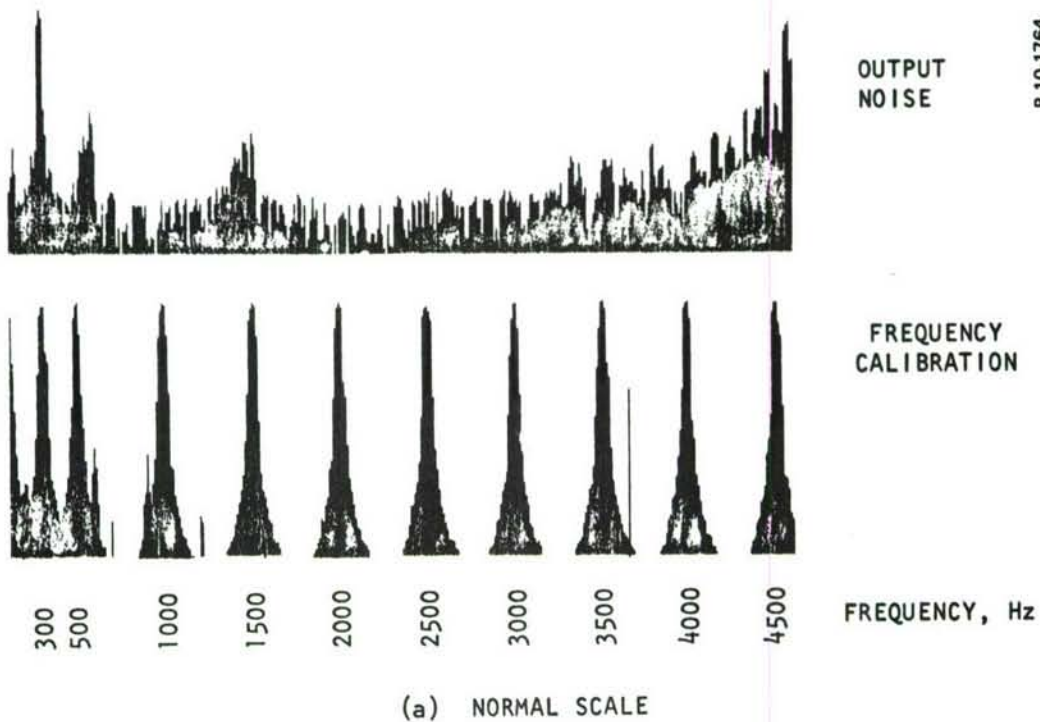


Figure 33 - Annular Slot Amplifier Model Noise



## SECTION 5

### SOUND GENERATOR DESIGN

An experimental fluidic sound generator was designed and fabricated. This generator consists of two stages, the first being the annular slot amplifier model described in the previous sections of this report, and the second being an annular slot amplifier scaled directly from the first stage such that flow passage areas are increased by a factor of ten. Thus, all experimental work described up to this point has been performed with the assembly that became the sound generator first stage.

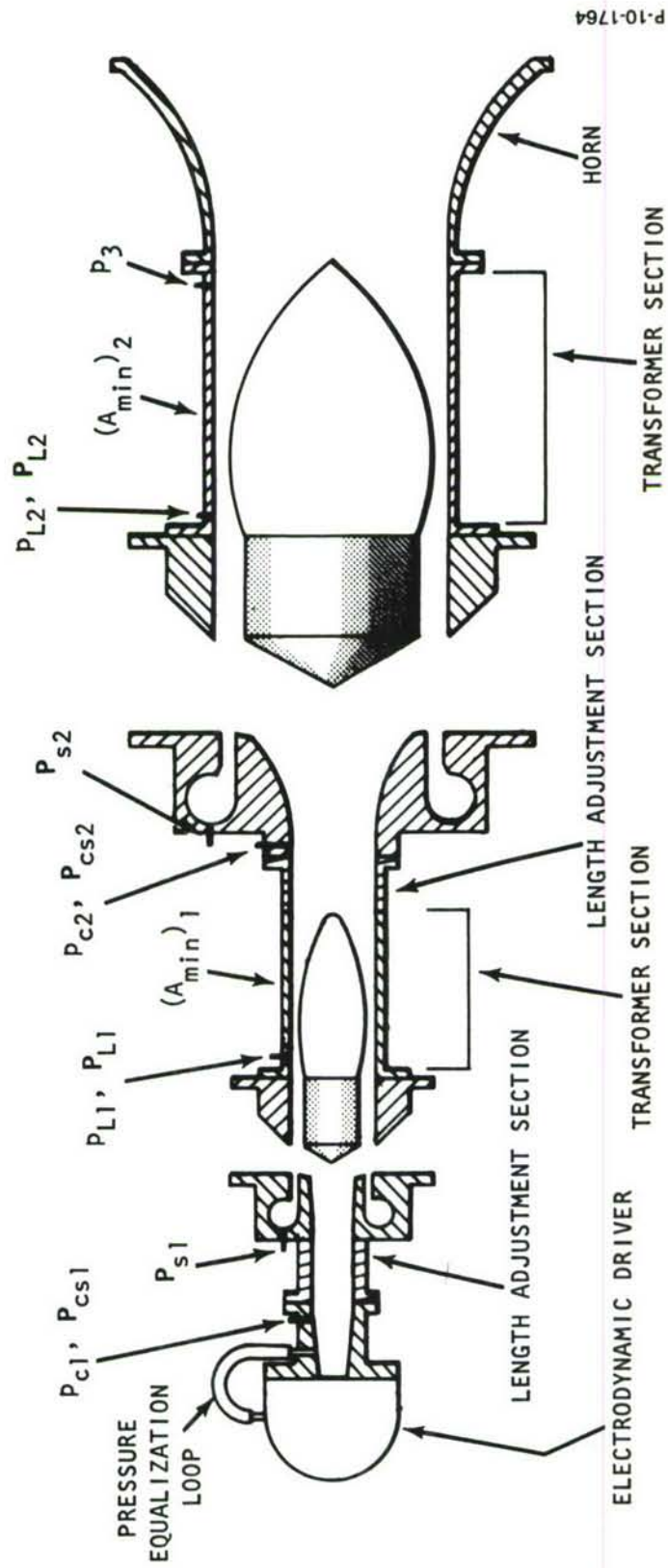
Reference 1 treats the scaling relationships for a fluidic sound generator. It is concluded that for a fixed supply pressure, the maximum output power capability is proportional to the square of the linear dimensions of the critical components. An equivalent relationship is that the maximum output power is proportional to the critical flow passage areas. Thus, the second stage of the present sound generator was scaled to yield a 10-times greater maximum output power than the first stage.

Figure 34 is a schematic diagram showing the arrangement of the generator components. Pressure tap locations are indicated in Figure 34. Following previous practice, upper case letters denote d.c. or steady state values, and lower case letters a.c. values. We must note that  $p_{c1}$  and  $p_{c2}$  in this case are not the effective control port a.c. pressures of their respective stages, but rather are the input or control line a.c. pressures. It was not physically possible to locate the pressure taps at the physical control ports. The measured control line a.c. pressures can differ from the effective control port a.c. pressures because of standing wave or reflection effects. There is no problem of this sort with the d.c. control pressures, however.

A photograph of the experimental generator is given in Figure 35.

As described in Section 3, the electric-to-pneumatic transducer which acts as the control flow source for the first stage is an electrodynamic loudspeaker driver, Altec Lansing Model 290E. The pressure equalization loop shown in the schematic diagram is to prevent any d.c. pressure differential from acting across the driver diaphragm. The passage areas in the pressure equalization loop are sufficiently small that the acoustic admittance of the loop is negligibly small.

The first stage control line duct has a conical shape. Pressure taps are provided in the duct for measuring the steady state and the a.c. control line pressures. A constant-area length adjustment section in the first stage control line allows adjustment in spacing the pressure



P-10-1764

Figure 34 - Sound Generator Schematic Diagram

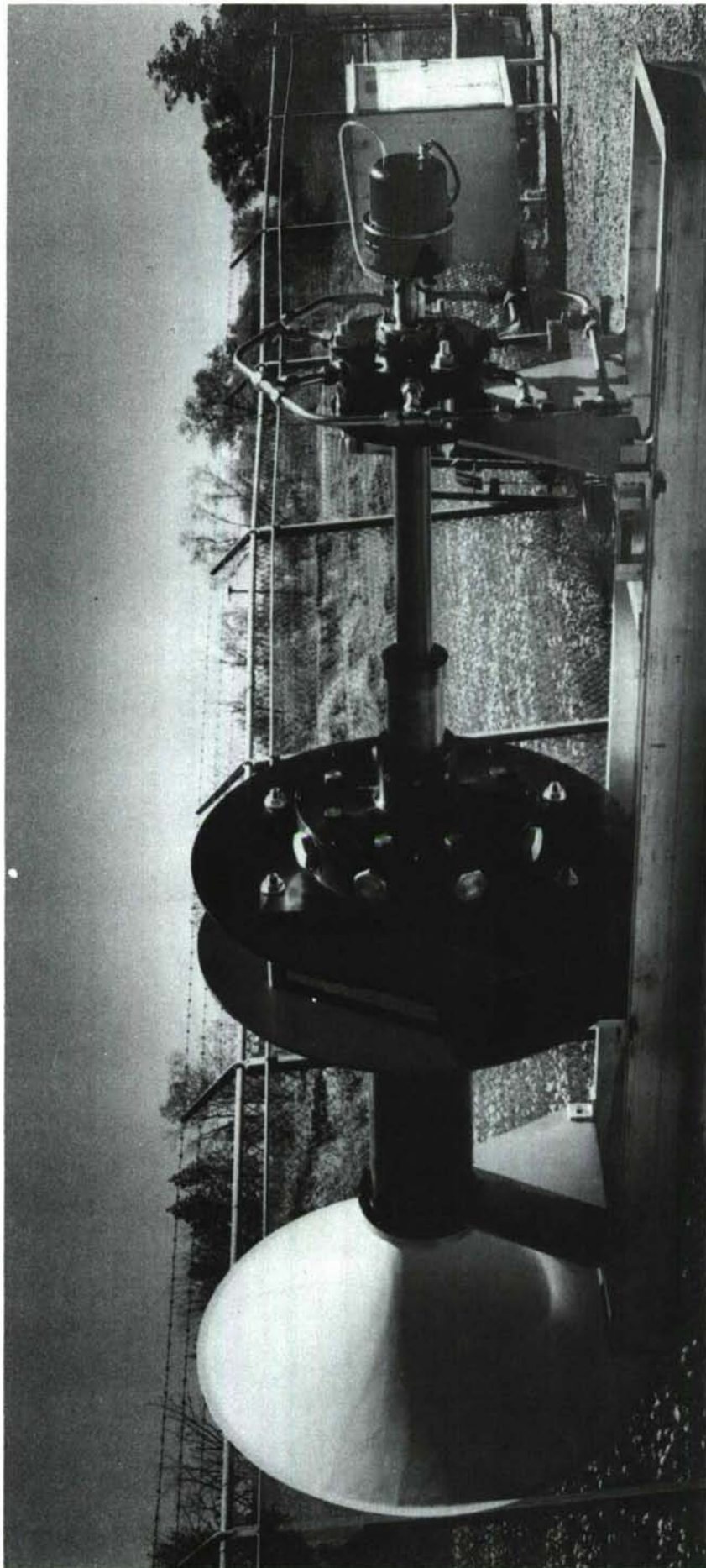


Figure 35 - Experimental Sound Generator



standing wave peaks and valleys over the frequency spectrum. A pressure tap for the steady state supply pressure for the first stage is also available.

At the outlet of the first stage receiver, an interstage transformer section is connected. This is an annular duct whose area varies exponentially with length. The cutoff frequency used to calculate the exponential form is 180 hz. To obtain the best a.c. performance of the first stage, the d.c. load on the first stage must be adjusted to the correct value. When this is done, the pressures  $P_{cs1}$  and  $P_{L1}$  and the d.c. load flow will be such that the amplifier is operating in the most favorable region of its characteristic map. The d.c. load is determined by the area  $(A_{min})_1$  in Figure 34. From the receiver exit, the transformer area decreases to  $(A_{min})_1$ , and then increases to blend into the control port of the second stage. With the d.c. load on the first stage set in this manner, an a.c. pressure wave from the first stage would be transformed, as it propagated down the transformer duct, by the square root of the duct area, if there were no losses. Actually, the a.c. pressure signal will suffer some attenuation due to friction. A constant-area length adjustment section is provided for the interstage transformer. This serves the same function as the length adjustment section in the first stage control line, namely the adjustment of the pressure standing wave peak and valley frequencies.

The second stage amplifier has pressure taps for measuring the steady state and the a.c. control line pressures, and also the steady state supply pressure. At the receiver exit, an exponential transformer section is attached. The cutoff frequency for this section is 180 hz also. Just downstream of the receiver exit are pressure taps for measuring the steady state and the a.c. load pressures.

The steady state operating point for the second stage amplifier is determined by the d.c. load, as in the first stage, and also by the d.c. component of control flow. The second stage d.c. control flow is, of course, equal to the first stage d.c. load flow. Because of the ten-times scale-up of the second stage, the d.c. control flow for the second stage is relatively small, and the second stage will operate in a nearly self-bias condition. The d.c. load on the second stage is set by the minimum area of the transformer section,  $(A_{min})_2$ .

The second stage transformer blends into a radiating horn, which continues the exponential, 180 hz-cutoff frequency form. Near the end of the transformer centerbody a tap is provided in the outer wall for measuring the a.c. pressure swing, denoted in Figure 34 as  $p_3$ .

Some critical dimensions of the first stage amplifier were given in Section 2. These are repeated here along with other dimensions of the first and second stages.

Distance from driver diaphragm to first stage physical control port* (without length adjustment section)	10.8 in
First stage physical control port diameter	1.95 in
First stage physical control port area	2.99 in <sup>2</sup>
First stage power jet outside diameter	2.738 in
First stage power jet inside diameter	2.600 in
First stage power jet area	0.58 in <sup>2</sup>
First stage receiver outside diameter	2.833 in
First stage receiver inside diameter	2.584 in
First stage receiver area	1.06 in <sup>2</sup>
First stage power jet-to-receiver distance	0.536 in
(A <sub>min</sub> ) <sub>1</sub> , interstage transformer minimum area	0.403 in <sup>2</sup>
Distance from first stage receiver entrance to second stage physical control port (with 10-inch length adjustment section)	42.75 in
Second stage physical control port diameter	6.160 in
Second stage physical control port area	29.8 in <sup>2</sup>
Second stage power jet outside diameter	8.658 in
Second stage power jet inside diameter	8.222 in
Second stage power jet area	5.83 in <sup>2</sup>
Second stage receiver outside diameter	8.962 in
Second stage receiver inside diameter	8.171 in
Second stage receiver area	10.63 in <sup>2</sup>

---

\*The physical control port is defined as that location along the control line duct where the area suddenly begins to flare out rapidly.

Second stage power jet-to-receiver distance	1.680 in
$(A_{\min})_2$ , output transformer minimum area	3.80 in <sup>2</sup>
Horn exit diameter	42.0 in
Horn exit area	1,385 in <sup>2</sup>
First stage power jet flow, calculated, $P_{s1} = 10$ psig, nitrogen, 50°F	0.33 lb/sec
Second stage power jet flow, calculated, $P_{s2} = 10$ psig, nitrogen, 50°F	3.28 lb/sec



## SECTION 6

### EXPERIMENTAL GENERATOR PERFORMANCE

As fabrication of the experimental sound generator progressed, several tests were run to obtain information prior to the generator's completion. Initially, the first stage was operated with the interstage transformer section attached but not the second stage amplifier. Next, the second stage amplifier with its transformer and horn load were added. Subsequently, the second stage amplifier vent region was modified to give a greater degree of similitude to the first stage vent region. Finally, the d.c. load point of the second stage was shifted. The significant experimental results for each of these generator conditions are given below.

In the tests performed on the experimental sound generator, the d.c. pressures were measured using laboratory-type Bourdon tube gages. The a.c. pressures were measured with Kistler model 601A pressure transducers with model 566 charge amplifiers.

#### 6.1 FIRST STAGE WITH INTERSTAGE TRANSFORMER

The interstage transformer consists of a constant-diameter cylindrical duct and a centerbody whose diameter varies with length (refer to Figure 34). This transformer physically connects the output of the first stage with the input of the second stage. The annular passage area of the transformer varies exponentially with length. Beginning at the first stage receiver exit, the passage area first decreases to a value  $(A_{\min})_1$ . Then the area stays constant for a short length before increasing to the full area of the circular duct. The area  $(A_{\min})_1$  establishes the d.c. operating point of the first stage amplifier. To set the value of  $(A_{\min})_1$ , the maximum diameter of the centerbody was cut down in increments until satisfactory values of  $P_{L1}$  and  $W_{L1}$  were obtained experimentally in d.c. runs. (The pressure  $P_{L1}$  is the d.c. output pressure and the weight flow  $W_{L1}$  is the d.c. output flow of the first stage.) An assumed value for  $P_{cs2}$ , the d.c. static control pressure of the second stage, was applied to the interstage transformer as a back pressure during these tests. The results were as follows:

Supply pressure	10 psig
$(A_{\min})_1$	$0.403 \text{ in}^2$
$P_{L1}$	3.07 psig

$W_1$	0.064 lb/sec
$P_{cs2}$	0.85 psig
$P_{cs1}$	0.80 psig

Next, the first stage and the interstage transformer were tested for a.c. performance. To minimize the effect of standing waves, a 50-foot extension was attached to the transformer's cylindrical duct. A gate valve was installed at the downstream end of the extension to establish the desired backpressure.

A frequency response test was first run with the dynamic pressure pickup in the normal position for measuring  $p_{L1}$  (the first stage dynamic output pressure). The purpose of this test was to determine how the frequency response of the first stage with the interstage transformer compared with earlier test results obtained without the interstage transformer.

Figure 36 shows the output pressure frequency response with the interstage transformer (solid line) and with the earlier concentric tube load (broken line). The latter is a replot of the data given in Figure 20 (b). The procedure followed in taking the data with the interstage transformer was somewhat different from that used in previous frequency response tests. The tracking filter amplifier was used in a different mode. The a.c. signal was effectively passed through a continuously-tuned filter having a Q of 25 and was not further processed. The advantage of this procedure is that a continuous recording is obtained when the frequency is swept over its range, as opposed to data points at discrete frequencies. The disadvantage is that rejection of noise is not as good.

We see from Figure 36 that for frequencies around 430 hertz, the output pressure with the interstage transformer is substantially greater than in the concentric tube load case. Throughout the rest of the frequency range, the two response curves do not match exactly, but they are comparable in magnitude.

The reason for the discrepancy at the low frequencies is not known. It was thought that the noise intensity in this frequency band might cause such a response peak, since the new frequency response procedure does not reject noise as effectively as the old procedure. However, subsequent noise measurements showed that while there are noise peaks around 300 and 600 hertz, their intensities are far too low to account for the overall increase in the response curve at low frequencies.

In the next test, the dynamic pressure pickup was moved from the  $p_{L1}$  position to a point just downstream of the end of the interstage transformer section. It will be recalled that a 50-foot cylindrical extension took the place of the sound generator second stage at this

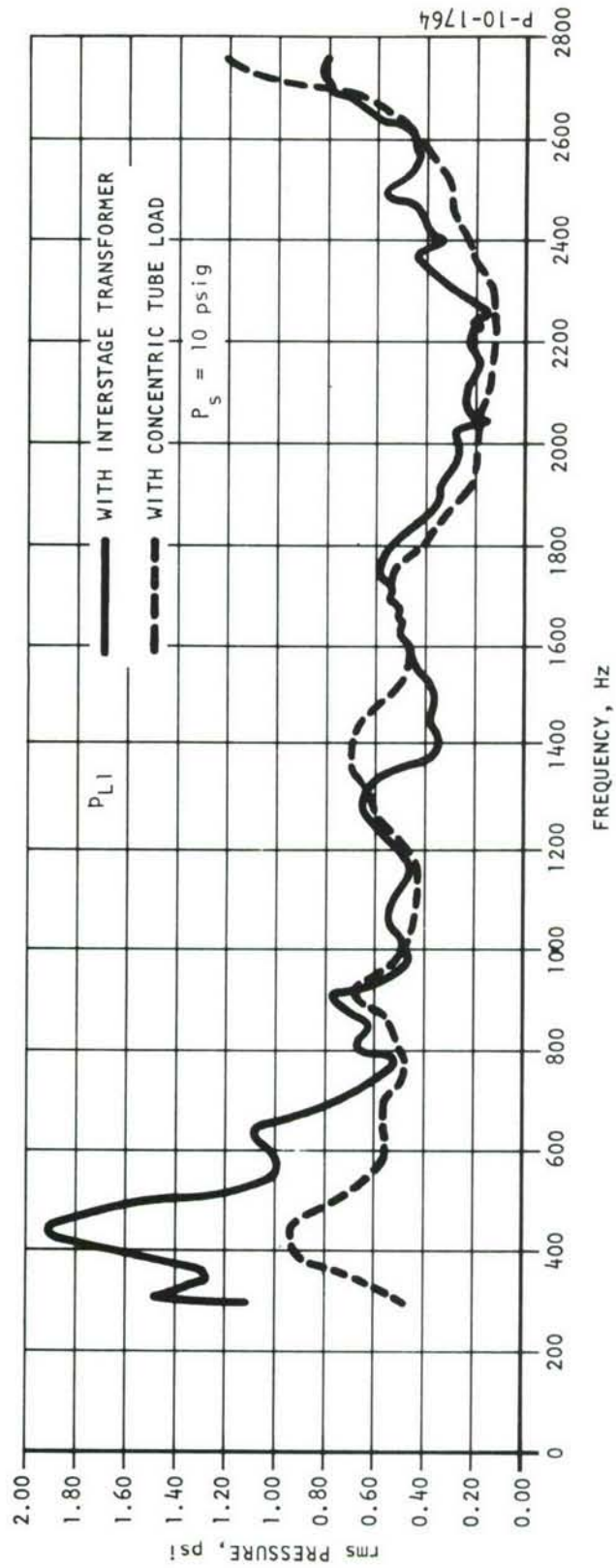


Figure 36 - First Stage Output Pressure Frequency Response with Interstage Interstage Transformer and with Concentric Tube Load



phase of the testing. Therefore, the pressure measured by the pickup in its new position was not  $p_{c2}$ . The purpose of this test was to determine how much acoustic power loss is suffered in the transformer section. This was done by comparing the frequency response curves for the new pickup position and the  $p_{L1}$  position.

From acoustic power considerations, the following relationship should hold at a given frequency:

$$\eta_t p_{L1}^2 (A_L)_1 = p_t^2 (A)_t$$

where

$p_{L1}$  = a.c. pressure magnitude just downstream of interstage transformer entrance

$p_t$  = a.c. pressure magnitude just downstream of interstage transformer outlet

$(A_L)_1$  = duct area where  $p_{L1}$  is instrumented

$(A)_t$  = duct area where  $p_t$  is instrumented

$\eta_t$  = dimensionless power loss factor for the interstage transformer

The loss factor was computed at several different frequencies and averaged. The result is:

$$\eta_t = 0.63$$

This corresponds to 2 db loss in the transformer section.

Another test run was made with the first stage and interstage transformer. This was to determine the effect of increasing the supply pressure from 10 to 20 psig. The data is shown in Figure 37. At the time this run was made, the value of  $(A_{min})_1$  was 0.250 in<sup>2</sup> and the transformer duct extension was 25 ft. long instead of 50 ft. For these reasons, the data of Figure 37 is not directly comparable to that of Figure 36. However, the two curves of Figure 37 do indicate the effect of a change in supply pressure alone. The increase in a.c. output pressure at 20 versus 10 psig supply varies with frequency. On the average, however, the a.c. output pressure increased about 50% when the supply pressure was doubled. On the basis of acoustic power, then, the output power was roughly doubled.

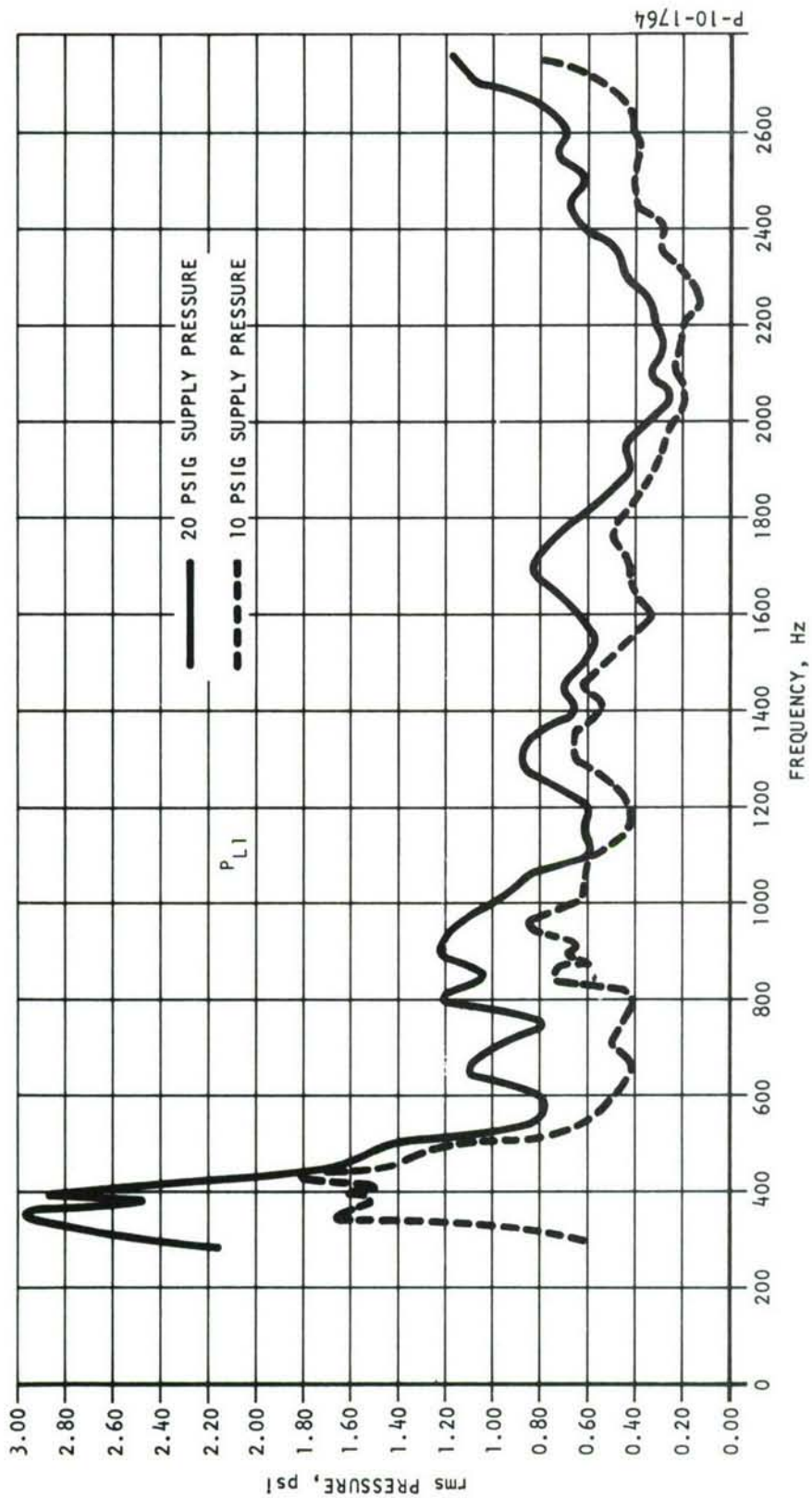


Figure 37 - Effect of Supply Pressure Change on First Stage Pressure Frequency Response

## 6.2 GENERATOR IN ORIGINAL CONFIGURATION

The complete sound generator, as depicted in Figure 34, was next assembled and tested. It is seen that a second transformer section joins the second stage receiver exit with the radiating horn. In the same way as in the interstage transformer, the value of  $(A_{\min})_2$ , the minimum transformer passage area, establishes the d.c. operating point for the second stage. After a number of trials,  $(A_{\min})_2$  was at the largest value which could be obtained without a fairly difficult machining operation. However, the data indicated that the area should be made still larger if the d.c. operating point of the second stage were to be close to that of the first stage. Before any major rework, data on the performance of the generator in its original configuration was obtained. Such data is given in this section.

For this test series, the following d.c. data applied:

$(A_{\min})_2$	2.45 in <sup>2</sup>
Second stage supply pressure	10 psig
$P_{L2}$	3.80 psig
$P_{cs2}$	0.73 psig
First stage supply pressure	10 psig
$P_{L1}$	3.10 psig
$P_{cs1}$	0.81 psig

The second stage is not operated in a "self-bias" condition as is the first stage. Rather, a d.c. flow component from the first stage passes through the second stage control line. Because of the 10-times scaleup of areas, the d.c. load flow component of the first stage should appear very small at the second stage control port.

To verify this, a test was run in which the second stage control line was blocked off. The resulting self-bias pressures were as follows:

$(A_{\min})_2$	2.45 in <sup>2</sup>
Second stage supply pressure	10 psig
$P_{L2}$	3.98 psig
$P_{cs2}$	0.71 psig



The second stage steady state load and control pressures were changed, but only slightly, from the previous coupled-stages data. This confirms that the d.c. control flow component of the second stage does not change the d.c. operating point grossly.

The a.c. performance is shown in Figures 38 and 39. Comparing the  $P_{L1}$  and  $P_{L2}$  traces, it is seen that the second stage output pressure is substantially lower than that of the first stage. Also, there are some interesting spikes and dips in all four curves at about 420 hertz. These are probably due to resonances.

Ideally, we would like to achieve a second stage output a.c. pressure level, away from the resonant peak, of the same order as that of the first stage. It is seen that the second stage output pressure level is lower than this ideal goal by roughly a factor of 4. Part of this reduction may be due to the fact that the second stage control a.c. pressure is not high enough to drive the second stage over the same range as the first stage is driven. Because the second stage control line length is relatively short (from the first stage receiver to the second stage physical control port), and because this line is not terminated at either end in its characteristic impedance, there are very likely multiple reflections and standing waves on the line. For this reason, calculation of the true second stage control port driving pressure is not a straightforward matter. However, rough estimates based on power considerations indicate that the second stage output a.c. pressure should be higher than that observed by a factor of two, given the observed second stage control a.c. pressure. Again, we are concerned with the part of the frequency response beyond the resonance centered at 400 hertz.

The results shown in Figures 38 and 39 suggested that the second stage may not have been performing as well as the first stage. The question arose as to whether the dynamic response of the second stage might be so slow that signals at frequencies beyond the resonant peak are not amplified. The previous investigation of the fluid sound generator approach (reported in Reference 1) concluded that the upper frequency limit of a sound generator stage scaled in inverse proportion to the linear dimensions of the stage. Therefore, the upper frequency limit of the present second stage would be lower than that of the first stage by a factor of  $\sqrt{10}$  or 3.16.

Experiments run earlier with the first stage alone showed there was good gain out to frequencies as high as 6500 hertz, which is about the frequency limit of the electrodynamic driver used. Therefore, the scaling principle indicates the second stage bandpass extends at least to  $6500/3.16$ , or beyond 2000 hertz.

Other causes were then sought for the low output pressure level of the generator second stage. Attempts were made to improve the generator performance by running at supply pressure conditions other

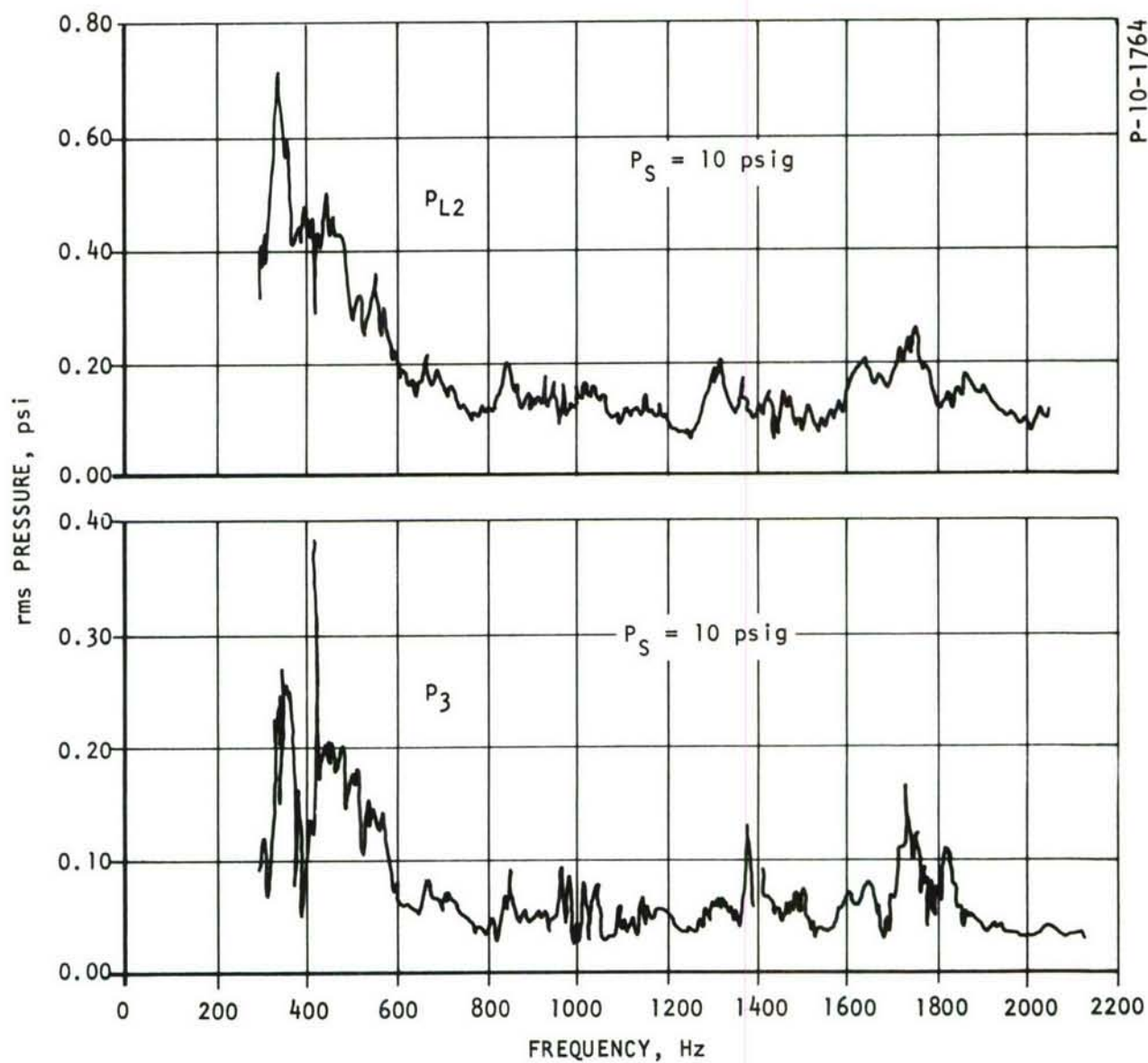


Figure 38 - Frequency Response of Generator in Original Configuration,  
 $P_{L2}$  and  $P_3$

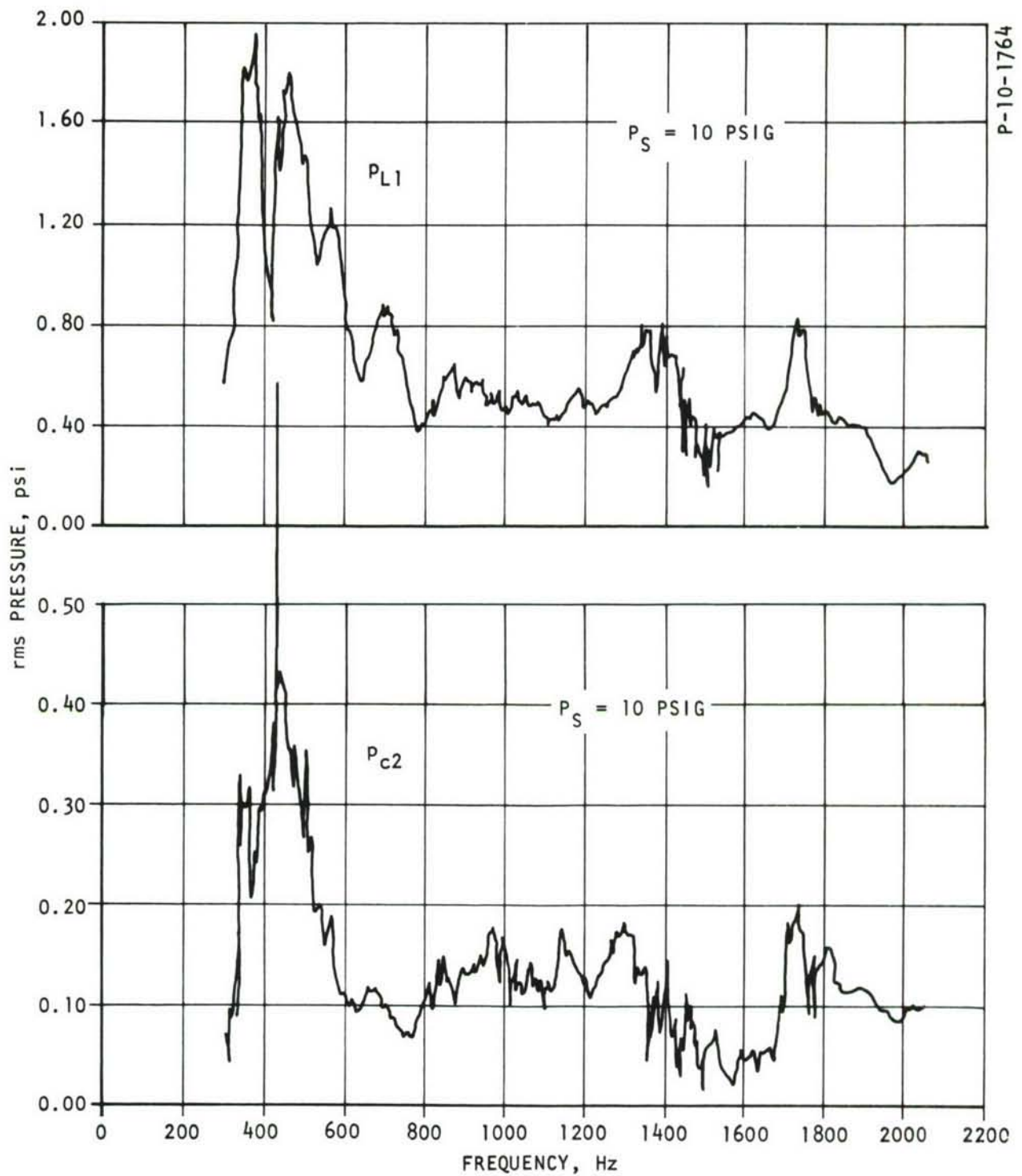


Figure 39 - Frequency Response of Generator in Original Configuration,  
 $P_{L1}$  and  $P_{C2}$



than 10 psig on each stage. The following combinations were tried:

$$P_{s1} = 20 \text{ psig}, P_{s2} = 10 \text{ psig}$$

$$P_{s1} = 5 \text{ psig}, P_{s2} = 10 \text{ psig}$$

The results were poorer than those with 10 psig on each stage.

While the critical dimensions of the jet interaction region were exactly scaled between the first and second stages, the vent region dimensions were not. The first stage vent region is defined by the structure of the supply pressure region and by the structure which supports the alignment rods and spacers. (Refer back to Figure 2.) The first stage vent region then consists essentially of a space between two concentric circular baffles perpendicular to the longitudinal axis of the amplifier.

In the original design of the second stage, the shape of the splitter member (which forms the outside of the receiver passage) was scaled for geometric similitude with the first stage. However, the region beyond the splitter's conical surface was not believed to be critical to the operation of the amplifier, as long as the venting flow was not unduly obstructed. Only a single circular baffle was provided to prevent a direct sound path from the second stage jet interaction region to the first stage jet interaction region.

As mentioned in Section 4, a possible explanation for the apparent regenerative feedback in the first stage is a distributed-path phenomenon in the vent region. Therefore, it was decided to modify the generator second stage to provide geometric similarity between the first and second stages in the vent region as well. This modification could be made with relatively little difficulty.

### 6.3 GENERATOR WITH VENT REGION SIMILITUDE

After modification to achieve geometric similarity of the vent regions for the first and second stages, the following d.c. data were obtained:

$(A_{\min})_2$	2.45 in <sup>2</sup>
Second stage supply pressure	10 psig
$P_{L2}$	3.40 psig
$P_{cs2}$	0.74 psig

First stage	
supply pressure	10 psig
$P_{L1}$	3.12 psig
$P_{cs1}$	0.82 psig

The modified second stage was also tested for its d.c. pressure levels at the self-bias condition (control line blanked off). The results were:

$(A_{min})_2$	2.45 in <sup>2</sup>
Second stage	
supply pressure	10 psig
$P_{L2}$	3.53 psig
$P_{cs2}$	0.71 psig

Comparing this d.c. data with that for the original configuration, we see that  $P_{L2}$  is lowered by 0.40 psig for full generator operation, and by 0.45 psig in the self-bias condition. All other d.c. pressures changed very little or not at all. Thus, the change in the second stage vent condition did definitely modify the d.c. operating characteristics of that stage, and this is manifested in the shift of  $P_{L2}$ .

Next, a.c. tests were run to determine whether the acoustic performance of the generator was changed. The results for the second stage output and control pressures are shown in Figure 40. Comparing these with the corresponding curves of Figures 38 and 39, we see that the output pressure level for the modified vent version is higher in the vicinity of the resonant peak, but is not substantially changed for higher frequencies. The control pressure level for the modified vent version is lower for virtually all frequencies, however. Beyond the resonant peak, the modified vent control pressure level is approximately 2/3 of the original configuration control pressure level. Thus, the vent change yielded an increased gain for the second stage, but no increase in acoustic output power for the frequency range beyond the resonant peak.

The next step taken was to attempt to reach even greater similarity between the second and first stages by increasing the d.c. load area of the second stage,  $(A_{min})_2$ .

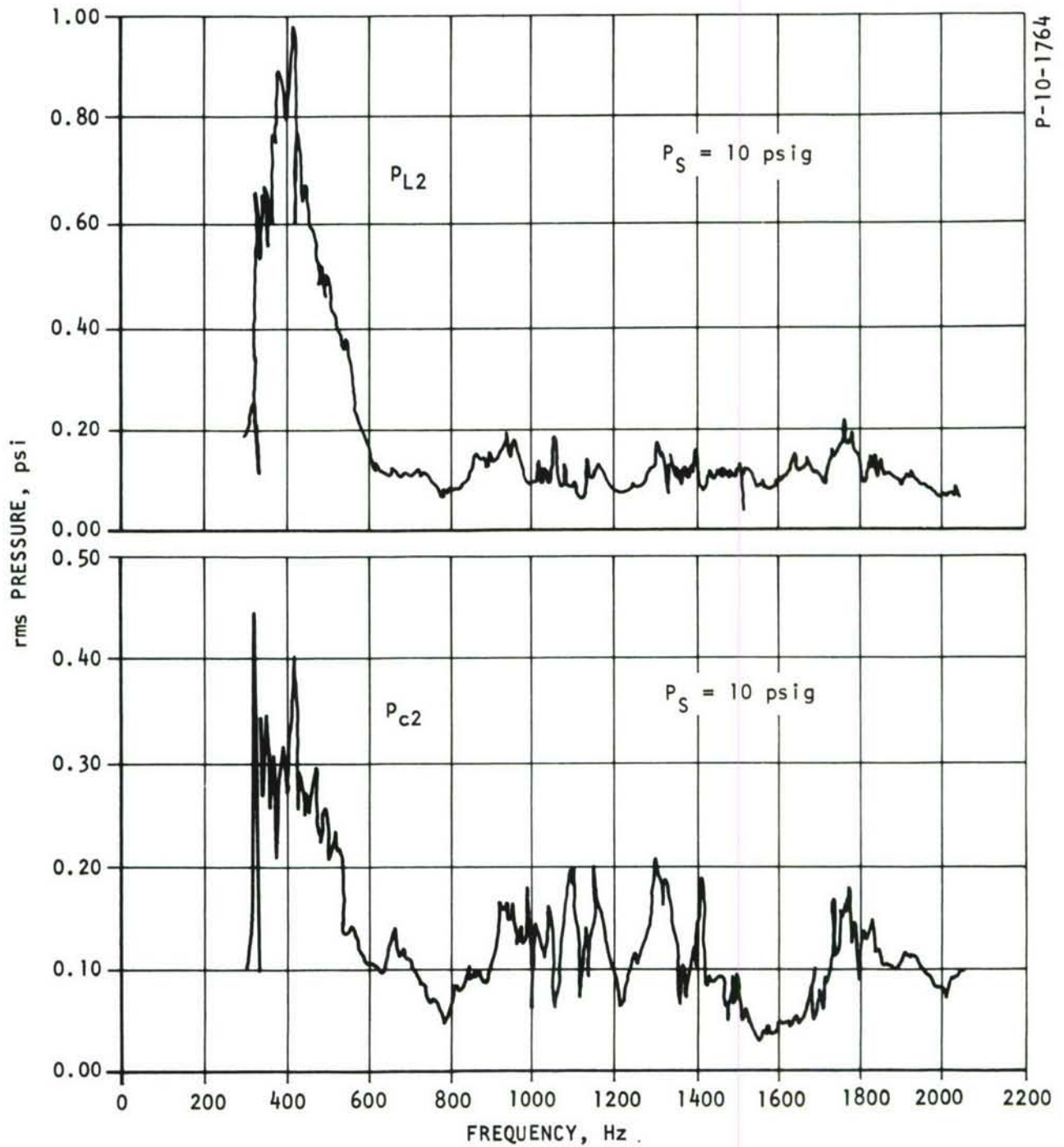


Figure 40 - Frequency Response of Generator with Modified Second Stage Vent Region,  $p_{L2}$  and  $p_{c2}$



#### 6.4 GENERATOR WITH VENT REGION SIMILITUDE AND CHANGED D.C. LOAD

After the machining operation to increase  $(A_{\min})_2$ , the generator was reassembled and the following d.c. data were obtained:

$(A_{\min})_2$	3.80 in <sup>2</sup>
Second stage supply pressure	10 psig
$P_{L2}$	2.72 psig
$P_{cs2}$	0.59 psig
First stage supply pressure	10 psig
$P_{L1}$	3.12 psig
$P_{cs1}$	0.81 psig

The value of  $(A_{\min})_2$  is 6% shy of being exactly ten-times the value of  $(A_{\min})_1$ . The d.c. value of the second stage output pressure,  $P_{L2}$ , is about halfway between the d.c. output pressure values obtained for the first stage with 50-ft. and 25-ft. concentric tube loads. The d.c. value of the second stage control pressure,  $P_{cs2}$ , is significantly lower than any corresponding value obtained with the first stage, however.

Tests were run to determine the d.c. pressures for the second stage in the self-bias condition, that is, with the second stage control line blocked off. The data are as follows:

$(A_{\min})_2$	3.80 in <sup>2</sup>
Second stage supply pressure	10 psig
$P_{L2}$	2.89 psig
$P_{cs2}$	0.67 psig

The first stage operates acoustically in the self-bias condition. The second stage cannot operate acoustically in the self-bias condition, since it must take its control flow from the first stage. For comparing d.c. operating points, however, the self-bias condition is very convenient. The self-bias value of  $P_{L2}$  is found to be within the range observed for  $P_{L1}$  near the optimum operating point, but the self-bias value of  $P_{cs2}$  is lower than that observed for  $P_{cs1}$  by some 12%. We interpret this as an indication that the d.c. characteristic curves for the second stage do not match exactly those of the first stage.

Next, an a.c. test series was run. Figure 41 gives frequency response curves for  $p_{L2}$  and  $p_{C2}$  with the changed d.c. load. Comparing these with the curves of Figure 40, we note that the a.c. pressure level of the second stage output has not been increased, and in some portions of the frequency spectrum it has been decreased slightly. The a.c. pressure level of the second stage control, on the other hand, has been increased by approximately 20%.

We conclude, then, that the second stage annular slot amplifier is still not performing in the same manner as the first stage amplifier.

Other data were taken on the a.c. pressures at the critical points in the fluidic circuit. The a.c. pressure levels were recorded directly in decible units of sound pressure level. This was done by processing the electrical signal from the tracking filter through a logarithmic amplifier. The output signal from this amplifier was then connected to the recorder input. The zero reference and sensitivity of the recorder were then adjusted to yield the correct decible values when a.c. calibration voltages were applied to the tracking amplifier input.

Figures 42 and 43 show the data obtained. The areas at each sensing station are noted, for purposes of comparison. (Figure 34 shows the sensing station locations on a schematic diagram of the generator.) The piezoelectric pressure transducer installation described previously was used at all stations except in the plane of the horn mouth. Here, a General Radio sound level meter type No. 1551-C with a General Radio standard ceramic microphone was used. The electrical signal from the sound level meter output jack was amplified by an auxiliary electronic amplifier and then connected to the tracking amplifier input.

We see that the highest sound pressure level observed was at the  $p_{L1}$  station, the first stage output. This also happens to be the station with the smallest area. In the resonant peak region, 177 db was recorded. In the plane of the horn exit, the largest area station, a maximum of 146 db was observed around the resonant peak. In the frequency range beyond the resonant peak, the sound pressure level was usually in the band from 130 to 135 db.

It will be recalled that in the standard frequency response procedure used in this program, the electrodynamic driver control flow source was operated at 45 watts electrical power input rather than the rated 100 watts. The reason was the short diaphragm life experienced at full power when the acoustic loading on the driver is highly reactive at several operating frequencies. However, one run was made on the complete generator with 81 watts electrical power input to observe the effect on the generator's operation. The 81-watt level was the highest power that could be obtained at the standard 500-hertz set-point, with the electronic amplifier used.

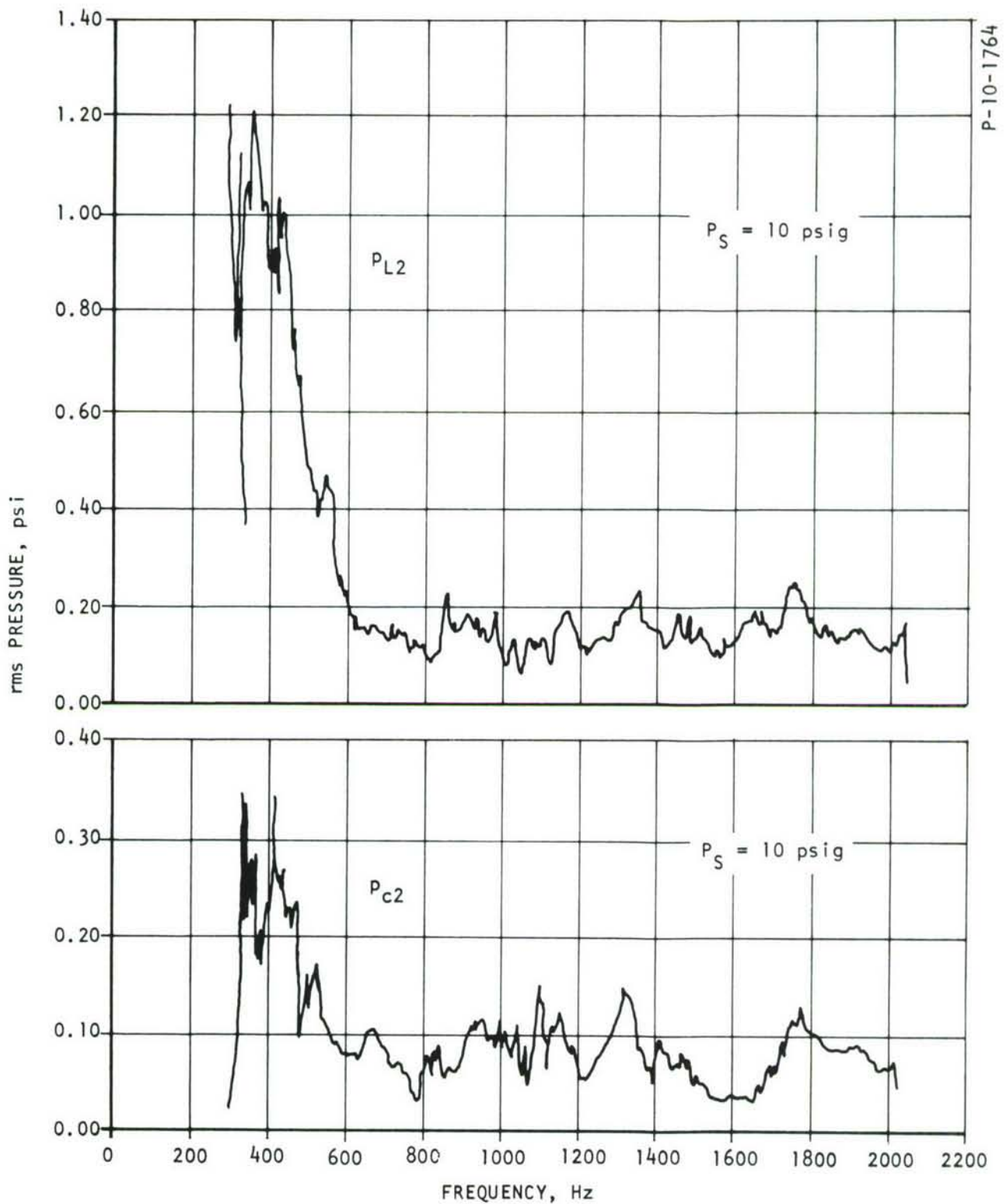


Figure 41 - Frequency Response of Generator with Modified Second Stage Vent Region and Changed d.c. Load,  $p_{L2}$  and  $p_{c2}$



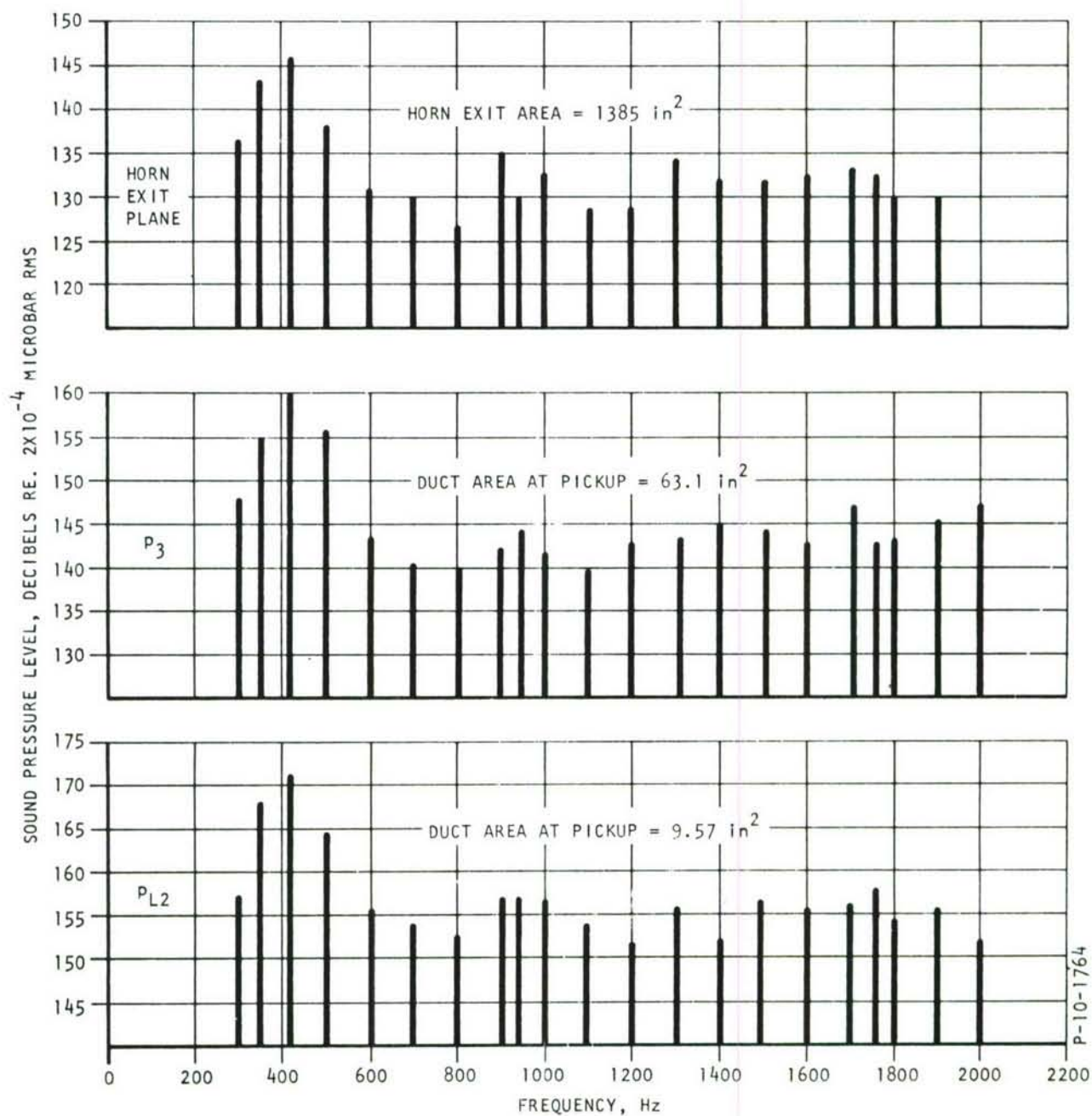


Figure 42 - Generator Frequency Response in Terms of Sound Pressure Level, Horn Exit, p<sub>3</sub> and p<sub>L2</sub>

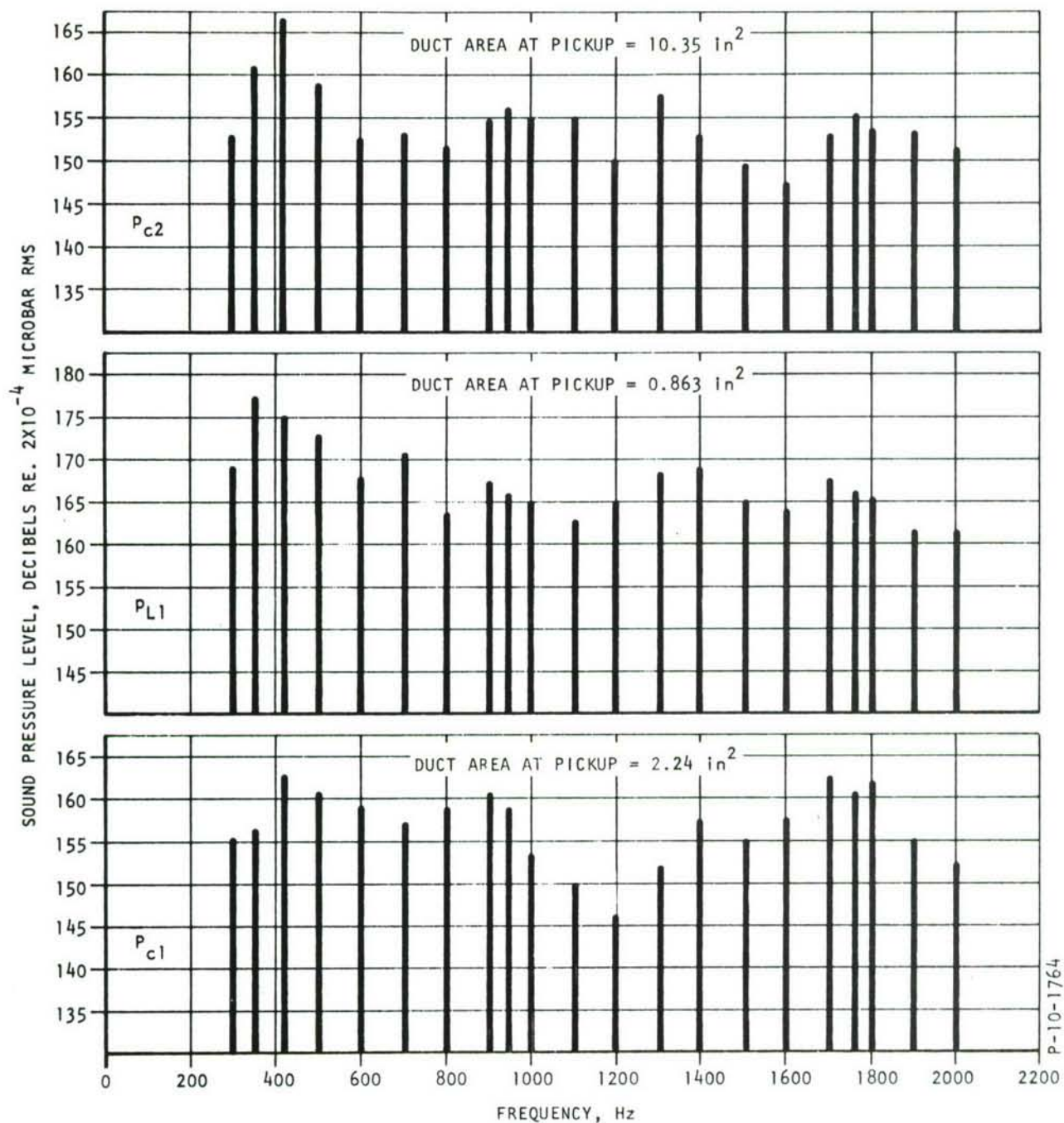


Figure 43 - Generator Frequency Response in Terms of Sound Pressure Level,  $P_{c2}$ ,  $P_{L1}$ , and  $P_{c1}$

Measurements were made with the sound level meter in the plane of the horn exit. These measurements showed the microphone output voltage was increased by an average of 25% over the frequency range of interest when the higher driver power was applied. If the system were completely linear, the microphone output voltage would have been increased in the same proportion as the driver input voltage, or 39%. The fact that the microphone output voltage experienced a smaller increase is attributed to one or both of the following:

- (a) the electrodynamic driver, the first stage fluidic amplifier and/or the second stage fluidic amplifier operating in a saturation range for a portion of a cycle, and
- (b) dissipation losses in the ducts increasing faster than the first power of the pressure amplitude.

The tests described above completed the experimental sound generator evaluation within the scope of this program. They are significant in that staged operation of two annular slot fluidic amplifiers was demonstrated. The results were somewhat disappointing due to the second stage amplifier not exhibiting as favorable performance as did the first stage. It is believed that the potential high-gain performance of the second stage can be realized eventually. This will be discussed further in Section 7.



## SECTION 7

### SUMMARY AND CONCLUSIONS

A new fluidic amplifier configuration using an annular slot power jet has been developed for use as a preamplifier or a final amplifier stage of a fluidic sound generator. This amplifier configuration evolved from a two-dimensional straight slot amplifier investigated in a previous phase of this effort. The annular slot configuration was considered advantageous for a sound generator application, particularly the final stage, because its single-ended output geometry provided a simple connection to a radiating horn.

In developing this amplifier configuration, it was found that considerably more static gain was present than anticipated, leading to the conclusion that some form of inherent regenerative feedback exists in this amplifier. This high gain design is viewed as beneficial in that it reduces the number of stages required to reach a given power level. However, the presence of the feedback leads to an amplifier input impedance that is markedly reduced over that ordinarily expected. An analysis carried out in Section 4, the results of which are illustrated in Figure 17, shows the input impedance to be about  $1/3$  of the control duct characteristic impedance. The output impedance is negative and of a magnitude slightly larger than the characteristic impedance of the receiver duct. The calculated impedances were confirmed experimentally and reported in Section 4.4.

The fact that the amplifier input impedance is lower than the control duct characteristic impedance causes a mismatch at the amplifier control port. The most direct design approach to eliminate the impedance mismatch, and the resultant signal reflections at the control port, is to increase the control duct area. Because of the geometry of the amplifier - the control duct is internal to the annular supply jet - there is no room to increase the control duct area. This circumstance, due to the unexpected regenerative feedback, resulted in considerable compromise in further development of the sound generator. A complete redesign might have solved the matching problem, as shown schematically in Figure 28. However, it was decided that even with the impedance mismatch at the amplifier control port, the staging of two different size amplifiers would yield useful design information. At this point, information still sought included design criteria for the interstage coupling transformer, and the behavior of an amplifier stage geometrically similar to the first stage but scaled up 10-times for power. In scaling up for 10-times the power, it was reasoned that no increase in stage pressure swing could be expected over that observed for the first stage. Thus, all linear dimensions of the second stage were increased by  $\sqrt{10}$  times those of the first stage.

Evaluation of the performance of this large second stage was found to be difficult because the stage could be driven only the first stage amplifier. The reflective loading situation - at both stages - caused considerable change in frequency response over that observed for the first stage when loaded with a nearly ideal acoustic load (50-foot concentric tube load). This can be seen by comparing the  $P_{L1}$  trace in Figure 39 with that of Figure 20b. There is considerably more output from the first stage at frequencies of 350, 440, 570, 700, 1400, and 1720 hz over that observed for the first stage with its 50-foot acoustic load. This increase in output is probably due to the reflective load presented by the second stage input port to the first stage output receiver.

A characteristic peak-and-valley occurs in the  $P_{L1}$  response of Figure 39 at a frequency interval of some 60 to 80 hz which corresponds to a quarter-wave-length line of some 40 inches, the approximate length of the interstage transformer.

The interstage transformer performed quite well showing an insertion loss of only 2 db. This transformer design, with its reduced throat area for setting the previous stage d.c. load point, can be stated to be a practical approach to staging amplifiers.

It must be recognized that although the two stages are geometrically similar, the output impedance of the electrodynamic driver is considerably different from the output impedance of the first stage. The electrodynamic driver output impedance of the first stage is positive and estimated to be some nine-times the driver throat characteristic impedance. The output impedance of the first stage is negative and approximately equal to the characteristic impedance of the output receiver. Because of this difference, total model similitude throughout the system is not possible. Therefore, conclusions as to the performance of the second stage in comparison to that of the first stage cannot be totally conclusive.

From the  $P_{L2}$  trace in Figure 41, there is a general conclusion that the second stage does not exhibit the same gain as the first. However, because of the control duct multiple reflection situation, it is not conclusive that the second stage is or is not functioning in the same manner as first.

Another consequence of the impedance mismatch at the driver end of the control duct (for either stage) is that reflected signals traveling upstream are reflected downstream again.

To circumvent the difficulties imposed by signal reflections in the control ducts, design changes should be undertaken to provide impedance matching looking downstream through the sound generator. Having matched in that direction, matching looking upstream through the sound generator is not required.



On the basis of the investigation performed, the application of annular slot fluidic jet amplifiers for the high-intensity sound generator task described in the Introduction (Section 1) requires the resolution of three problems:

- (a) a satisfactory breadboard control flow source for the first stage,
- (b) a tuning technique or a modified geometry to minimize the reflection effects in control lines which presently have mismatched terminations, and to minimize the effect of frequency-dependent amplifier gain, and
- (c) a better understanding of the annular slot amplification mechanism so that high-gain performance can be achieved on scaled units.

None of these problems appears insolvable. The most straightforward approach to the control flow source is to use two generator types to cover the frequency range. A generator type equipped with a modulating valve control flow source might be used for frequencies from 20 to 300 hertz. Another generator type equipped with an electrodynamic driver control flow source (as in the current program) would be used for the frequencies beyond 300 hertz. An electronic crossover network would command both types of generators in parallel. Other approaches to the control flow source problem might be suggested also.

Tuning techniques utilizing selected and fixed control line lengths between the stages of a generator, and between the control flow source and the first stage amplifier, can very likely result in a moderately smooth frequency response. However, if a very smooth response curve is required, more sophisticated tuning approaches or a modified amplifier geometry would have to be developed, perhaps involving feedback loops in the fluidic stages.

The need for further understanding of the amplification problem is pointed up by the performance of the second stage amplifier of the current program as compared to that of the first stage amplifier. It is believed that a very fruitful area for more careful study will be the control port geometry. In the first stage amplifier, which performs very well, the control line duct approaches the physical control port with a shallow conical taper. The included angle is 3 degrees. In the case of the second stage amplifier, the control line duct is an exponential transformer section, and the "bellmouth" at the second stage physical control port is considerably greater than a 3-degree included angle. It is possible that the control line duct immediately upstream of the physical control port is highly influential for the amplifier a.c. performance. Of course, other aspects should not be overlooked in seeking to obtain the full performance capability of scaled annular slot stages.



## REFERENCES

1. B. R. Teitelbaum and A. A. Seleno, "Fluid State High-Intensity Sound Generation," Air Force Flight Dynamics Laboratory Technical Report AFFDL-TR-67-112, June 1967.
2. L. B. Taplin, "The Admittance Properties of a Jet Proportional Amplifier," SAE SP-348, May 1969.
3. J. E. Emswiler and F. L. Schwartz, Thermodynamics, McGraw-Hill, 1943.
4. W. G. Johnson, Transmission Lines and Networks, McGraw-Hill, 1950.
5. R. N. Miller, "Dynamic Characteristics of Blocked Concentric Cascaded Pneumatic Transmission Lines," Thesis, Air Force Institute of Technology, U.S.A.F., March 1968.
6. J. G. Truxal, Automatic Feedback Control System Synthesis, McGraw-Hill, 1955.
7. H. F. Olson, Acoustical Engineering, D. Van Nostrand, 1957.

Unclassified

Security Classification

## DOCUMENT CONTROL DATA - R &amp; D

(Security classification of title, body of abstract and indexing annotation must be entered when the overall report is classified)

1. ORIGINATING ACTIVITY (Corporate author) Bendix Research Laboratories Southfield, Michigan 48075		2a. REPORT SECURITY CLASSIFICATION Unclassified	
		2b. GROUP N/A	
3. REPORT TITLE Investigation of Fluidic High Intensity Sound Generator			
4. DESCRIPTIVE NOTES (Type of report and inclusive dates) Final Report - 26 February 1968 through 24 April 1970			
5. AUTHOR(S) (First name, middle initial, last name) Bernard R. Teitelbaum Lael B. Taplin			
6. REPORT DATE May 1971		7a. TOTAL NO. OF PAGES 115	7b. NO. OF REFS 7
8a. CONTRACT OR GRANT NO. F33615-68-C-1406		9a. ORIGINATOR'S REPORT NUMBER(S) AFFDL-TR-70-98	
b. PROJECT NO. 4437			
c. Task 443705		9b. OTHER REPORT NO(S) (Any other numbers that may be assigned this report) 5335	
d.			
10. DISTRIBUTION STATEMENT This document has been released for public release and sale; its distribution is unlimited.			
11. SUPPLEMENTARY NOTES N/A		12. SPONSORING MILITARY ACTIVITY AFFDL/FYA Wright-Patterson AFB, Ohio 45433	
13. ABSTRACT This report summarizes the results of an investigation of a fluidic high-intensity sound generator concept. The investigation concerned the evaluation of a new type of proportional fluidic amplifier geometry, the annular slot amplifier. This amplifier was found to have significantly higher pressure gain than the conventional planar jet proportional amplifier, 4 to 12.5 versus 3 to 5. An annular slot amplifier model was tested over a frequency range from 300 Hz to over 2000 Hz. Its control port impedance was studied particularly, and the impedance as well as the amplifier gain were found to vary with frequency. The frequency dependence is attributed to a distributed-parameter feedback phenomenon in the vent region.  An experimental two-stage sound generator was designed, fabricated, and tested. The second stage is an annular slot amplifier with its critical areas scaled up ten times over those of the first stage. The first stage control flow source is an electro-dynamic driver of the kind used with conventional loudspeakers. The second stage power jet area is 5.78 in <sup>2</sup> , and the supply pressure is 10 psig. The radiating horn is exponential with a cutoff frequency of 180 Hz and an exit diameter of 42 inches.			

Unclassified

Security Classification

KEY WORDS	LINK A		LINK B		LINK C	
	ROLE	WT	ROLE	WT	ROLE	WT
Acoustics Fluidics Sound Generation						

Unclassified

Security Classification